



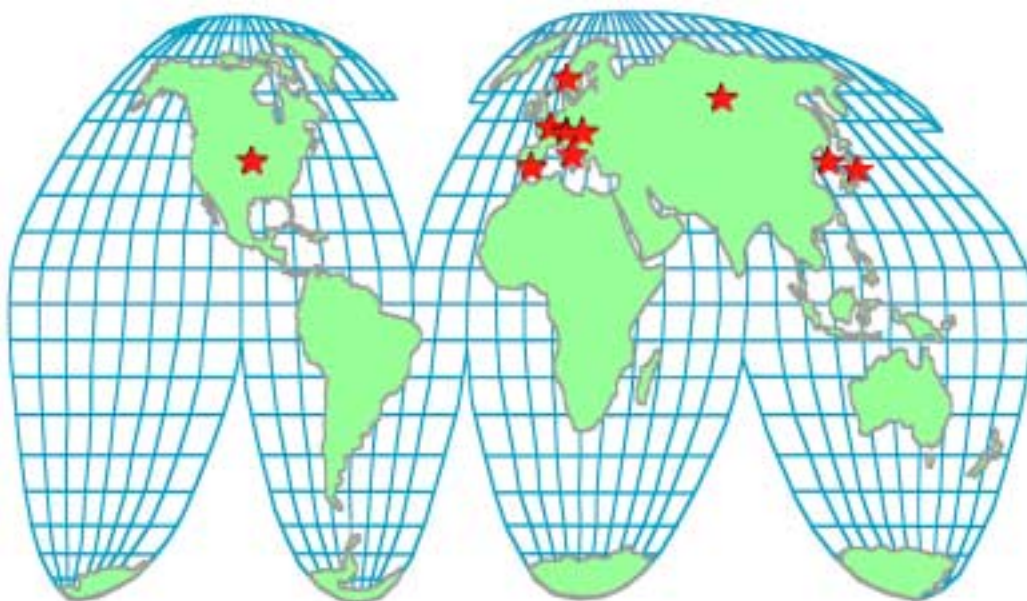
AAA-PDO-GEN-01-0057

31 Oct 2001

AAA Quarterly Report July–Sept 2001

LA-UR-01-6111

***Through the AAA Program, the U.S. Joins International
Efforts to Evaluate the Potential of Partitioning and
Transmutation and Advanced Nuclear Fuel Cycles***



Los Alamos National Laboratory, Argonne National Laboratory
Oak Ridge National Laboratory, Sandia National Laboratories
Brookhaven National Laboratory, Lawrence Livermore National Laboratory
Burns & Roe, Enterprises, Inc., General Atomics, Westinghouse Savannah River Company
University of Nevada, University of Michigan, University of California, University of Texas

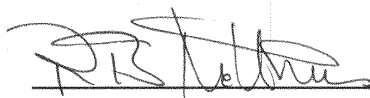
This page left intentionally blank

**AAA Technical Quarterly Report
July–September 2001**

LA-UR-01-6111

AAA-PDO-GEN-01-0057

Approval



Date 11/13/01

R. Bruce Matthews
AAA Program Director
Advanced Accelerator Applications

This page left intentionally blank

Table of Contents

Major Contributors	viii
Acronyms.....	ix
I. INTRODUCTION	1
II. HIGHLIGHTS	3
III. TECHNOLOGY DEVELOPMENT	7
1. Fuels Development.....	7
Scope	7
Highlights	7
Fabrication Development	8
TRU-Oxide Fuel Fabrication.....	8
Metal Fuel Fabrication	8
Nitride Fuel Fabrication	9
Irradiation Testing	10
ATW-1	12
Fuel Design.....	14
Model Description	14
Summary.....	17
2. Separations Technology	20
Scope	20
Highlights	20
UREX Process Demonstration.....	21
Evaluation of the Stability of AHA	21
3. Accelerator Development	22
3.1 Low-Energy Demonstration Accelerator	22
Scope	22
Highlights	22
100-mA Beam Halo Measurements.....	23
Layout of the Quadrupole Magnet FODO Lattice.....	23
Measurements of Beam Halo in the Quadrupole Magnet Lattice	23
Measurement of the Beam Emittance at Halo-Channel Entrance	25
CCDTL Section 2.....	25
Tuning and Installation on the Hot Model Test Stand	26
Initial RF Power Tests on the Hot Model Test Stand	28
Likely Cause of Frequency Detuning.....	28
Retuning	29
RF Retest Results.....	30
Summary of RF Test Results	30
Milestone and DDN Documentation Progress	30

3.2 High-Energy Linac	31
Scope	31
Highlights	31
Spoke Cavity Development	31
Cavity Testing	33
APT SCRF DDN Work	35
Other SCRF Activities	35
4. Transmuter Development	37
Scope	37
Highlights	38
Analysis Support	38
Nuclear Codes and Data	38
Thermal-Hydraulic Codes	39
Natural Circulation with Fluid Decay Heat	39
Modeling of Oxygen as a Trace Species in the ADTF	40
Laboratory Experiments	40
Irradiation Tests	43
Corrosion Experiments	43
Sodium Activation Experiments	44
Hydrogen and Helium Production Experiments	46
Neutron Yield and Spectrum Tests for LBE Targets	47
University Collaboration	48
5. Spallation Target Development	50
Scope	50
Highlights	51
LBE Technology – Materials Test Loop	52
Materials Research	53
PNNL Activities	53
ORNL Activities	54
Materials Handbook Activities	55
Temporary Assignment at PSI	56
LANL Hot-Cell Analyses	56
Air Corrosion DDN	56
IV. ENGINEERING DESIGN & DEVELOPMENT	589
6. APT Engineering Design	59
Scope	59
Highlights	59
Preliminary Design Status	59
Top-Level Documents	60
System Design Descriptions	60
Technical Reports, Calculations, and Models	60
Design Changes	61
Drawings and Specifications	62

7. Accelerator-Driven Test Facility	62
Scope	62
Highlights	63
7.1 Systems Integration	64
Overall Facility Design and Arrangement	64
ADTF Missions, Functions, and Requirements	65
Cost Estimate	65
7.2 ADTF Target and Material Test Station	66
TMT Design	66
Target Design Options	67
Annular Target Geometry Option	68
Conclusion	73
ADTF Subcritical Multiplier - 100 MW (SCM-100) Design	73
Sodium-Cooled Fast-Spectrum SCM Design	74
SCM Neutron Physics Design	76
SCM Target Designs	77
LBE Target Design	77
Solid Tungsten-Target Design	80
Shielding Design	81
Other SCM Design Team Activities	81
Coordination With Other ADTF Activities	81
ADTF EIS Support Activities	82
International Collaboration - DOE/CEA Work Package on ADTF Design	82
7.3 Balance of Facility Design	85
TMT and Hot Cell Building	85
SCM Building	86
U. PROJECT INTEGRATION	87
8. Systems and Technology Integration	87
Scope	87
Highlights	87
Multi-Strata Evaluations	87
Improve long-term public safety	88
Provide benefits to the repository program	88
Reduce proliferation risk from plutonium in commercial spent fuel	88
Improve prospects for nuclear power	88
9. University Programs	91
Scope	91
Highlights	91
Technical Progress	93
10. Collaborations	93
Scope	93
Highlights	94

Major Contributors

Fuels Development:	D. Crawford (ANL) K. Chidester (LANL) M. Meyer (ANL) S. Hayes (ANL) R. Margevicius (LANL) K. McClellan (LANL)
Separations Technology:	J. Laidler (ANL)
Accelerator Development:	R. Sheffield (LANL) V. Smith (LANL) D. Chan (LANL) P. Colestock (LANL) R. Wood (LANL)
Transmuter Development:	K. Pasamehmetoglu (LANL) B. Hill (ANL) M. Chadwick (LANL) J. Spore (LANL) M. Farmer (ANL) S. Wender (LANL)
Spallation Target Development:	K. Pasamehmetoglu (LANL) N. Li (LANL) S. Maloy (LANL)
APT Engineering Design:	C. Rodriguez (BREI/GA) R. Chuebon (BREI/GA) J. Tooker (BREI/GA) A. Baxter (BREI/GA) G. Campbell (BREI/GA) D. McEachern (BREI/GA) B. Boore (WSRC) L. Parme (BREI/GA)
Accelerator-Driven Test Facility:	M. Cappiello (LANL) S. McConnell (LANL) K. Pasamehmetoglu (LANL) J. Roglans (ANL) R. Guffee (LANL) H. Cohen (BREI/GA) J. Herceg (ANL) E. Pitcher (LANL)
Systems & Technology Integration:	G. Van Tuyle (LANL) D. Bennett (LANL)
University Programs:	D. Beller (LANL) A. Hechanova (UNLV)
Collaborations:	G. Van Tuyle (LANL)

Acronyms

AAA	Advanced Accelerator Applications
AC	Accelerating cavities
ADS	Accelerator-Driven System
ADTF	Accelerator-Driven Test Facility
AES	Advanced Energy Systems (formerly Northrup-Grumman Corp.)
AET	Ability Engineering Technology
AHA	Acetohydroxamic acid
AMUSE	Argonne Model for Universal Solvent Extraction, the generic TRUEX model expanded to include UREX and PUREX processing
ANL	Argonne National Laboratory
ANRC	Amarillo National Research Center
ANS	American Nuclear Society
ANSYS	structural analysis modeling code
appm	atomic parts per million
APT	Accelerator Production of Tritium
ASME	American Society of Mechanical Engineers
ATR	Advanced Test Reactor (INEEL)
ATW	Accelerator Transmutation of Waste
BBE	Backbone Beam Enable System
BCCM	Bridge-Coupler Cold Model
BCM	Beam-Current Monitor
BCP	Baseline Change Proposal
BCP	Buffered Chemical Polishing
Beta (β)	Ratio to the speed of light
BNFL	British Nuclear Fuels, Ltd
BNL	Brookhaven National Laboratory
BOF	balance of facility
BOL	beginning of life
BOP	Balance of Plant
BOR-60	Sodium-Cooled Fast Reactor (Dimitrovgrad, Russia)
BPM	Beam-Position Monitor
CCDTL	Coupled-Cavity Drift-Tube Linac
CCL	Coupled-Cavity Linac
CCT	Coupled-Cavity Tuning computer code
CEA	Commissariat à l'Energie Atomique (France)
CEM	Cascade Exciton Model code (Model-based Monte-Carlo particle transport code)
CERCA	Compagnie Pour L'Etude Et La Realisation De Combustibles Atomiques
cercer	ceramic-ceramic
cermet	ceramic-metal
CFD	Computational Fluid Dynamics
CLWR	Commercial Light-Water Reactor
CMR	Chemistry and Metallurgy Research (facility at LANL)
CONCERT	COmbined Neutron Center for European Research and Technology
CTR	Cryogenic Test Rig
cw	continuous wave (100% duty factor)
DACS	Data Acquisition and Control System
DAS	Data Acquisition System
DCR	Design Change Request
DDN	Design Data Need
dpa	displacements per atom
EBR	Experimental Breeder Reactor

ED&D	Engineering Development and Demonstration
EEV	English Electric Valve
EFPD	Effective Full-Power Day
EIS	Electrochemical Impedance Spectroscopy
EIS	Environmental Impact Statement
EOI	end of irradiation
EOL	end of life
EPICS	Experimental Physics and Industrial Control System
ERANOS	Computer modeling code
ERC	External Review Committee
ES&H	Environmental, Safety, and Health
ESS	European Spallation Source
ESSAB	Energy System Acquisition Advisory Board (DOE)
FDD	Facility Design Description
FFTF	Fast Flux Test Facility
FMF	Fuel Manufacturing Facility
FODO	focus-drift-defocus-drift
FWHM	full width half maximum
FZK	Forschungs Zentrum Karlsruhe (German Laboratory)
FZJ	Forschungs Zentrum Jülich (German Laboratory)
fpv	full-power year
HCP	Hazard Control Plan
GSI	Gesellschaft für Schwerionenforschung (Darmstadt, Germany)
GT-MHR	Gas Turbine Modular Helium Reactor
HEBT	High-Energy Beam Transport
HEU	highly enriched uranium
HFR	High Flux Reactor (Petten, Netherlands)
HFIR	high flux isotope reactor (ORNL)
HIP	Hot Isostatic Process (for bonding materials)
HM	heavy metal
HPRF	High-Power Radio Frequency
HS/WS	halo-scraper/wire-scanner (diagnostic device)
HX	heat exchanger
I&C	Instrumentation and Control
IAEA	International Atomic Energy Association (Vienna, Austria)
ICS	Integrated Control System
IFMIF	International Fusion Materials Irradiation Facility
IFR	Integral Fast Reactor
IHX	Intermediate Heat Exchanger
IMS	Information Management System
INEEL	Idaho National Engineering and Environmental Laboratory
IOT	Inductive-Output Tube
IPBT	In-Pile Beam Tube
IPPE	Institute of Physics and Power Engineering, Obninsk, Russia.
ISTC	International Science and Technology Centre (Moscow)
ITER	International Thermonuclear Experimental Reactor
JAERI	Japan Atomic Energy Research Institute
JCNNM	Johnson Controls Northern New Mexico
JLAB	Jefferson Laboratory (VA)
KEK	National Laboratory for High-Energy Physics (Tsukuba, Japan)
LAHET	Los Alamos High-Energy Transport
LANL	Los Alamos National Laboratory
LANSC	Los Alamos Neutron Science Center
LBE	Lead-Bismuth Eutectic
LBHM	Low- β Hot Model
LEBT	Low-Energy Beam Transport

LEDA	Low-Energy Demonstration Accelerator
LINAC	a computer code based on PARMILA that has been modified to include CCDTL and SCRF elliptical cavities as options
LLFP	Long-Lived Fission Product
LLNL	Lawrence Livermore National Laboratory
LLRF	Low-Level Radio Frequency
LMR	Liquid-Metal Reactor
LWR	Light-Water Reactor
MA	minor actinide
mb	millibarn
MCNP	Monte Carlo N-Particle Transport Code
MCNPX	Merged code - Los Alamos High-Energy Transport (LAHET) and Monte Carlo N-Particle Codes (MCNP)
MEGAPIE	MEGAwatt Pilot Experiment
MOX	Mixed oxide fuel
MT	metric ton
MTL	Materials Test Loop
n/p	neutrons per proton
NDA	NonDestructive Analyses
NEA	Nuclear Energy Agency (Paris)
NEPA	National Environmental Protection Agency
NERAC	Nuclear Energy Research Advisory Committee
NERI	Nuclear Energy Research Initiative
NFF	nonfertile fuel
O&M	Operations and Maintenance
OECD	Organization for Economic Cooperation and Development (Paris)
OPO	Operations Project Office
ORIGEN	A computer code system for calculating the buildup, decay, and processing of radioactive materials
ORNL	Oak Ridge National Laboratory
P&ID	Piping and Instrumentation Diagram
PACS	Personnel Access Control System
PARMTEQM	RFQ simulation code
PFD	Process Flow Diagram
PHA	preliminary hazards assessment
PHENIX	Fast Reactor in France
PIE	Post-irradiation examination
PNNL	Pacific Northwest National Laboratory
POP	Proof of performance
PPO	Plant Project Office
PRAD	Proton Radiography
PRISM	Power Reactor Innovative Small Module
PSAR	Preliminary Safety Analysis Report
PSS	Personnel Safety System
PSI	Paul Scherrer Institute (Switzerland)
PUREX	Plutonium-Uranium Extraction
PWR	Pressurized Water Reactor
PYRO	Pyrochemical process
Q	Quality factor
QA	Quality Assurance
QAC	<u>Quick ATW Costing</u>
RAMI	Reliability, Availability, Maintainability, and Inspectability
RERTR	Reduced Enrichment for Research and Test Reactors program
RF	Radio Frequency
RFQ	Radio-Frequency Quadrupole
RCCS	Resonance-Control Cooling System

RIA	Rare Isotope Accelerator
RIAR	Russian Institute of Atomic Reactors
Rms	root mean square
RRR	Residual Resistance Ratio
RTD	surface temperature detector
RTTB	Room Temperature Test Bed
SAR	Safety Analysis Report
SC	Superconducting
SCRF	Superconducting RF
SDD	System Design Description
SEM	Scanning Electron Microscopy
SHR	shutdown heat-removal
SINQ	Spallation Neutron Source at Paul Scherrer Institute (Switzerland)
SNF	Spent nuclear fuel
SNL	Sandia National Laboratory
SRS	Savannah River Site
SRTC	Savannah River Technology Center
Star-CD	Computational fluid dynamics code
STAYSL2	A computer code used to analyze the results of the activation foil measurements in both a proton and neutron flux
STP	standard temperature and pressure
STIP	Spallation Target Irradiation Program (at PSI)
T/p	Tritons (nucleii of tritium atoms) per proton
T/B	Target / Blanket
TBP	tri- <i>n</i> -butyl phosphate or "TriButylPhosphate"
TDO	Technology Development Office
TEM	Transmission Electron Microscopy
TESLA	International Collaboration on a TeV Superconducting Linear Accelerator
TGA	Thermal Gravimetric Analysis
TJNAF	Thomas Jefferson National Accelerator Facility
TMT	Target and Materials Test Station
TRAC	Transient Reactor Analysis Code
TRACE 3-D	Interactive computer code that calculates the envelopes of a bunched beam through a user-defined transport system
TRISPAL	Refers to the French APT Program
TRL	Technical Readiness Level
TRU	transuranics (plutonium, neptunium, americium, and curium)
TSF	Tritium Separation Facility
UFP	University Fellowship Program
UNLV	University of Nevada Las Vegas
UPP	University Participation Program
UREX	Uranium Extraction (an aqueous partitioning process)
URP	University Research Program
USQD	Unreviewed Safety Question Determination
WBS	Work Breakdown Structure
WNR	Weapons Neutron Research (facility at LANL)
WPPT	Working Party on Partitioning and Transmutation
WS/HS	Wire Scanner / Halo Scraper (beam diagnostic device)
WSRC	Westinghouse Savannah River Company
ZPPR	Zero Power Physics Reactor

Advanced Accelerator Applications

Quarterly Report

July–September 2001

I. INTRODUCTION

The Advanced Accelerator Applications (AAA) Program is a Department of Energy program commissioned last year by Congress. Los Alamos leads a national effort consisting of DOE laboratories (Los Alamos, Argonne, Savannah River, Livermore, Oak Ridge), industry (Burns and Roe Engineering Inc, General Atomics) and universities (UC-Berkeley, Texas, Michigan, Nevada). The primary mission of the AAA Program is to develop the technology base for the transmutation of nuclear waste and to demonstrate its practicality and value for long-term waste management.

The AAA Program was constituted by combining two programs: The Accelerator Production of Tritium (APT) Program and the Accelerator Transmutation of Waste (ATW) Program. The APT Program was established in 1995 with a commercial light-water reactor (CLWR) program as part of a dual-path strategy for development of a new tritium-production technology for the nation. From 1995 through 2001, Defense Programs (DOE) invested in the design and development of an accelerator to produce tritium, including a full-scale prototype of the front-end of the accelerator. In December 1998, the Department chose the CLWR as the primary technology for tritium production, assigning APT the role of a backup technology, which affords Defense Programs the opportunity to establish a robust backup technology to assure the nation's capability to produce tritium. The Accelerator Transmutation of Waste (ATW) Program, funded by Congress in FY00, has been investigating the feasibility of accelerator-driven systems to transmute long-lived toxic components of spent nuclear fuel. Together, these two programs benefit by integrating common technologies.

The goal of the AAA Program is to evaluate the effectiveness of transmutation of spent nuclear fuel against the following criteria:

- (1) reduce the long-term radiological impact of waste;
- (2) enable development of a simpler, cheaper repository;
- (3) reduce proliferation risk; and
- (4) improve long-term prospects of nuclear power.

Improving the long-term prospects of nuclear power means not only demonstrating through proof-of-performance the practicality of the transmutation of nuclear waste and its meaningful impact on nuclear materials, waste management, and economics, but also defining and executing activities designed to support the country's nuclear science and engineering infrastructure. In addition to these goals, the AAA Program will continue technology development and demonstration applicable to a backup tritium-production capability, should national security needs dictate.

For the short term, the AAA Program has focused its efforts on (1) evaluating the most effective systems for transmutation of spent nuclear fuel, (2) developing separations technologies to partition long-lived radioactive waste from reusable nuclear material,

(3) developing and testing potential transmutation fuels, (4) developing, constructing, and demonstrating both the low-energy portion and the superconducting RF technology for the high-energy portion of the accelerator, which is required for production of tritium and for testing transmutation fuels, (5) developing a spallation target to provide an effective environment for transmutation, (6) establishing and supporting a national university program to reenergize development and training in nuclear-related fields, and (7) collaborating in international research efforts with nations involved in evaluating nuclear waste management. Through these focused efforts, the AAA Program is defining key experiments, analyses, and facilities needed to demonstrate the technical viability of partitioning and transmutation of long-lived nuclear wastes.

A key future objective of AAA is the construction of an accelerator-driven test facility (ADTF). The goal of the facility would be to demonstrate the transmutation of nuclear waste and to function as a national nuclear science and engineering user facility.

II. HIGHLIGHTS

Fuels Development

- ZrN has been shown through ion irradiation testing to resist amorphization to a fluence of 5×10^{16} Xe/cm². This is the first positive indication that the ZrN may be a good choice as an inert fuel matrix material for actinide-ceramic fuel forms.
- Collaboration between LANL and ANL-E has been initiated to perform ion irradiations at energies higher than achievable at LANL.
- The ATW-1 experiment capsules will be placed in the Advanced Test Reactor (ATR) East Flux Trap positions, which recently became available.
- A simple model was formulated to gauge the feasibility of utilizing plutonium-amercurium nitride dispersions as waste transmutation targets.

Separations Technology

- Pilot-plant demonstration of the UREX process flowsheet was carried out, achieving uranium recovery of 99.999%.
- Direct electro-refining experiments with simulated metal-alloy fuel have shown that the PYRO-B process is preferred over the molten-salt chloride-volatility process. Direct electro-refining is now the reference process for treatment of this transmuter fuel type.

Accelerator Development

- We completed beam-halo measurements with a 100-mA RFQ output beam into the halo channel.
- We completed installation and testing of the CCDTL Section 2 on the hot-model test stand, and a final report is being prepared.
- A contract for fabricating two $\beta=0.175$, 2-gap superconducting spoke cavities was awarded, with delivery of the cavities scheduled for the summer of 2002.
- We completed all APT-related SCRF Design Data Need (DDN) documentation work, including that for the $\beta=0.64$ 5-cell cavities and for the APT power couplers.

Transmuter Development

- Sodium and lead-bismuth eutectic (LBE) compatibility experiments were started. We obtained time-temperature traces, clearly showing exothermic reactions.
- Sodium activation tests were performed in the Blue Room with an 800-MeV proton beam. The data have been analyzed and a final report is being written for the ⁷Be and ²²Na evaluations.

Spallation Target Development

- The readiness review for the Materials Test Loop was completed. The melt tank has been loaded with lead-bismuth eutectic.

- Final reports were released on the tensile data produced at PNNL, the fatigue crack-growth and weld tensile-properties tests performed at ORNL, and the air corrosion Design Data Need.

APT Engineering Design

- The *Preliminary Design Status Report* was released, meeting a Level 1 APT milestone on schedule. Fifteen Level 3 milestones were completed this quarter with the release of system design descriptions (SDDs) for APT systems and structures.

Accelerator-Driven Test Facility

- The ADTF Missions, Functions, and Performance Requirements document was approved and issued.
- A revised ADTF preconceptual cost estimate was prepared to define the direct construction cost of the Target and Material Test (TMT) and Subcritical Multiplier (SCM) stations.
- Calculations were performed, indicating that an annular target geometry for the Target and Material Test station can provide twice the fast flux as achieved with the side geometry.
- The assessment of the four options being considered for the SCM design was completed, and the vertical entry option was selected. A reference design for the lead-bismuth target has been completed for the SCM vertical entry configuration.
- A conceptual design for the structure supporting a high-energy beam transport above the SCM was completed.

Systems & Technology Integration

- The Systems and Technology Integration Team completed the extensive multi-tier evaluations and produced the technical report entitled "Candidate Approaches for an Integrated Nuclear Waste Management Strategy—Scoping Evaluations."

University Programs

- The ten University Fellowship Program Fellows began their academic programs with the start of the Fall Semester at their respective universities. Several have begun their research projects.
- Three students completed summer internships, two at LANL and one at ANL-W.
- Contracts were awarded to the University of Michigan and to the University of California at Berkeley for work in support of reactor design and analysis, systems studies, planning for experiments, and repository performance studies.
- DOE/NE sponsored five students (two fully and three partially) to attend the Glenn T. Seaborg Institute for Transactinium Science (GTS-ITS) Summer School at Lawrence Livermore National Laboratory.

Collaborations

- The report, “Internal Plan for International Technical Cooperation,” summarizing opportunities for international collaborations, was finalized and published with a limited distribution.

This page left intentionally blank

III. TECHNOLOGY DEVELOPMENT

1. Fuels Development

Scope

AAA fuel development activities are directed toward the development and qualification of fuels for safe transmutation of actinides at maximal rates. The objective is to provide one (or more) transmutation fuel form(s) at Technical Readiness Level (TRL) 6 at the time that transmutation technology overall is to begin integral demonstration. Thus far, requirements for such fuels include nonfertile compositions in forms suitable for fast-spectrum transmuters and a homogenous fuel cycle (i.e., all minor actinides would be maintained in the same fuel and processing stream). However, the AAA transmutation program is considering additional transmuter architectures, the use of which would imply different requirements for fuels; therefore, the fuel development program is evolving as the nature of and approach for the overall transmutation mission evolves.

The specific R&D activities include development of techniques to fabricate transmutation fuels from LWR fuel-derived actinide feed and from actinide feed recycled from transmuters. As-fabricated samples are chemically and microstructurally characterized to evaluate the success of fabrication processes and to better understand the nature of the fuel materials. Evaluation of proposed fuel forms requires irradiation testing, so near-term irradiation tests are being planned and will be performed through the course of this program. Finally, the understanding of in-service fuel behavior is best demonstrated through the development and validation of fuel behavior models that are eventually incorporated into fuel performance codes. Such models are being developed, concurrent with an effort to develop thermal models that allow calculation of fuel and cladding temperatures in service and during testing.

Highlights

- Standard cold-press/sinter processing of nitrides for ATW-1 irradiation fuel pellet geometries has been shown to be unsuitable for achieving final ATW-1 fuel densities, and therefore, a sintering aid study has been initiated.
- ZrN has been shown through ion irradiation testing to resist amorphization to a fluence of 5×10^{16} Xe/cm². Phase stability is an important characteristic for a suitable matrix material to withstand high burnup conditions. This is the first positive indication that the ZrN may be a good choice as an inert fuel matrix material for actinide-ceramic fuel forms.
- DyN has been identified as a surrogate for AmN with respect to volatilization. Tests to characterize this material's vaporization behavior have started.
- Collaboration between LANL and ANL-E has been initiated to perform ion irradiations at higher energies than are achievable at LANL.

- The ATW-1 experiment capsules will be placed in the Advanced Test Reactor (ATR) East Flux Trap positions, which recently became available. Design calculations for these new positions, which are larger in diameter, are now in progress.
- The Pu-238 contamination in the ANL Casting Laboratory glovebox was removed sufficiently to allow resumption of activities.
- Development of welding parameters for ATW-1 rodlet closure is underway. A welding qualification plan was approved.
- A simple model was formulated to gauge the feasibility of utilizing plutonium-amerium nitride dispersions as waste transmutation targets. It can be used to gauge the relative effects of particle size, volume loading, temperature, and americium content on stress within the dispersion fuel zone.

Fabrication Development

TRU-Oxide Fuel Fabrication

A key furnace for the production of TRU-oxides has been upgraded and is now operational. Key modifications include new heating elements, a heat exchanger, and an insulation package. These modifications have allowed the furnace to attain a temperature of 1700°C at less than 100% power. This high temperature may be important in the sintering of some of the actinide oxides.

Metal Fuel Fabrication

The Pu-238 decontamination effort in the ANL Casting Laboratory glovebox continued and will be completed in September. This decontamination effort is required to allow access to the glovebox for installation of a bench-scale arc melter, which will be used to prepare samples for the ATW-1 experiment. Preparations were made for preventive maintenance on the glovebox purification system.

Weld development continued for the ATW-1 experiment. Prototypic ATW-1 fuel rodlets were "closure welded" using two different orbital welding systems. Blowout of some weld material from the closure (top) weld occurred during initial testing due to gas expansion in the small fuel plenum space. Changing of the weld process parameters to allow a cooling period prior to completion of the weld mitigated this problem. Metallographic examination was performed on several specimens; the examination showed that complete penetration was not achieved on top closure welds, despite good visual appearance. A modified end-plug was designed, and development of weld parameters continued.

Other efforts included the preparation of a draft weld qualification plan. The weld qualification plan is required by ANL-W welding procedures to ensure that ATR quality assurance requirements for the ATW-1 experiment will be met. Specific welds to be addressed with the plan are the end-plug/closure welds on the ATW-1 rodlets and outer capsules.

Equipment Preparation - Gloveboxes for the Fuel Manufacturing Facility (FMF) equipment installation are being modified in the Engineering Development Laboratory and the ANL-W machine shop. Because personnel resources are not available as originally envisioned, the progress has been slower than planned. In addition, design

reviews and evolutions in design requirements have increased the scope of engineering design work beyond what was originally envisioned. For those reasons the milestone to have the FMF equipment installation complete will likely be delayed about three months.

Nitride Fuel Fabrication

TRU-Nitride Equipment Preparation - Carbothermic reduction of some of the actinide oxides will require the use of a 94%-nitrogen / 6%-hydrogen gas mixture. Currently, this gas is not available in the required furnaces. It has been plumbed and requires a simple gas manifold outside on the plutonium facility dock (a work request has been submitted). The furnaces capable of synthesizing and sintering nitride compounds have been idle for more than two years, so some repair and upgrade are required. A water-flow monitor in the water-coolant supply line to one of the furnaces is being repaired. One of the high-temperature inert furnaces is being leak-checked and seals are being replaced as needed. The vacuum pumping station of another furnace is being repaired.

Cold Press/Sinter Processing of NonTRU-Nitride Pellets - An RF-heated furnace chamber has been designed and built for high-temperature sintering of nitride materials under controlled atmospheres. This furnace permits operation to higher temperatures ($>1700^{\circ}\text{C}$). This furnace has also been designed for thermal cycling for a thermal fatigue study beginning in FY02.



Figure 1. ZrN pellets fired to ~80% theoretical density under ultra high-purity nitrogen atmosphere within a standard ceramic muffle tube using a Zr foil wrapper to prevent oxidation.

ZrN with an L/d (length to diameter ratio) of ~0.5 can typically be cold pressed to a "green density" of 75% of theoretical density, and additional densification can be achieved with sintering above $\sim 1600^{\circ}\text{C}$ for fine mesh powders (sieve size -325). However, with the anticipated L/d ~ 1.5 for fuel pellets for the ATW-1 irradiation, we will not be able to reach the desired final density of 85% without use of a sintering aid to allow significant densification at $\leq 1400^{\circ}\text{C}$. A sintering aid study has been initiated.

Synthesis of DyN Surrogate - DyN has been identified as a surrogate for AmN with respect to volatilization. Since a commercial vendor for DyN has not been found, a study was initiated to examine kinetics of the formation of DyN from Dy metal. Dy metal powder was reacted in a Thermal Gravimetric Analysis (TGA) under N_2 and N_2/H_2 atmospheres. Figure 2 shows an example of a TGA curve showing weight gain with increasing temperature. DyN begins to form at low temperatures but oxidation also occurs due to the undesired presence of small quantities of oxygen. At the beginning of FY02, the system/process will be changed to reduce even trace quantities of oxygen from the process to separate the kinetics of nitriding from those of oxidation.

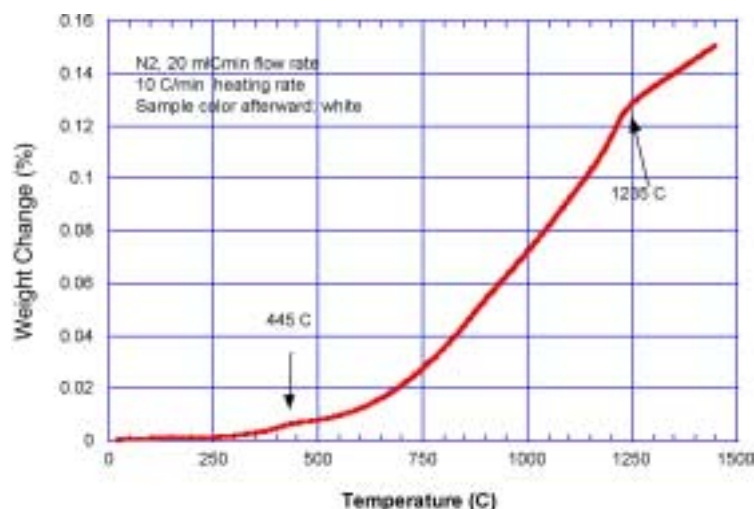


Figure 2. Weight gain with increasing temperature for Dy metal under flowing ultra-high-purity nitrogen. Two transitions can be seen on the curve, indicating change in the reaction kinetics and/or in the nature of the chemical reaction.

Irradiation Testing

Assessment of Radiation Tolerance - Radiation damage studies using heavy ions have shown that ZrN is surprisingly radiation-tolerant and is comparable to some of the most damage-tolerant oxides. ZrN has been shown to resist amorphization to a dose of 5×10^{16} Xe/cm². An example of microstructure of irradiated and nonirradiated ZrN is shown in Fig. 3. Most of the nonirradiated substrate microstructure (bottom of micrograph) is too thick for observation by transmission electron microscopy (TEM). Some of the ZrN grains in the electron transparent region (upper part of micrograph) are oriented for Bragg diffraction and dark mottled contrast features are apparent. These features arise from the strain associated with radiation-induced defects. Twins are also visible in the irradiation-induced microstructure (twins do not exist in the nonirradiated ZrN microstructure). Small voids or bubbles are also often found (not visible here), due possibly to the aggregation of Xe atoms (the peak Xe concentration in the irradiated region corresponds to several atomic percent, due to the implantation of about 50 monolayers of Xe).

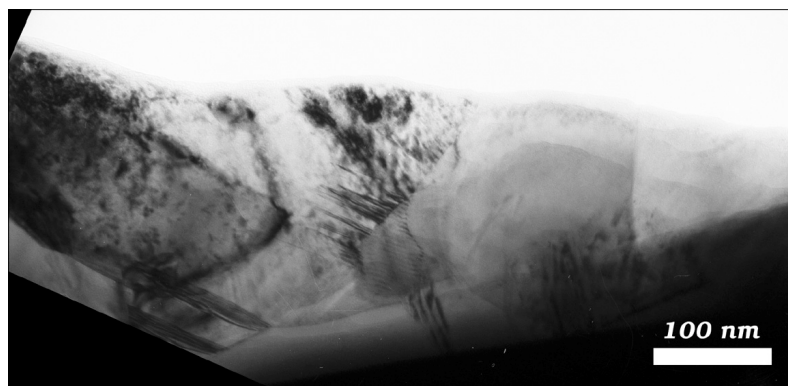


Figure 3. Bright-field transmission electron micrograph showing the microstructure of ZrN following 300 keV Xe⁺⁺ ion irradiation to a fluence of 5×10^{16} Xe/cm² at 100 K. Xe ions entered the ZrN material from the top of this cross-sectional TEM image.

The irradiated microstructure appears to extend far beyond the range of the 300 keV Xe ions used in this radiation-damage experiment. Damage features have been observed extending to a depth of about 300 nm in the material, though the range of the Xe ions was only about 55 nm (20 nm longitudinal straggling).¹ This is attributed to the migration of radiation-induced defects (presumably interstitials) into the substrate during irradiation. This effect is probably enhanced due to large surface stresses that accompany the accumulation of Xe atoms in the near-surface region. This effect has been observed previously in Xe ion irradiations of cubic-stabilized zirconia.² Also, some micro-twins in the ZrN microstructure appear at depths well below the range of the implanted Xe ions. A similar effect to this has been observed in the radiation damage microstructure of rutile (TiO₂) following 360 keV Xe⁺⁺ ion irradiation.³ In this case, planar defects protruding to depths of about 300 nm were observed, though the Xe range was only about 100 nm. Again, these extended defects may nucleate to relieve some of the high stresses that arise in the irradiated region of the substrate.

Collaboration with Argonne National Laboratory (ANL-E) was also initiated to perform high-energy ion irradiations of nitride compounds. The principal investigator at ANL-E is in the Materials Science Division.

Thin film samples of ZrN on Zr metal were ion irradiated to produce a ZrN sample in which the ion beam-induced damage is distributed over a large depth within the target. Previous ion irradiation experiments on ZrN performed at LANL had produced damage layers with very limited ion range (a few hundred angstroms as noted above). The ZrN was irradiated with 3 MeV Kr⁺ ions at ambient temperature to a fluence of 2×10^{16} Kr/cm².

Based on Monte Carlo ion-solid interaction simulations, the following irradiation damage conditions were achieved:

- Depth of peak concentration of implanted Kr⁺ ions: 750 nm
- Longitudinal FWHM of implanted Kr⁺ ion distribution: 170 nm
- Displacement damage profile (dpa=displacements per atom):
 - Peak damage on Zr sublattice = 36 dpa
 - Peak damage on N sublattice = 24 dpa
 - Damage on Zr sublattice at sample surface = 12 dpa
 - Damage on N sublattice at sample surface = 10 dpa
 - Damage on Zr sublattice at approx. center of damage profile = 24 dpa
 - Damage on N sublattice at approx. center of damage profile = 16 dpa

The microstructural damage in these samples will be characterized at the beginning of FY02.

¹ Calculations based on the Monte Carlo simulation code TRIM by Ziegler et al. in J. F. Ziegler, J. P. Biersack and U. Littmark, *The Stopping and Range of Ions in Solids* (Pergamon Press, New York, 1985).

² Yu, N., K.E. Sickafus, P. Kodali and M. Nastasi, "In Situ Observation of Defect Growth Beyond the Irradiated Region in Yttria-Stabilized Zirconia Induced by 400 keV Xenon Ion-Beam at -90 and 30°C," *J. Nucl. Material.* **244** (1997) 266-272.

³ Li, F., M. Ishimaru, P. Lu, I.V. Afanasyev-Charkin, and K. Sickafus, "Damage Evolution in Xe-Ion Irradiated Rutile (TiO₂) Single Crystals," *Nucl. Instr. Meth. B* **166-167** (2000) 314-321.

ATW-1

The design of the ATW-1 fuels irradiation experiment was revised substantially early this quarter due to evolving options and emphases within the program, namely, the serious consideration of a dual-strata approach to actinide transmutation and destruction. The proposed fuels test matrix for ATW-1 has been adjusted in order to provide timely performance data on an array of transmutation fuel compositions that attempt to cover the spectrum conceivable at this point in time. As has been anticipated for some time, the ATW-1 experiment has evolved into a series of experiments designed to survey candidate fuel types as well as actinide composition ranges. The Conceptual Design Description for the first four ATW-1 irradiation vehicles, designated ATW-1A, ATW-1B, ATW-1C and ATW-1D, has been completed in fulfillment of the relevant deliverable contained within the FY01 work package. This document will be issued separately under the title of "Experiment Description for ATW-1A, ATW-1B, ATW-1C and ATW-1D."

Interaction with the Advanced Test Reactor (ATR) Experiment Group continued following the submission of the Experiment Description for ATW-1A, -1B, -1C and -1D. Calculations were begun to reevaluate the experiment powers and to appropriately size the hafnium shrouds based on the finalized test matrix. The seven capsule drop-in positions presently configured in the East Flux Trap of the ATR have unexpectedly become available to the program. They offer the advantage of a large number of positions that are larger in diameter than the previously considered outboard A-holes. It was determined that the ATW-1 series of experiments would utilize these East Flux Trap positions.

Each of the four irradiation vehicles contains six fueled rodlets. The rodlet test matrix is shown in Table 1, and a summary of the experiment schedule is shown in Table 2. These first four irradiation experiments will focus on the nitride and metallic fuel candidates. Experimental vehicles are also planned containing oxide and dispersion fuel candidates, to be delivered to the ATR for irradiation early in the fiscal year 2003. Figure 4 shows the rodlet design for the nitride fuels. The metallic fuel design is identical except for a reduction in the fuel column height from 2.0 inches to 1.5 inches to reduce the fuel volume and increase the plenum volume; this is in anticipation of higher fission gas release rates from the actinide metallic fuels.

Table 1. ATW-1A, -1B, -1C, and -1D Fuel Test Matrix

Rodlet	Fuel Test Matrix	
	ATW-1A & -1C*	ATW-1B & -1D†
1	(Pu _{0.2} ,Am _{0.8})N-X·ZrN	Pu-12Am-40Zr
2	(Pu _{0.8} ,Am _{0.2})N-X·ZrN	Pu-10Am-10Np-40Zr
3	(Pu _{0.5} ,Np _{0.5})N-X·ZrN	Pu-40Zr
4	PuN-X·ZrN	Pu-12Am-40Zr
5	(Pu _{0.50} ,Am _{0.25} ,Np _{0.25})N-X·ZrN	Pu-30Np-40Zr
6	(Pu _{0.5} ,Am _{0.5})N-X·ZrN	Pu-60Zr

*X denotes weight fraction of inert ZrN diluent.

†Alloy composition expressed in weight percent.

Table 2. Overview of the ATW-1A, -1B, -1C, and -1D Experiments

ATR Experiment Designation	Fuel Form	ATR Insertion	Target Discharge Burnup*
ATW-1A	Nitride	Sept-2002	5-7%
ATW-1B	Metallic	Sept-2002	5-7%
ATW-1C	Nitride	Sept-2002	~20%
ATW-1D	Metallic	Sept-2002	~20%

*Burnup in percent of initial heavy metal.

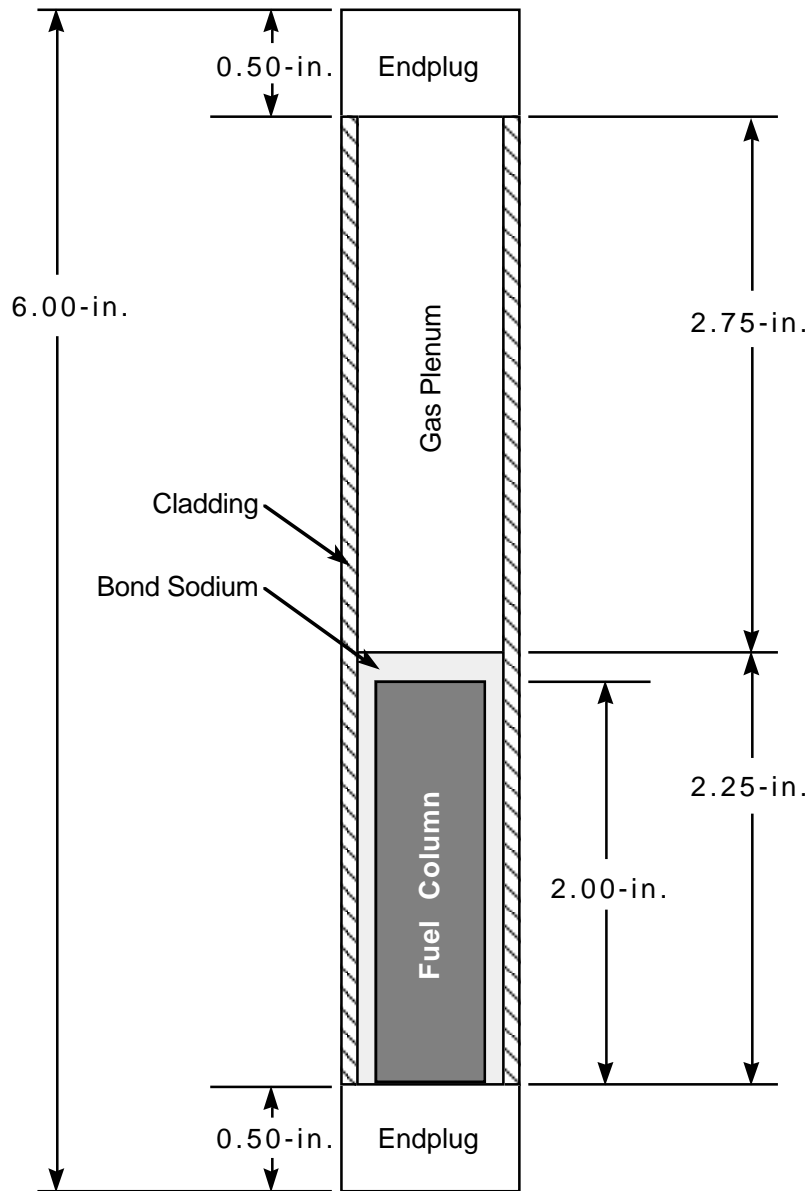
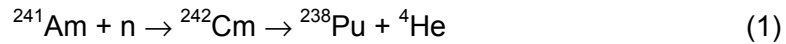


Figure 4. Nitride-fueled rodlet design for ATW-1A and -1C.

Fuel Design

Dispersion fuels have been shown to be capable of very high burnup—in certain cases, far exceeding the ATW goal burnup of 30%. Properly fabricated UO_2 dispersions in stainless steel have been shown to be capable of ^{235}U burnup >70% at 93% enrichment. This experience is not directly applicable to an americium-bearing fuel, however, because of additional stress exerted on the matrix by helium gas production. Neutron capture by ^{241}Am and subsequent decay of the ^{242}Cm capture product leads to production of helium gas as shown in Eqn. 1:



This helium generation adds to the total gas inventory, which can become significantly higher than that due to fission.

Dispersion fuels are heterogeneous mixtures of fuel particles dispersed in a matrix material that provides mechanical restraint and an efficient path for heat conduction away from the fuel.⁴ An ideal dispersion consists of spherical particles uniformly distributed throughout a chemically and neutronically inert matrix material. In order to minimize the damage done to the matrix by fission fragment recoil from the fuel particles and retain matrix strength, fuel particles should be large compared to the fission-fragment range in the matrix, and the fuel particle volume fraction should be low enough to ensure that damage zones do not overlap.⁵ A simple model was formulated to gauge the feasibility of utilizing plutonium-ameridium nitride dispersions as waste transmutation targets. This simple model does not predict failure, but can be used to gauge the relative effects of particle size, volume loading, temperature, and americium content on stress within the dispersion fuel zone. The impact of other sources for gas production, such as Cm, is not considered.

Model Description

The fuel dispersion was modeled as a single spherical fuel particle surrounded by a thick-walled pressure vessel of matrix material. Gas pressure in the sphere generates a stress in the sphere wall, which can be compared as a function of particle size, americium content in the fuel, and particle volume loading. This simple model does not account for particle-particle interaction, chemical compatibility of the fuel and cladding, or stress introduced by gas-driven or solid fission product swelling of the fuel particles. The thickness of the wall surrounding the particle is a function of the particle size and the volume fraction of the fuel and is given by Eqn. 2:

$$t = \frac{D}{2} \left[\frac{1}{\left(V_f \right)^{\frac{1}{3}}} - 1 \right] \quad (2)$$

⁴ Weber, C.E. and Hirsch, H.H., "Dispersion-Type Fuel Elements," *International Conference on the Peaceful Uses of Atomic Energy*, Geneva, Switzerland, P/561 (1955).

⁵ Weber, C.E., "Progress on Dispersion Elements," *Progress in Nuclear Energy Series V: Metallurgy and Fuels*, 2 295-362 (1959).

where D is the diameter of the particle and V_f is the volume fraction of the fuel particle.⁶ The thickness of the undamaged matrix material surrounding the particle is calculated as

$$t_u = t - \lambda \quad (3)$$

where λ is the fission fragment range, taken as a constant for a particular matrix material. Using this model, any matrix material within the fission fragment range is assumed to be degraded and makes no contribution to pressure vessel strength.

Fission gas yield was estimated based on ORIGEN calculations performed at ANL; the results are shown in Table 3. The percent release of fission gas is calculated by a best-fit correlation equation from uranium-nitride (UN) fuel data:

$$R = 100 / [\exp(0.0025 \{90TD^{0.77}/B^{0.09} - T\}) + 1] \quad (4)$$

where TD is the fraction of theoretical density, B is the burnup fraction, and T is the absolute temperature.⁷

Helium gas yield was also estimated using ORIGEN output and is also shown in Table 3. The helium release rate from the fuel particles was taken as five times the fission gas release (5 x Eqn. 4) for this initial investigation. The 5:1 ratio is a conservative value based on results of the EFFTRA-T4 test, which reached 28% actinide burnup (97% transmutation), given in Table 4.

Table 3. Parameters and Results of Gas Generation Calculations

Fuel Composition	Pu-40Zr	Pu-6Am-40Zr	Pu-20Am-40Zr	Am-20Pu-40Zr
Fission gas yield	0.246	0.235	0.207	0.141
Helium generation (ml He/g ²⁴¹ Am)	0.0	47.2	46.8	46.6

Table 4. Gas Inventories and Release at End of Life in EFFTRA-T4.⁸

Gas species	Inventory, moles	Release, moles	%Release
He	1.37E-03	2.66E-04	19.4
Kr	8.92E-06	1.07E-06	11.9 ^a
Xe	2.20E-04	1.08E-05	4.9
He:fission gas ratio	6.0	22.3	4.0 ^a

a) The authors Weber and Hirsch (Footnote 4) consider this value suspect, since the measured quantity of Kr was near the detection limits of the apparatus. He:FG release ratio is thus based on ratio of He:Xe.

Released fission gas and helium are assumed to expand into pores within the fuel particle, which generates pressure inside of the hollow sphere of matrix material. The pressure is calculated using the ideal gas law, where the expansion volume is taken to be the free space inside the spherical shell due to fuel particle open porosity.

⁶ Holden, A.N., *Dispersion Fuel Elements*, Gordon and Breach Science Publishers (1967).

⁷ Storms, E.K., "An Equation which Describes Fission Gas Release from UN Reactor Fuel," *Journal of Nuclear Materials* **158** 119-129 (1988).

⁸ Konings, R.J.M. et al., "The EFFTRA-T4 Experiment on Americium Transmutation," *Journal of Nuclear Materials*. 282 (2000) 159-170.

The stresses at a distance, R , from the center of a thick-walled pressure vessel in spherical co-ordinates are given by:

$$\sigma_R = \frac{p_i a^3 (b^3 - R^3)}{R^3 (a^3 - b^3)} \quad (5)$$

$$\sigma_\theta = \sigma_\phi = \frac{p_i a^3 (2R^3 + b^3)}{2R^3 (b^3 - a^3)} \quad (6)$$

where p_i is the internal gas pressure, a is the inner radius of the matrix shell, b is the outer radius of the matrix shell, and R is the radial distance within the shell.⁹ Substituting, we get

$$a = \frac{D}{2} + \lambda \quad (7)$$

and

$$b = \frac{D}{2(V_f)^{\frac{1}{3}}} \quad (8)$$

where λ is the fission fragment range and V_f is the fuel volume fraction, which yields

$$\sigma_R = \frac{p_i \left(\frac{D}{2} + \lambda \right)^3 \left[\frac{D^3}{8V_f} - R^3 \right]}{R^3 \left[\left(\frac{D}{2} + \lambda \right)^3 - \frac{D^3}{8V_f} \right]} \quad (9)$$

and

$$\sigma_\theta = \sigma_\phi = \frac{p_i \left(\frac{D}{2} + \lambda \right)^3 \left[2R^3 + \frac{D^3}{8V_f} \right]}{2R^3 \left[\frac{D^3}{8V_f} - \left(\frac{D}{2} + \lambda \right)^3 \right]} \quad (10)$$

for the radial and tangential stresses. The stresses are dependent on the location within the shell matrix and reach a maximum at the inner shell radius and then decrease to a minimum at the outer shell radius.

The distortional energy density (von Mises) criterion is used as a relative indicator of the effects of particle size, volume loading, americium content, and temperature on the matrix. The distortional energy density criterion is given by Eqn. 11:

⁹ Timoshenko, S.P. and J.N. Goodier, *Theory of Elasticity*, McGraw-Hill, Inc. (1970).

$$Y = \frac{1}{\sqrt{2}} \left[(\sigma_\theta - \sigma_R)^2 + (\sigma_\theta - \sigma_\phi)^2 + (\sigma_R - \sigma_\phi)^2 \right]^{1/2} \quad (11)$$

which reduces to

$$Y = \sigma_\theta - \sigma_R \quad (12)$$

in this case, since $\sigma_\theta = \sigma_\phi$ in the spherical geometry. This is the same approach used by Weir in an earlier model.¹⁰ Other dispersion fuel models have used creep failure, recoil damage zone overlap, and full plasticity of pressure vessel walls due to fission gas release, as failure criteria.

Summary

All comparisons made here are at a point in the shell wall a distance of 0.75 times the wall thickness from the fuel particle surface, and at the target transmuter burnup level of 30% heavy metal (HM). Fuel particle composition is assumed to be 0.6(Pu,Am)N-0.4ZrN. The reference fuel particle volume loading is 25%, and fuel particle density is held constant at 85% of theoretical. Helium-to-fission-gas release rate is held constant at 5:1, unless otherwise noted.

The effect of particle size at 500°C on the magnitude of the stress criterion (Eqn. 12) is shown in Fig. 5, which shows that doubling the particle size from 50–100 μ results in a 44% reduction in effective stress at a fuel particle volume loading of 25 vol.%. Further increasing particle size to 200 microns reduces the stress to a level 57% lower than the 50- μ case. These results are consistent with the fact that particle size and shape control are effective means of increasing dispersion fuel service life.

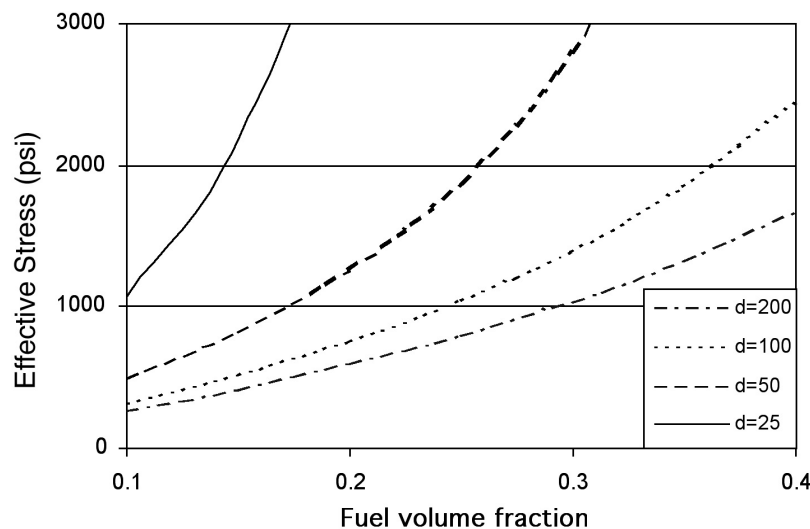


Figure 5. Effective stress (psi) at 30% HM burnup as a function of fuel particle volume fraction for particle diameters (d) ranging from 25–200 μ m (10 wt.% AmN, 500°C).

¹⁰ Weir, J.R., *A Failure Analysis for the Low-Temperature Performance of Dispersion Fuel Elements*, ORNL-2902 (1960).

Figure 6 shows the effect of AmN content on effective stress for a 25 vol.% dispersion at 500°C (773 K) for spherical particle sizes ranging from 50–400 μ . The inflection in the curves is due to discontinuous data on helium generation (Table 3). The reference (single strata) 840 MWt sodium-cooled core would reach equilibrium at about 6.8 wt.% ^{241}Am . A dual-strata transmutation system would use feed with much higher Am contents. Figure 6 illustrates the effect of Am content on effective stress. For a typical 100- μ particle size at 25 vol.% loading, stress increases by a factor of 2.2 when AmN content is increased from 10 to 30 wt.%. Stress increases more rapidly for smaller particle sizes due to the larger ratio of damaged to undamaged matrix. Temperature effects (Fig. 7) are also quite substantial in this model scenario due to the dual effects of increased fission gas and helium release with temperature (Eqn. 12) and increased ideal gas pressure. Increasing the temperature from a nominal 500°C (773 K) to 727°C (1000 K) results in a stress increase of 222%.

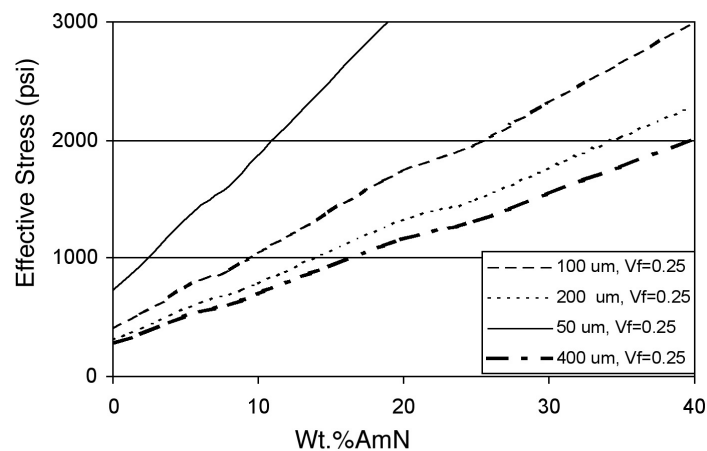


Figure 6. Effective stress as a function of AmN content for xAmN 0.6-xPuN, 0.4ZrN for fuel particle sizes ranging from 50–100 μm (volume loading 25%, 500°C).

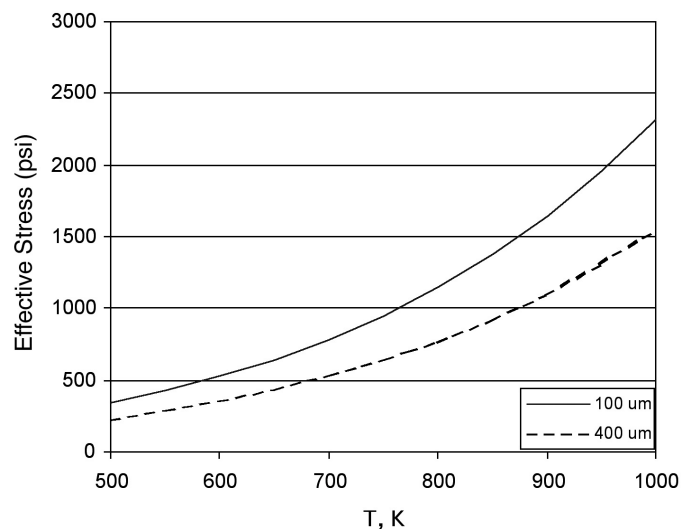


Figure 7. Effective stress as a function of temperature for a 25 vol.% loading of 10AmN-50PuN-40ZrN.

Since there are no data for helium release rates in minor actinide (MA) nitrides, the assumption of five times the release rate was made based on EFTTRA-T4 oxide data. Helium release rates play a major role in determining the matrix stress in this model. Figure 8 illustrates the stresses generated for release rates from 1–20 times the fission gas release rates for americium nitride contents of 10%, 20%, and 40%. As is intuitively obvious, the release rate becomes a major issue at high americium content. At low americium content, control of particle size is adequate to maintain reasonable stress values, even at high release rates. At high americium content, however, an increase in particle size and a reduction in particle volume fraction are required to maintain reasonable stresses at high release rates. This may be an important consideration for accidents if helium release rates are found to exhibit high sensitivity to temperature.

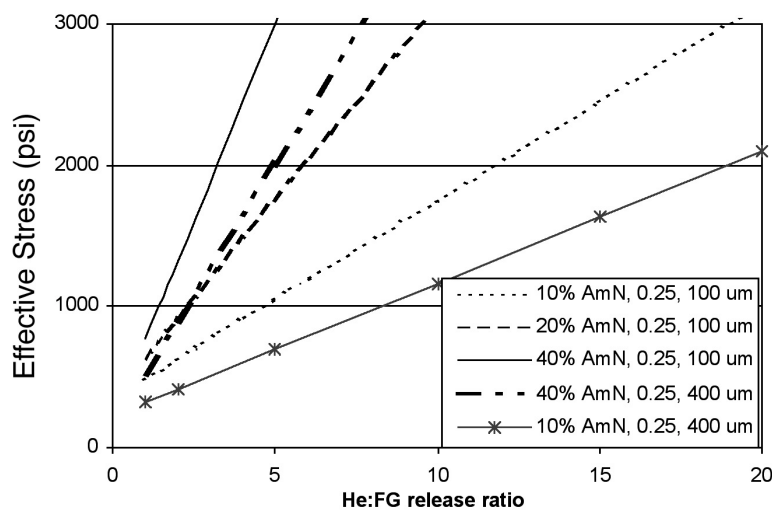


Figure 8. Effective stress as a function of He:FG release ratio for particle sizes of 100 μm and 400 μm and AmN contents of 10%, 20%, and 40% in $x\text{AmN} (0.6-x)\text{PuN} 0.4\text{ZrN}$.

Some fuel performance data are available on dispersions of UO_2 in stainless steel. If one assumes that the assumptions made here about the mechanism for generating matrix stress are reasonable, this data can be used to generate an order of magnitude estimate of the stresses required to cause failure. Of particular interest is a data set consisting of 62 dispersion fuel plates produced during development of SS-347 matrix fuel for the SM-1 and SM-2 military reactors.¹¹ The onset of matrix cracking was found to occur at approximately 74 at.% HEU burnup (2.8×10^{27} fissions/ m^3) for 23 vol.% dispersions at 538°C. Using the methodology described above, the effective stress in the matrix for this fuel is calculated to be 14.5 Mpa (2100 psi). Note that Eqn. 12 was used to calculate fission gas release in the absence of high-burnup low-temperature data for UO_2 . Comparing this value to those shown in Figs. 5-8 indicates that for helium release rates similar to those measured in the EFTTRA-T4 test, fuels with high americium content, operated at moderate temperatures, with fuel volume loadings in the range of 25%, and with particle size on the order of 400 μm , the matrix stress calculated by this model at 30% burnup is similar to values calculated for high burnup UO_2 dispersions.

¹¹ Schaffer, L. D., "Army Reactors Program Annual Progress Report," ORNL-3386 (1962).

2. Separations Technology

Scope

The AAA Separations Technology activity consists of three tasks addressing the various stages in the process of partitioning irradiated fuels for subsequent fissioning of transuranic elements and transmutation of long-lived fission products.

- **Light-Water Reactor Spent Fuel Treatment** – This task involves the development and demonstration of efficient and economic means for the separation of uranium, transuranic elements, specific long-lived fission products, and other fission products from LWR spent fuel. An aqueous partitioning process (UREX) is envisioned for the initial treatment of LWR fuel, involving the extraction of uranium for disposal as a low-level waste. This will be followed by a pyrochemical process (PYRO-A) to separate the transuranic elements from fission products.
- **Transmuter Blanket Fuel Treatment** – Nonfertile blanket fuel that has been irradiated in the AAA transmuter to fission transuranic elements must be processed to recover and recycle the unburned transuranics and to extract newly generated long-lived fission products for transmutation. This task accomplishes the development and demonstration of the means for processing that blanket fuel. A pyrochemical process (PYRO-B) is planned for the separation of unburned transuranics and long-lived fission products. Such processes are favored because the reagents are stable under high radiation fields and because the processes are normally operated at elevated temperatures with the use of molten salts, and can thus accommodate high levels of decay heat.
- **Waste Form Production** – One of the overarching criteria for AAA separations technology development is the minimization of high-level waste generation. Design of the LWR fuel treatment process has been oriented toward the elimination of liquid high-level waste streams, and the pyrochemical processes are similarly being designed to minimize high-level waste volumes. This task involves the development and qualification of durable high-level waste forms to accommodate the two principal waste streams (salt and metal) that emanate from the separations process, as well as the waste form for the disposal of the pure uranium extracted from spent LWR fuel.

Highlights

- **Demonstration of UREX Process** – Demonstration of the Pilot-Plant UREX process was carried out with a prepared dissolver solution, using 2-cm centrifugal contactors operating in countercurrent mode. The UREX flowsheet was established by optimizing the solution concentrations and number of stages per section with the AMUSE code. A uranium recovery of 99.999% was achieved. Plutonium recovery, however, was only 99.7%; this is attributed to the use of fewer extraction stages than necessary. Improvements to the AMUSE code for optimizing the UREX flowsheet are required.

- **PYRO-B Process Development** – Direct electro-refining experiments with simulated metal alloy fuel have shown that this method is preferred over the molten-salt chloride-volatility process. Direct electro-refining is now the reference process for treatment of this transmuter fuel type.

UREX Process Demonstration

A pilot-scale countercurrent demonstration of the UREX process flowsheet was successfully completed using two banks of 2-cm centrifugal contactors. The UREX flowsheet was established by optimizing the solution concentrations and number of stages per section with the AMUSE code. Uranium performance was close to AMUSE code predictions, with 99.999% of the uranium being extracted and recovered in the uranium strip product. Neptunium performance was also as expected, with all of the neptunium being complexed by the AHA in the extraction/scrub sections and exiting in the raffinate stream. The behavior of both plutonium and technetium deviated from code predictions; the plutonium complexes with acetohydroxamic acid (AHA) appear to be weaker than predicted. This resulted in a significant fraction (0.29%) of the plutonium being extracted into the organic phase and subsequently recovered in the technetium and uranium product streams. Technetium did not extract as well as expected, with about 5% exiting in the raffinate stream. This demonstration, although successful in showing that the UREX process is capable of achieving AAA process goals, shows that additional work is needed to improve the AMUSE model predictions. Additional work is needed to improve the AHA-Pu speciation model and the Tc extraction model. In the current model, the complexation constant for Pu(IV)-AHA was estimated to be three times as large as that for Np(IV)-AHA; clearly, measured values are needed.

Evaluation of the Stability of AHA

Progress has been made in understanding the stability of AHA in nitric acid. The effect of temperature on the stability of AHA under process-relevant conditions was established by experiment. The fairly strong temperature effect noted will be an important consideration in the design of the extraction process. Scoping studies to establish the key aqueous interactions between AHA and neptunium species were also completed. It was found that Np(V) and Np(IV) are the two most important neptunium oxidation states in the nitric acid-AHA system and will likely coexist under process-relevant conditions. Np(VI), which is rapidly reduced in the presence of AHA, does not appear to be an important species in this system. The speciation of neptunium in the presence of AHA under acidic conditions was determined, showing that NpO_2^+ is not complexed by AHA under a wide range of AHA concentrations. Np(IV) forms at least three complexes with AHA over a wide pH range, but only one species predominates at the lower pH values used in the UREX process.

3. Accelerator Development

3.1 Low-Energy Demonstration Accelerator

Scope

Construction and operation of the Low-Energy Demonstration Accelerator (ED&D) is confirming the design and demonstrating the viability (at full power) of the technically challenging initial stages of the accelerator. It is providing the first opportunity to look for possible beam halo at low energies (<8 MeV), the development of a commissioning and operating plan for a continuous mode (cw) system, and the opportunity to prototype the entire low-energy accelerator.

The LEDA beam activities are being conducted in three distinct stages (listed below). LEDA operates predominantly in cw, but short periods of pulsed operation are used during commissioning to permit use of interceptive diagnostics.

- **Stage I** – Install and test a 75-keV, 110-mA proton injector (completed).
- **Stage II** – Add a 350-MHz radio-frequency quadrupole (RFQ) accelerator to accelerate a 100-mA proton beam to 6.7 MeV (completed). Measure the formation and development of beam halo in a magnet lattice after the RFQ, including detailed beam profiles at multiple points along the transport line, perform analysis and compare with profiles predicted by the beam-simulation codes, using the results to make corrections (if needed) to beam codes (near completion).
- **Stage III** – Add a 700-MHz coupled-cavity drift-tube linac (CCDTL) section to accelerate 6.7-MeV beam to ~ 8 MeV to confirm beam matching from the 350-MHz RFQ into the 700-MHz CCDTL. Complete CCDTL structure fabrication, assembly, and tuning.

Highlights

- **Beam-Halo Experiment** – We matched a 100-mA RFQ output beam to the halo channel and intentionally introduced breathing-mode and quadrupole-mode mismatches into this beam. We completed measurements of the effects of those mismatches with the wire-scanner halo-scraper (WS/HS) devices located at the center and at the end of the quadrupole magnet lattice.
- **CCDTL Section 2 RF Tests** – We completed installation and testing of the CCDTL Section 2 on the hot-model test stand. Despite design changes, rapid temperature transients still caused monotonic decreases in the resonant frequency in this structure. Although we are not certain of the exact cause of these frequency shifts, indications are that they result from the copper near the ends of the coupling slots undergoing plastic deformation during thermal transients. Testing was completed, and a final report is being prepared.

100-mA Beam Halo Measurements

Layout of the Quadrupole Magnet FODO Lattice

A schematic of the beam-halo channel is shown in Fig. 9. This 11-m-long FODO lattice consists of 52 quadrupole singlet magnets and several beam diagnostics devices. The wire-scanner halo-scraper (WS/HS) devices have one wire scanner and two halo scrapers per unit. The central profile of the beam is measured with the wire (wire scan), and the profile in the periphery of the beam is obtained by using the halo scrapers, one on each side of the beam. The wire scanner data and the halo scraper data are acquired with overlapping position intervals and then joined to form one data file, giving about five orders of magnitude peak-signal-to-noise ratio for the beam-profile measurements. The beam current and transmission through the halo channel is measured with the A/C current toroids. The steering magnets are used to center the beam in the halo channel—the location of the beam being determined with the beam position monitors (BPMs). Beam loss is detected with the photo-multiplier-tube-based beam-loss monitors (BLMs).

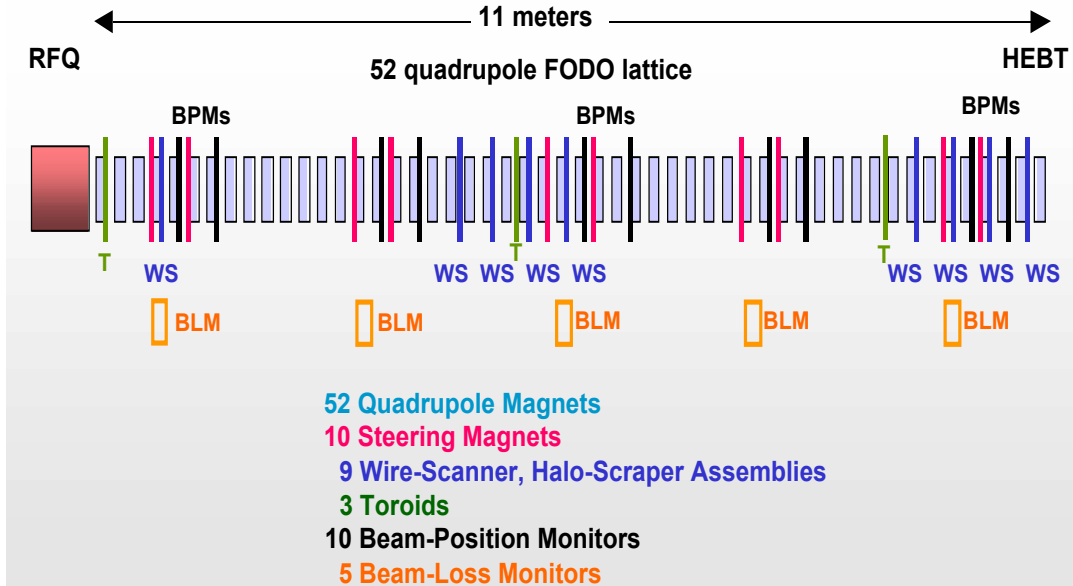


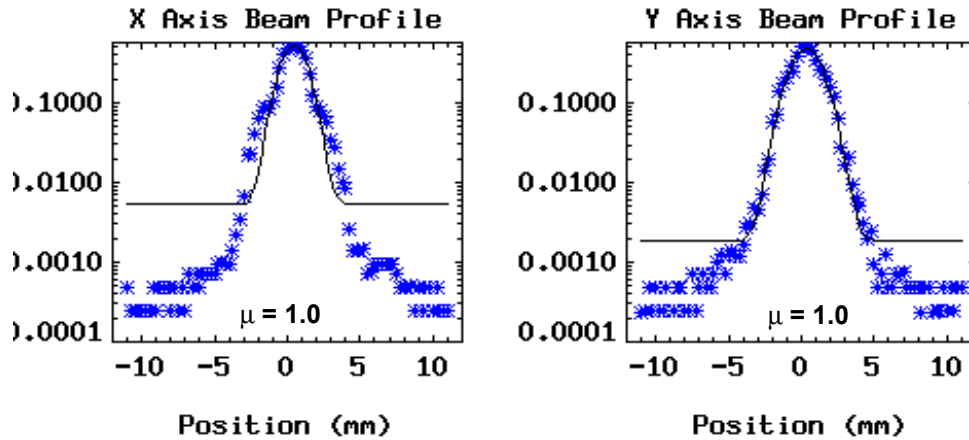
Figure 9. Schematic of the beam-halo channel, including the location of the diagnostic devices. The 6.7-MeV RFQ output H^+ beam enters from the left and exits to the right.

Measurements of Beam Halo in the Quadrupole Magnet Lattice

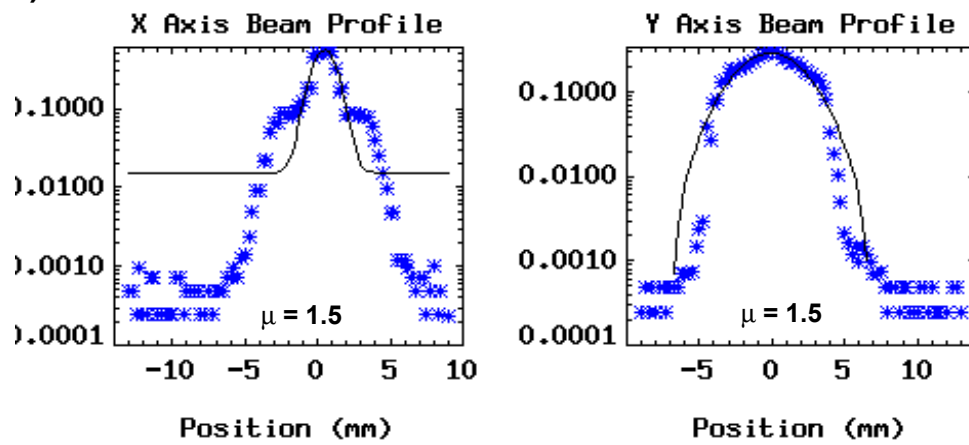
At each current level, the WS/HS devices are used to measure the profiles of the beam as injected into the magnet lattice with the initial matching quadrupole settings (first 4 quadrupoles), determined from beam simulations. Based on these measurements, the matching quadrupoles are then adjusted to obtain a better match. Typically, after two iterations, the beam size is uniform, about $1.1 \text{ mm} \pm 0.05 \text{ mm}$, as measured with each wire scanner in the two blocks of four HS/WS assemblies. The results for 16-, 50-, and 75-mA beams were given in the previous quarterly report (April-June 2001). This quarter, we made breathing-mode and quadrupole-mode mismatch scans for 100-mA beams, and the data are currently being analyzed. A series of wire scan measurements, taken at position midway down the halo channel, is shown in Fig. 10. As in the 16-mA, 50-mA, and 75-mA data, the shoulders in the

periphery of the beam grow as the mismatch of the beam to the halo channel is increased from the matched condition ($\mu=1.0$) to higher values. Analysis of this data is still in progress.

a)



b)



c)

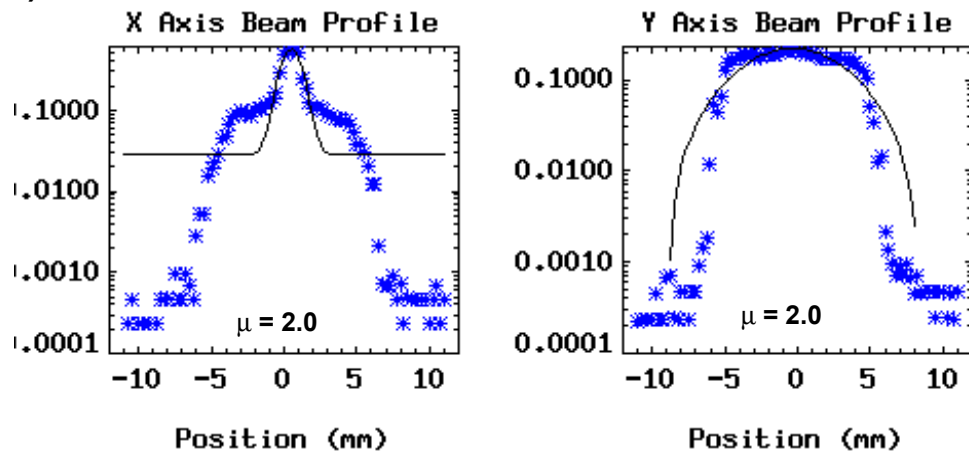


Figure 10. X and Y beam profiles at halo channel mid-point location 20 for breathing-mode mismatches of (a) $\mu=1.0$ (matched), (b) $\mu=1.5$, and (c) $\mu=2.0$.

Measurement of the Beam Emittance at Halo-Channel Entrance

The data collected for the 100-mA breathing-mode and quadrupole-mode mismatches will allow us to determine the root-mean-square (rms) beam emittance at the center and at the end of the halo channel as a function of mismatch factor. That data for 16-mA and 75-mA beam currents were presented in the last quarterly report (April–June 2001). Analysis of the 50-mA and 100-mA data is still in progress.

For the 100-mA beam, we have a preliminary determination of the beam emittance at the entrance to the halo channel (at the exit of the RFQ). The data were obtained by first matching the 100-mA beam to the halo channel (through adjustment of quadrupole magnets 1-4), then sequentially adjusting each of the first four quadrupole magnets to +50%, +100%, -50%, and -100% of their matched values. We then fit the measured rms widths of the beam, using computer codes TRACE 3-D and LINAC. The resulting emittance values, and the PARMTEQM predictions, for the horizontal (x) and vertical (y) planes are shown in Fig. 11 for beam current values of 16 mA, 50 mA, 75 mA, and 100 mA. Only the 100-mA TRACE 3-D analysis is shown in Fig. 11. The LINAC analysis is still in progress.

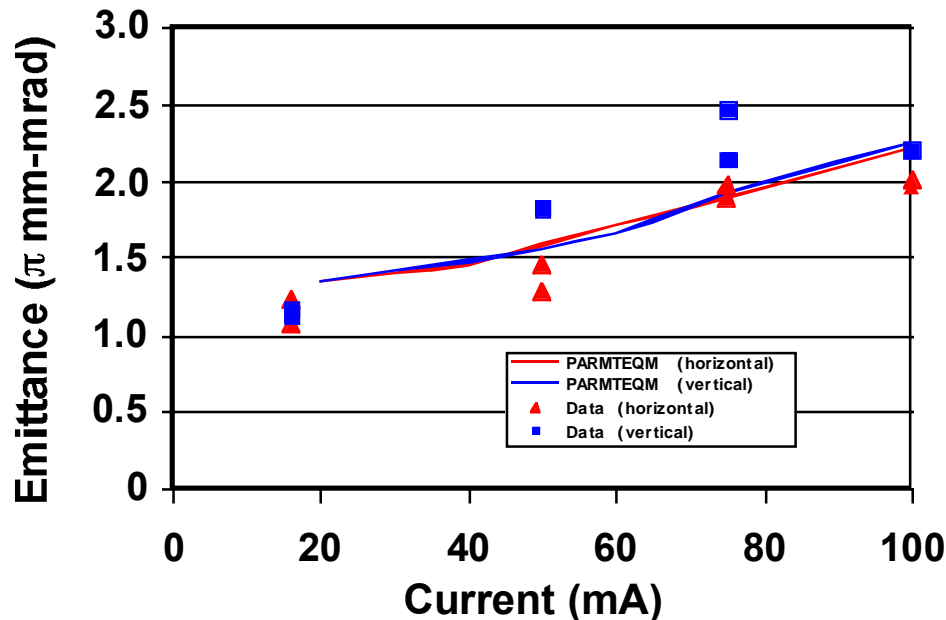


Figure 11. The RFQ output beam emittance (determined by both TRACE 3-D and LINAC analyses) as a function of RFQ output beam current. Note that the LINAC prediction for the 100-mA RFQ output beam emittance is not shown on this figure; that analysis is still in progress.

CCDTL Section 2

Following the results of testing the CCDTL Low Beta Hot Model (LBHM), the design of the CCDTL was modified in several significant ways to greatly improve its chances of success. The new design used on Section 2 of the CCDTL is shown in Fig. 12. In addition to significant changes in the cooling system, the new structure does not have any 3-gap accelerating cells, so there is no *transition* coupling cavity and no mid-

plane accelerating cavity flanges. Also, Section 2 end walls are about 25% thicker than on the LBHM, so they should be roughly double the axial stiffness. It also has removable inter-segment beam tubes, a critical feature.

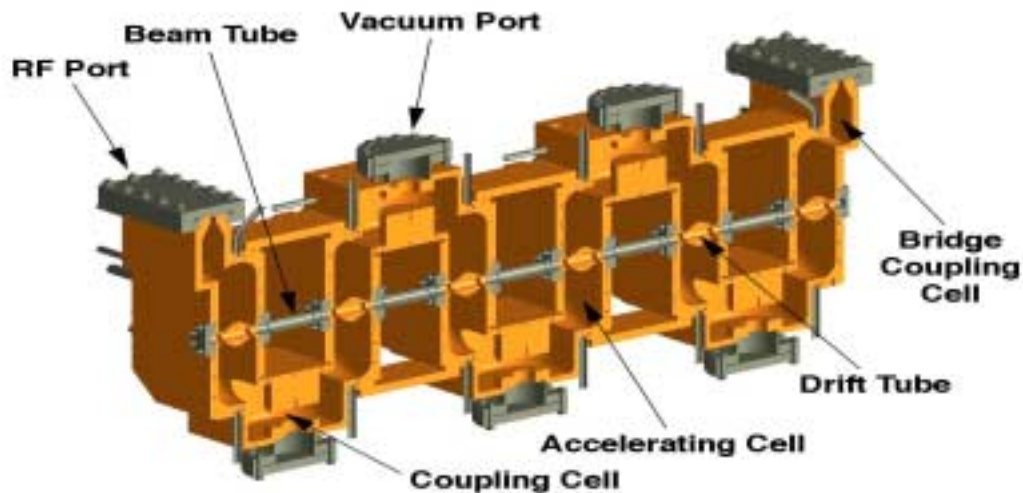


Figure 12. An isometric cross-sectional view of CCDTL Section 2. Unlike the CCDTL LBHM, CCDTL Section 2 has removable beam tubes between the accelerating cavities, allowing the frequency of each accelerating cavity to be adjusted, if necessary.

The inter-segment beam tubes on the LBHM were permanently attached (via furnace braze). There was no easy way to insert a tool to symmetrically crush the end-walls inward for final tuning (or retuning), and there was no way to pull out an end wall to raise the frequency. This design flaw was eliminated on Section 2. The stainless steel mounting flange on each end-wall provided an easy location for both pushing in and pulling out the cavity end-wall. Thus, we were able to intentionally tune these cavities a bit too high prior to the stack braze, then to fine tune them by pushing in on the end-walls after the braze.

Tuning and Installation on the Hot Model Test Stand

As reported in the last quarterly report, fabrication of CCDTL Section 2 was completed in May 2001. The field distribution was set and the cavity frequencies adjusted in the laboratory before Section 2 was mounted on the Hot Model Test Stand. The relative field distribution of the six accelerating cavities (AC) was measured using the bead-perturbation technique. The design field distribution calls for a linear ramp with a +1% field tilt. The initial measurement showed an average tilt of $\sim -0.75\%$. Both are shown in Fig. 13. This field error was corrected by enlarging two of the coupling slots. Following these modifications, new bead pull data were taken. The result (Fig. 13) is in good agreement with design.

Five of the six accelerating cavities were tuned to a lower frequency by squeezing the end-walls and reducing the gaps. This resulted in a nominal operating frequency slightly below 700 MHz. A measurement of the mode spectrum with Section 2 under vacuum showed the stopband to be ~ 0 kHz; therefore, no tuning was performed on the coupling cavities.

After tuning CCDTL Section 2, and after adjusting the field tilt to the design value, it was mounted on the Hot Model Test Stand for RF tests as shown in Fig. 14.

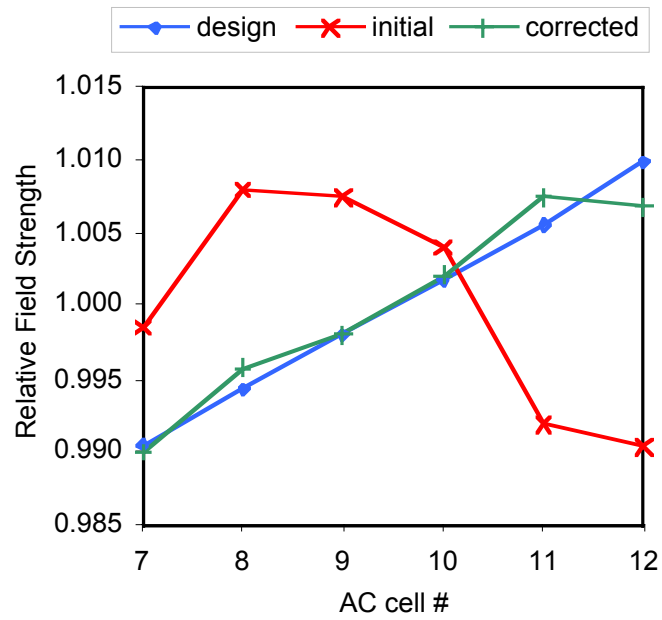


Figure 13. CCDTL Section 2 initial and corrected relative field distributions compared to the design values.



Figure 14. CCDTL Section 2 mounted on the Hot Model Test Stand in the LEDA Building.

Initial RF Power Tests on the Hot Model Test Stand

The hot model test stand setup utilized the vacuum, cooling system, and RF equipment which had been previously assembled for the LBHM in the LEDA building. The vacuum pumping behavior of this structure was much improved over the LBHM. More appropriate care had been taken to keep the inside of this structure clean during the post-braze tuning and handling. As a result, the structure conditioned much quicker, and relatively high RF power levels were achieved in a matter of hours rather than days. Surface temperature sensors (RTDs) were strategically placed on coupling cavities and other critical spots suggested by the LBHM tests and the Advanced Energy Systems finite-element analysis. Five of these sensors were placed in key points that we expected would give us the best average outer body temperature.

By the end of the second day of operation, we had achieved a cavity power level of 30 kW (where ~43 kW cw is full power). Unfortunately, we observed a resonant frequency drop of ~12 kHz. At that point, the focus on testing shifted to a more thorough investigation of the detuning phenomenon. The system was run for several days thereafter, eventually reaching full power. During this time, the structure was subjected to various loading and unloading cycles and control schemes, in a continuing attempt to pinpoint the cause of the frequency drop.

The rate of frequency drop was not steady and was often unpredictable. There was clear evidence that the step downward was bigger if the rise to full power was rapid and/or the ramp down abrupt (as in a vacuum or klystron trip). It is impossible to say whether simply achieving a new highest power caused a permanent frequency drop, because increasing power to new record levels was always accompanied by one or more vacuum bursts that tripped off the RF power. In the absence of RF trips, we were able to produce a detuning effect or an equivalent frequency drop by manually ramping up and down abruptly.

The main conclusion that should be drawn from these tests is that, although the cooling improvements succeeded in reducing the rate of drop of resonant frequency, they were inadequate to prevent it. There is evidence that the rate of drop is slowing, that it will eventually reach an asymptote. This suggests that one could simply tune the structure to a higher frequency, operate it and let it detune some, and then manually tune it to the correct final frequency. As this is not a rigorous solution, it will not be recommended.

Likely Cause of Frequency Detuning

Figure 15 shows a cross section of the CCDTL, cut through the center of one of the coupling cavities and the support strap opposite it. In the current cooling design, the crosshatched regions are usually very close to the same temperature, but from time to time, the central, double-cross-hatched region is significantly different. It appears that even the added cooling passages are inadequate to prevent the inner nose of this coupling cavity from overheating. In addition, its large thermal mass causes it to lag behind changes in any other part of the structure. Our theory is that external air pressure on the accelerating cavity end-wall biases the stresses, producing a slight inward motion of the AC end-wall each time material anywhere around the periphery yields for whatever reason. In these very low- β cavities, it only takes 0.000009 inches (0.2 μm) inward movement of the end-wall to produce a -2 kHz shift as was seen in each cycle.

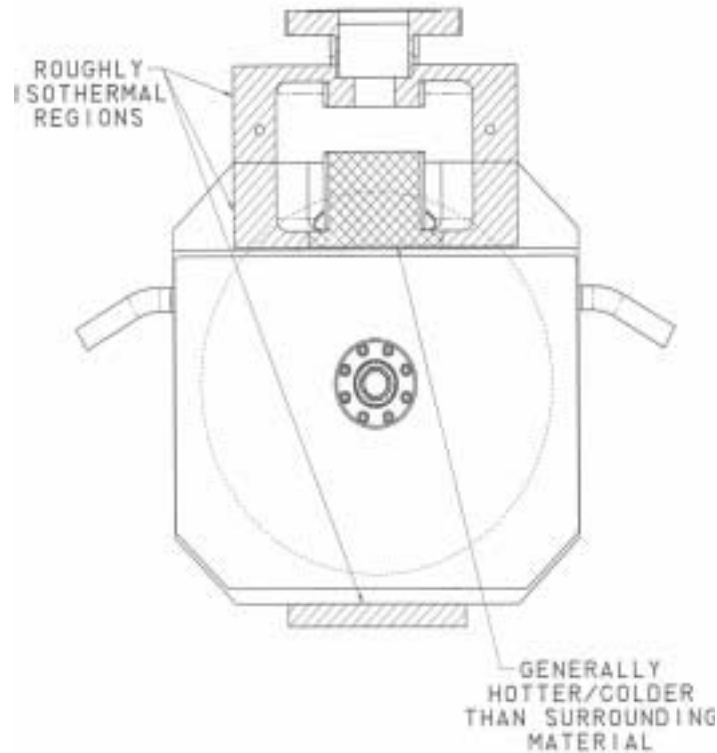


Figure 15. Cross-sectional view of CCDTL sideways coupling cavity and opposing strap. Thermal expansion or contraction of the central double-cross-hatched region is over-constrained, and results in high stresses at the ends of the coupling slot.

Retuning

Upon completion of the initial high power tests, Section 2 of the CCDTL was prepared for retuning. Prior to retuning, measurements were made of the individual cavity frequencies. The average frequency drop in the accelerating cavities was ~160 kHz while the average frequency drop in the sideways coupling cavities was ~56 kHz. For the accelerating cavities (ACs), the largest drop in frequency occurred at the ends of the structure. When the individual AC data were combined with the frequency shifts resulting from the tuning phase prior to high power operation, it appears that the end AC cells total drop in frequency following the stack braze was about half that of the inner four AC cells. This result could be related to the fact that both end-walls of the four inner AC cells are joined to a sideways coupling cavity while only one of the end-walls on the outer two AC cells is so connected.

Based upon the individual cavity and structure mode measurements, the average AC cell frequency needed to be raised about 190 kHz to return the operating mode to 700 MHz. An end-wall puller was fabricated for this purpose. On three ACs, we intentionally over-shot the correct frequency several times, using the puller and the pusher alternately, in an attempt to work-harden the critical areas. Additional frequency measurements were made to determine how much to raise the average of the sideways coupling-cell frequencies to achieve a positive stopband. A DISPER analysis of the final Section 2 mode spectrum showed a stopband of +90 kHz. A new tuning slug was fabricated for the bridge coupler to adjust its frequency and minimize the power in the adjacent longitudinal coupling cell.

Finite-element analysis of this tuning procedure showed that the highest stresses occur at the cavity nose, not at the end-wall periphery. Therefore, the work-hardening achieved by mechanical tuning was in the wrong location (i.e., we did not work-harden the area nearest the coupling slots).

RF Retest Results

After retuning, the CCDTL Section 2 was replaced on the hot model test stand. Following ~2 1/2 days of high power operation at levels up to full power, we observed a drop of ~55 kHz in the $\pi/2$ frequency. Following completion of this phase of high power tests, the individual cavity frequencies were measured. Except for one cell whose frequency dropped 120 kHz, the other five cells dropped an average of ~46 kHz. As expected, there appears to be no difference between the three cavities that were intentionally work hardened and the three that were not. The cumulative frequency shifts from detuning during all high power RF operations was the largest at the end cells.

In this series of tests, we found the frequency of the end cavities dropped as much as or more than those in the interior. If the detuning mechanism was caused by thermal ratcheting in the sideways coupling cavities, then we should have seen twice as much drop in the interior cavities. For this reason, it appears we did not identify the true cause.

Summary of RF Test Results

Despite our design changes, we were unable to stop the monotonic drop in the CCDTL Section 2 resonant frequency. Even if we were to tune the structure "too high" in frequency to begin with, and perform a final tuning step after the self-detuning, this approach would only work if the detuning eventually reached some asymptote. In our testing period, the structure detuning had definitely slowed, but had not stopped.

Milestone and DDN Documentation Progress

The following Design Data Need documentation reports were completed this quarter:

- *Summary of RFQ Performance*, Rev. 0, July 2001, second part of "RFQ Construction/Performance Documentation," was submitted to the IMS in August.
- *Interim Report on LEDA Beam Halo Experiment*, Rev. 0 (September 28, 2001), was completed, meeting the Level 2 milestone "Complete Beam-Halo Experiment Report."
- *Final Report: LLRF Ripple Response* documentation was completed, and is in the final signature stage. This work was deferred until after the 06/08/01 beam-halo completion date so as to not impede the beam-halo experiment.
- *CCDTL Hot Model Performance Documentation* and *CCDTL Stop Band Performance Documentation* are addressed in the report LANSCE-1:01-044(TN), *LEDA CCDTL Final Report* (September 26, 2001). A formal response to these two DDNs is being prepared.

3.2 High-Energy Linac

Scope

The scope of the high-energy linac work includes the development and demonstration of superconducting RF linac technology required to build the Accelerator-Driven Test Facility linac for the AAA Program. Work in FY01 included:

- **Spoke Cavity Development** – The spoke cavity is a superconducting accelerating structure that may be used at low energies, as low as 6.7 MeV (RFQ exit energy) to ~100 MeV. Development work will lead to the design and fabrication of spoke cavities that will be beam tested on LEDA.
- **Cavity Testing / SC Laboratory Operation** – Testing of superconducting cavities and related components (e.g., power couplers) is being performed in the LANL Superconducting Laboratory. In FY01, spoke cavities were tested in support of spoke-cavity development. Elliptical cavities were also tested to improve their performance. General-purpose instrumentation for cavity testing and the bench testing of other components related to SCRF linacs were developed.
- **Completion of SCRF APT DDN Work** – Work related to the development of the APT SCRF high-energy linac will be completed and documented.

Highlights

- **Spoke Cavity Development** – Spoke cavity development was officially requested by a Design Data Need. A contract for fabricating two $\beta=0.175$, 2-gap spoke cavities was awarded with delivery of the cavities scheduled for the summer of 2002. Design of the power coupler to be used with these cavities was reviewed, and we are proceeding with fabrication.
- **Superconducting Laboratory Operation** – A commissioning run was completed of a diagnostic system that can map cavity-wall temperature and emitted x-rays (from field emissions due to cavity impurities) of an elliptical cavity. Results showed that some improvements needed to be made in the equipment and data-acquisition system.
- **Completion of SCRF APT DDN Work** – We completed all APT-related SCRF DDN documentation work, including that for the $\beta=0.64$ 5-cell cavities and for the APT power couplers. Documentation, including that related to the deferred prototype cryomodule work, has been submitted to the IMS.
- **Other SCRF Activities** – We attended the 10th Workshop of RF Superconductivity held in Japan. Our work in SCRF development of high-current proton linacs, especially efforts on the spoke cavities, was well recognized.

Spoke Cavity Development

Spoke-Cavity DDN - In the present low-energy linac for the ADTF facility, spoke-cavity structures will be used to accelerate the proton beam. This type of structure has not previously been used for accelerating 100 mA of cw proton beam, and there

is minimal information available on spoke cavities designed for high-current applications. A Design Data Need entitled *Spoke Cavity Performance* was prepared to direct ED&D work to be done on these structures. This DDN requests the TDO to characterize spoke cavities and couplers designed for high-currents and obtain data on their performance with a cw proton beam.

Spoke Cavity Procurement - After completing a statement of work and a set of engineering drawings of a $\beta=0.175$, 2-gap, 350-MHz spoke cavity, we solicited US and foreign vendors for their interest in providing a firm, fixed-price quotation for the fabrication of two such cavities. The procurement was carried through BREI. Of the four bids received, three were within 15% of the average quoted price. The order was placed with the lowest bidder, E. ZANON SpA, of Shio, Italy. Delivery of the first cavity is scheduled for June of 2002, with the second cavity to be delivered at the end of July of 2002. After delivery, these cavities will be tested in the vertical cryostat at the LANL SCRF Laboratory before being tested with beam on LEDA.

Spoke Cavity Power Coupler - Work continued on a power-coupler design to be used for a spoke-cavity beam test. Power couplers of such design can carry up to 212 kW of cw power at 350 MHz, as required for the Accelerator-Driven Test Facility with a cw current of 100 mA. The coupler design, shown in Fig. 16, is an antenna-type coaxial coupler similar to the APT power coupler. RF power is transferred to the coaxial coupler via a half-height WR2300 waveguide section. At the transition from the waveguide to the coaxial line, there is a 4.8-mm-thick cylindrical ceramic window. The outer conductor of the coaxial line has a diameter of 103 mm and an impedance of 75 ohms. The inner conductor is cantilevered off a shorting plate that terminates the coaxial line at the end away from the cavity. RF transmission from the waveguide to the coaxial line was maximized by correctly terminating the waveguide and the coaxial line. This coupler has a large pumping port to ensure good vacuum and short conditioning time. Thermal analyses of the window and center conductor for the testing up to 500 kW are in progress.

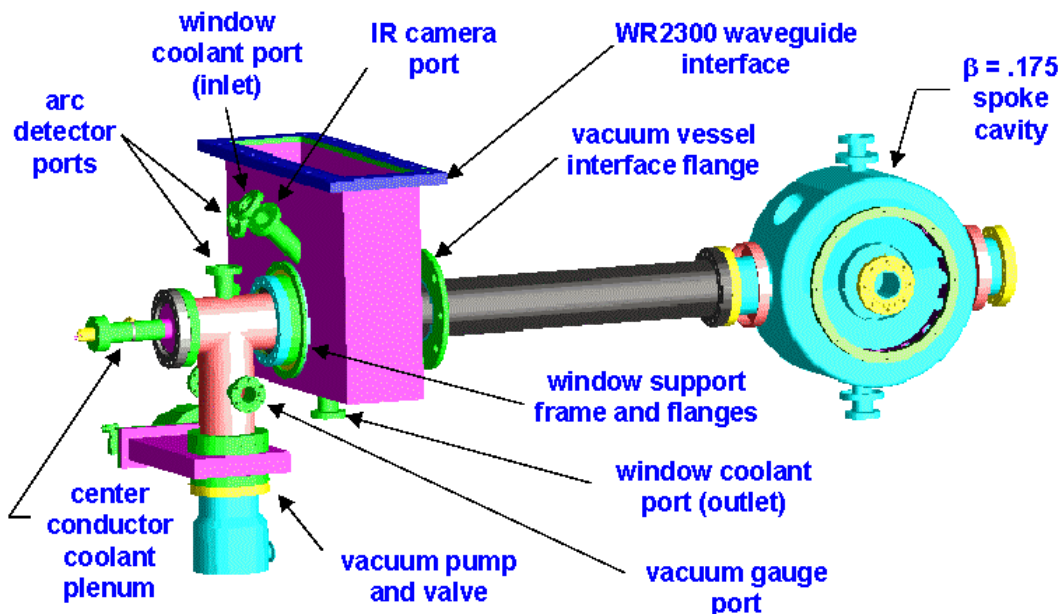


Figure 16. Spoke-cavity power coupler.

An external design review of the spoke-cavity power coupler design was held on August 2, 2001. The review panel consisted of power coupler experts from SNS, LLNL, and LANL. The panel found the design principle and procedure reasonable, and recommended we proceed with fabrication. The results of their review can be found in the report LANSCE-1:01-081.

LEDA Beam Test - We started a conceptual design of a simple cryomodule for beam testing the $\beta=0.175$, 2-gap, 350-MHz spoke cavity on the LEDA beamline. The design utilizes a modified commercial cryostat. The cavity and tuner are immersed in the liquid helium while suspended by the power coupler from the upper flange of the cryostat. Figure 17 shows the cavity and the piezoelectric tuner. A piezoelectric tuner is chosen to demonstrate the capability of detuning a cavity off resonance in under 300 msec to accommodate failure of an RF cavity unit without interruption of beam delivery.

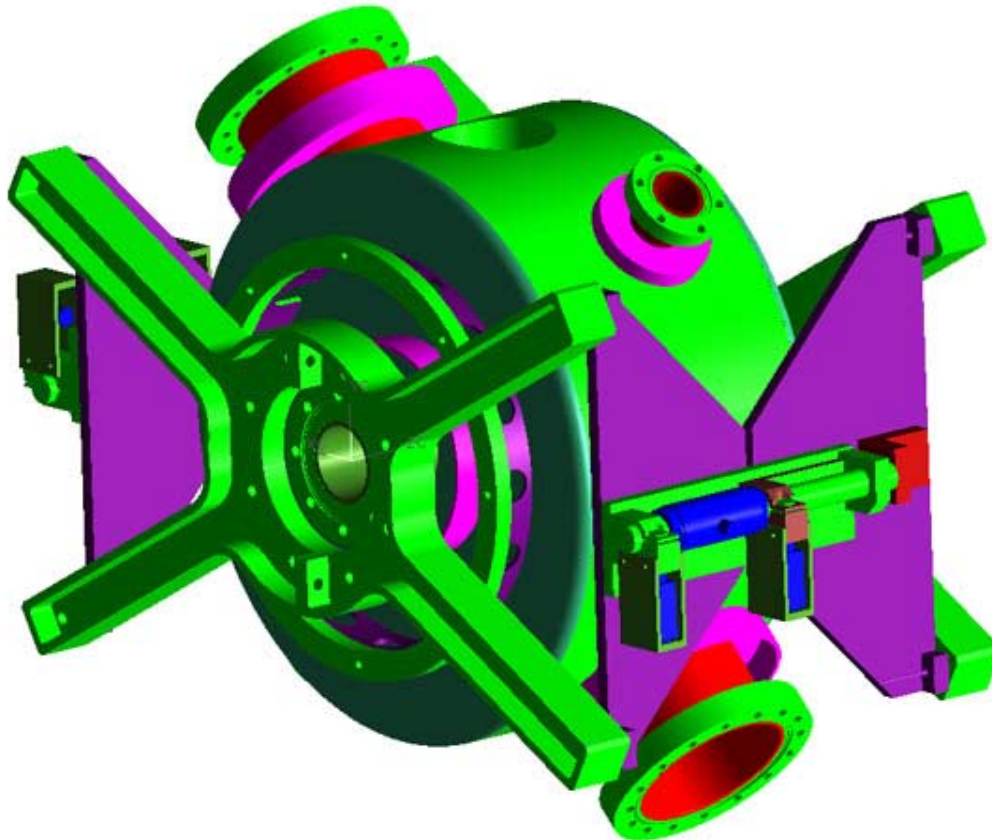


Figure 17. Spoke cavity with piezoelectric tuner.

Cavity Testing

Diagnostic System for Elliptical Cavities - We completed the fabrication of a diagnostic system to measure the temperature and x-ray profile of the outer surfaces of the $\beta=0.64$ 5-cell elliptical cavities, and completed an initial test. Figures 18 and 19 show the cavity with the sensors of the diagnostic system and a close-up photo of the

attached sensors, respectively. Unfortunately, we encountered a number of problems in installing the equipment due to the different sizes of the cells. The differences in size occurred when the cavity was squeezed to obtain the field flatness in each cell. We also experienced difficulties in our data-taking software. A new test is planned in December, after completing improvements of the equipment and data acquisition system.



Figure 18. Temperature and x-ray sensors mounted on a $\beta=0.64$ 5-cell cavity.

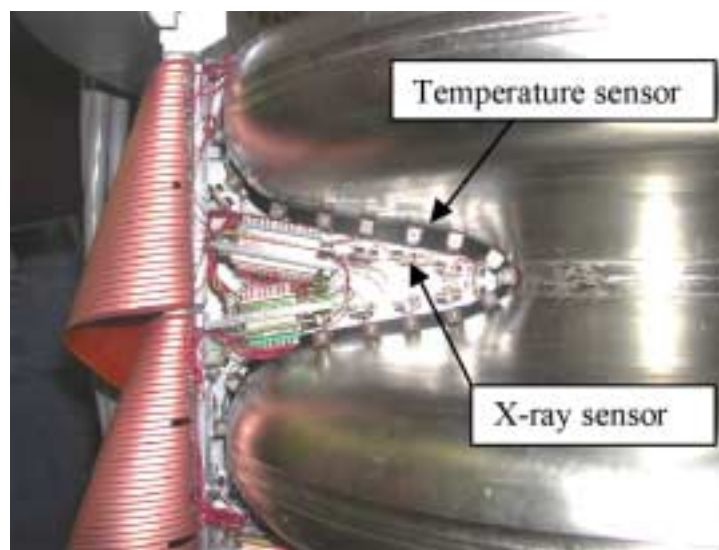


Figure 19. Close-up of temperature sensors (carbon resistors) and x-ray sensors (PIN diodes) mounted on the cavity.

APT SCRF DDN Work

We completed the DDN documentation, entitled *RF Coupler/Window HE Linac*, and a final report was published.¹² With the completion of this DDN, we completed all the APT-related DDN work.

We completed the installation of the outer helium vessels on two of the $\beta=0.64$, 5-cell cavities (Fig. 20). Diagnostics and heaters were also installed. These cavities will be required in FY02 for testing with the APT power couplers in the Saclay CRYHOLAB.



Figure 20. Installation of outer helium vessel.

Other SCRF Activities

Upgrade of LEDA Facility to 600 MeV - A preliminary study has launched for a possible upgrade of the LEDA facility to 600 MeV as a low-cost option for a Target Material Test (TMT) station facility. By taking advantage of the existing infrastructure of the LEDA facility, we can achieve significant reductions in cost and schedule when compared to constructing a TMT facility at a new site. With a lower beam-current requirement of 13 mA, the focusing lattice requirements can be relaxed compared to an APT-like linac, allowing the use of spoke cavities with more than two accelerating gaps. We started RF-cavity analysis and mechanical design of a $\beta=0.125$, 5-gap cavity, a concept shown on Fig. 21. At higher energies, spoke cavities with up to seven accelerating gaps are being considered. In the current design, we are considering the use of spoke cavities for velocities as high as $\beta=0.5$.

¹² Report No. TPO-E42-R-TNS-X-00049.

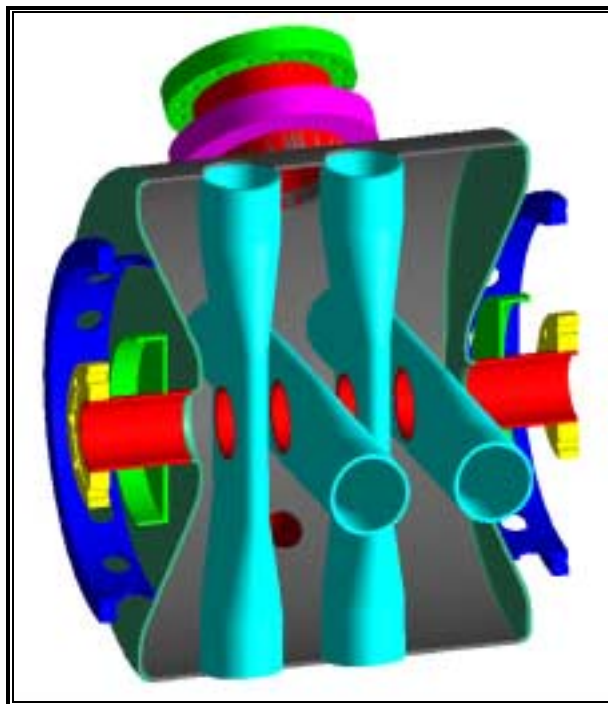


Figure 21. A $\beta=0.125$ five-gap 350-MHz spoke cavity.

10th Workshop on RF Superconductivity - The 10th Workshop on RF Superconductivity was held in Tsukuba, Japan, in September. It is a biennial gathering of SCRF experts worldwide to report the technical progress of different laboratories and to exchange and collect ideas and information. Four technical staff from the SCRF ED&D team represented the AAA Program. They presented eight papers, including three invited talks, in relation to our efforts. Our achievements in the past two years, especially our efforts on the spoke cavity, were well recognized. Information obtained during the workshop and associated visits to Japanese laboratories and industries was documented in a trip report (LANSCE-1:01-079).

The following is a list of the papers presented:

- “Design & Fabrication of SCRF Cavities for the AAA Continuous-Wave Proton Linac” (R. C. Gentzlinger).
- “Status of Multicasting Simulation Capabilities for SCRF Applications,” invited talk (F. L. Krawczyk).
- “Design of $\beta=0.175$, 2-Gap Spoke Resonator” (F. L. Krawczyk).
- “Results of the APT RF Power Coupler Development for Superconducting Linacs” (E. N. Schmierer).
- “Design of the Spoke Cavity ED&D Input Coupler” (E. N. Schmierer).
- “Superconducting Technologies for the Advanced Accelerator Applications Program,” invited talk (R. L. Sheffield).
- “Status of the LANL Activities in the Field of RF Superconductivity,” invited talk (T. Tajima).
- “Test Results of $\beta=0.64$, 700 MHz, 5-Cell Elliptical Cavities” (T. Tajima).

4. Transmuter Development

Scope

- **Analysis Support** – Includes analytical assessments to guide overall transmuter development—specifically, experimental needs and data quality objectives. FY01 focus is assessing damage and gas production in structures surrounding the target.
- **Nuclear Codes and Data** – Includes development of analytical methods for the nuclear design of the transmuter, with focus on nuclear design codes and data, including evaluation of fission cross sections of key Pu isotopes, assessment of the lead-bismuth scattering cross-sections, improvement of the subactinide fission and fission fragment model for MCNPX, benchmarking results and comparing with the higher order methods, and coupling of higher order and deterministic codes and revisions to deterministic codes to account for subcritical source-driven behavior.
- **Thermal-Hydraulic Codes** – Includes assessment of the liquid metal and gas system models incorporated into the Transient Reactor Analysis Code (TRAC), such as benchmarks and quantification of some of the transport equations, thermal-transients in the structures from beam interrupts, natural convection potential in LBE, etc.
- **Laboratory Experiments** – Includes experiments to investigate the fundamentals of chemical reaction between LBE and sodium to address concerns with current design concepts about a possibility of severe sodium reactions with lead or bismuth due to a leak. Preparation for a series of small, scoping-type tests is underway to provide quick, pseudo-quantitative data on the nature and extent of the sodium reaction.
- **Irradiation Experiments** – For FY01, four sets of scoping experiments were approved by the steering committee:
 - “Influence of Proton Irradiation on the Corrosion Kinetics of Structural Materials in LBE Coolant Systems” will irradiate material samples with protective oxide layers.
 - “Cross-Sections for the Activation of Sodium by Protons” will investigate the production of the longer-lived isotopes in an AAA target assembly with sodium as a coolant, providing a benchmark for testing the nuclear physics codes used for target design.
 - “High-Energy Neutron Leakage from a Spallation Target” will provide experimental verification of expected flux distributions and evaluate the effectiveness of a buffer in reducing the leakage of high-energy neutrons, which produce gas and limit the lifetime of structural materials.
 - “Measurement of Hydrogen and Helium Production with Neutrons up to 100 MeV” will determine hydrogen and helium production on materials proposed for the AAA Program with neutron energies up to 100 MeV.

Highlights

- Sodium and lead-bismuth eutectic compatibility experiments were started. Temperature-vs-time traces were obtained by mixing sodium-lead and sodium-bismuth, which show a clearly exothermic reaction. The temperature rise with bismuth was approximately twice as large for the temperature rise as with lead. The remaining tests in the test matrix are ongoing.
- Blue Room irradiation experiments were begun.
 - Initial scooping tests were performed for the LBE corrosion and oxide film capacitance measurements.
 - Sodium activation tests were performed with an 800-MeV proton beam. Data analyses were performed, and a final report is being written for the ^7Be and ^{22}Na evaluations.
 - The helium and hydrogen production test chamber is ready for commissioning.
 - Target design continued for the LBE target neutron-yield and spectrum experiments, while a number of pre-test evaluations were performed to guide the design.

Analysis Support

We started a set of analyses to compare the spallation and activation products for an LBE and a sodium-cooled tungsten target under similar irradiation conditions. For this comparison, we are using a beam energy of 1 GeV and a beam current of 15 mA. We will evaluate the reaction products at the end of a 9-month continuous irradiation period and as a function of cooling time. This analysis is ongoing and results will be included in subsequent reports.

Nuclear Codes and Data

CEM2k Documentation - A report was written on the Recent Developments of the Cascade Exciton Model (CEM2k Code) of Nuclear reactions by S.G. Mashnik and A.J. Sierk (LA-UR-01-5390). A detailed discussion of the improvements was included in the previous quarterly report (April-June 2001).

Pu-239 (n,f) ENDF Evaluations - The final evaluation was completed (results were described in the previous quarterly report) and the new ENDF file will be delivered to AAA shortly.

Evaluation of the Data Libraries - We have established a list of actinide cross-section uncertainties for the AAA Program. These are summarized in Table 5. The “achieved” uncertainties have been assessed through the study of the available nuclear data libraries¹³ while the *required* ones are essentially based on the numerical simulations of the integral experiments.¹⁴

¹³ See “Present Status of Minor Actinide Data,” NEW/OECD report, WPEC Vol. 8 (1999).

¹⁴ Koscheev, V.N. et al., “Nuclear Data for Plutonium and Minor Actinides,” *Proc. 3rd Int. Conf. on ADTTA*, Praha, 11-17 (June 1999).

Table 5. Actinide Cross-Section Uncertainties, Achieved and Required (in bracket).

Nuclide	Half-life	$\delta\sigma_c(\%)$	$\delta\sigma_f(\%)$	$\delta\sigma_{in}(\%)$
Pa-232	1.3d	-	-	-
Np-237	2.1×10^6 y	15 (5)	7 (3)	30 (15)
Np-238	2.1d	-	-	30 (15)
Pu-238	87.7y	25 (10)	10 (5)	30 (15)
Pu-239	2.41×10^4 y	6 (4)	4 (2)	20 (15)
Pu-240	6.56×10^3 y	10 (5)	5	30 (15)
Pu-241	14.3y	15 (5)	5 (3)	30 (15)
Pu-242	3.73×10^5 y	-	-	30 (15)
Pu-244	8×10^7 y	-	-	30 (15)
Am-241	432.7y	10 (5)	10 (5)	30 (15)
Am-242	16.0h	-	-	30 (15)
Am-242m	141.0y	30 (10)	20 (5)	30 (15)
Am-243	7.37×10^3 y	30 (10)	10 (5)	30 (15)
Cm-242	162.9d	50 (10)	50 (5)	30 (15)
Cm-243	28.5y	50 (10)	50 (5)	30 (15)
Cm-244	18.1y	30	20 (5)	30 (15)

Thermal-Hydraulic Codes

The following two TRAC-ATW tasks, which were completed this quarter, are noted here and further described below:

- The effect of decay heat within the coolant on natural circulation within the LBE ADTF target was investigated. The analysis of the results was completed and a report is in progress.
- Trace-material calculations for the ADTF with oxygen as the trace material, including solubility models, were completed. A draft report was completed describing the new numerical solution for the trace materials and the results of the test calculations.

Natural Circulation with Fluid Decay Heat

Several natural circulation cases were run with TRAC-ATW for the lead-bismuth eutectic ADTF target to test TRAC's ability to model natural convection for liquid metal systems. For all cases, the loop was run to a steady state for ~30 min. Five megawatts were deposited in the beam region, with 1% of that power deposited uniformly by volume in the fluid after it exited the beam to model the initial decay heat. At 2000 seconds (~33 min), the beam and pump were tripped. For all cases, the full steady-state flow of helium continued at the same inlet temperature on the

secondary side of the heat exchanger. The calculations were run out to ~58,000 seconds (~16 hrs) to obtain quasi-steady conditions.

The quasi-steady conditions were found to be very sensitive to the heat losses through the ADTF target-loop piping walls. If the heat losses through the pipe walls are ignored, then late in the natural circulation transient, energy continues to be transferred from the target loop primary side to the secondary side of the heat exchanger. Relative to the rest of the loop, the fluid temperature at the outlet of the primary side of the heat exchanger was lower than the rest of the LBE primary loop. These relatively colder temperatures result in a relatively large LBE density in the primary side of the heat exchanger, which in turn causes the quasi steady-state natural circulation velocities to be negative relative to the normal operating fluid flow direction.

However, as piping heat losses for the primary side of the ADTF target loop are added to the model, the quasi steady-state flow direction can become positive relative to the normal operating-fluid flow direction. If the piping heat losses are sufficient to bring the average temperature of the primary loop fluid below the inlet temperature of the secondary side of the heat exchanger, then the energy transfer through the heat exchanger reverses (i.e., heat is transferred from the secondary side to the primary side). With the change in heat transfer, the fluid in the primary side of the heat exchanger will be at a higher temperature than the rest of the fluid in the primary loop, and therefore, the density of the fluid on the primary side of the heat exchanger will be lower relative to the rest of the target loop primary fluid; thus, the flow will be in the same direction as the normal operating-fluid flow direction.

Modeling of Oxygen as a Trace Species in the ADTF

The explicit method for solving the trace species transport model described by Spore¹⁵ was found to be too costly in terms of computing time and lost accuracy for relatively long transients. However, the existing TRAC-M implicit numerical solution for boron concentration tracking was modified to be used by the trace species transport model.¹⁶ With the implicit numerics, the computing cost for the trace species transport calculation has been significantly reduced (by an order of magnitude) and the accuracy has been significantly increased. Calculations were completed for ADTF with oxygen as the trace species. This calculation includes solubility models that were recently incorporated into the ATW version of TRAC.

Laboratory Experiments

The first two months of the fourth quarter were used to complete the design and fabrication of an instrumented test apparatus. An existing glovebox was outfitted to support assembly and disassembly operations, and a data acquisition system (DAS) based on LabView software was assembled. Detailed operating procedures and a safety plan were developed and subsequently approved for the tests.

¹⁵ Spore, J.W., "Accelerator Transmutation of Waste Updates for TRAC-M," LA-UR-01-3660 (June 2001).

¹⁶ Spore, J.W. and D.R. Liles, "Improvements to the Accelerator Transmutation of Waste Updates for TRAC-M, DRAFT report.

A schematic of the assembled apparatus for these tests is shown in Fig. 22. The experimental approach is quite simple: small quantities of the two metals to be investigated are heated above their melting points in separate crucibles, and the two metals are mixed together to initiate the reaction. As shown in Fig. 22, up to 100 cc of sodium is heated with a clamshell heater in a 500-cc stainless steel crucible. The sodium temperature is measured with four tantalum-sheathed Type-C thermocouples (2300°C temperature range). A slow bleed of argon gas is introduced into the bottom of the sodium crucible to promote mixing when the two metals are combined. Immediately above the sodium crucible is a second stainless steel crucible containing LBE, Pb, or Bi. The second crucible is also heated with the clamshell heater. The temperature of the heavy metal is measured with an alloy-718-sheathed Type-K thermocouple. The bottom of the crucible containing the heavy metal is fabricated with a thin (5 mil) replaceable tantalum bottom, which can readily be punctured. After the desired temperature in the two pools is achieved, the bottom of the crucible containing the heavy metal is perforated with a remotely actuated lance driven by a small pneumatic cylinder affixed to the top of the reaction isolation container. The heavy metal pours into the underlying sodium pool, thereby starting the interaction. Once it is mounted in the secondary container, the lower end of the test section containing the test materials is insulated to achieve adiabatic conditions to the greatest extent possible. The secondary container has a flowing argon cover gas during the test. For safety, the entire assembly is placed within an existing ventilated hood during the experiment.

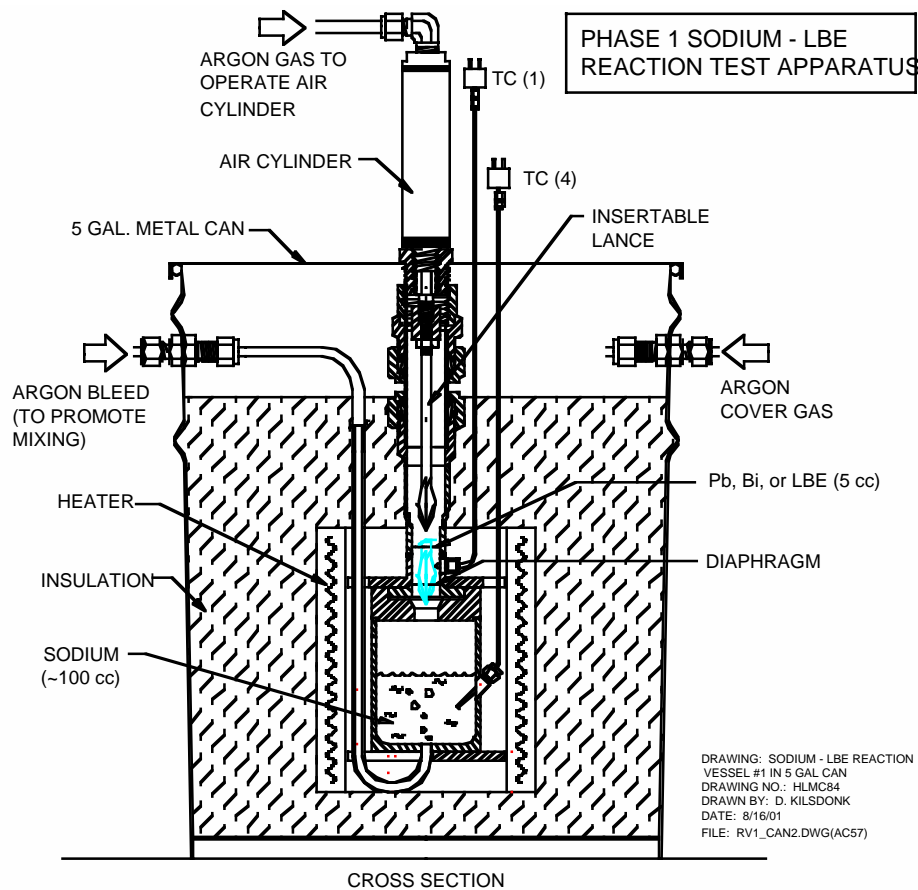


Figure 22. Test apparatus.

Initial tests indicated that the volumes of the test materials needed to be reduced for the planned tests (shown in test matrix, *AAA Quarterly Report Apr-Jun 2001*). The exothermic reaction caused by mixing 2.5 cc of lead with 100 cc of sodium at 400°C was so active that material was transported up to and even beyond the perforated tantalum diaphragm. Reacted lead and sodium were found immediately above and below the diaphragm during post-test examination of the first two initial tests. The volumes of lead and sodium were scaled down by half in subsequent tests at 400°C to ensure that all reaction products remained within the mixing crucible. The checkout tests were useful in evaluating other facets of the hardware and the DAS performance, which led to modification of several features of the test section and secondary containment before beginning the compatibility tests.

The exothermic reaction initiated by mixing Pb or Bi with Na leads to an easily measurable, nearly instantaneous temperature increase within the mixing crucible. This is illustrated in Fig. 23 with plots of temperature data from two separate tests in which 1.25 cc of molten Pb and Bi at 400°C were respectively mixed with 50 cc of Na at 440°C.

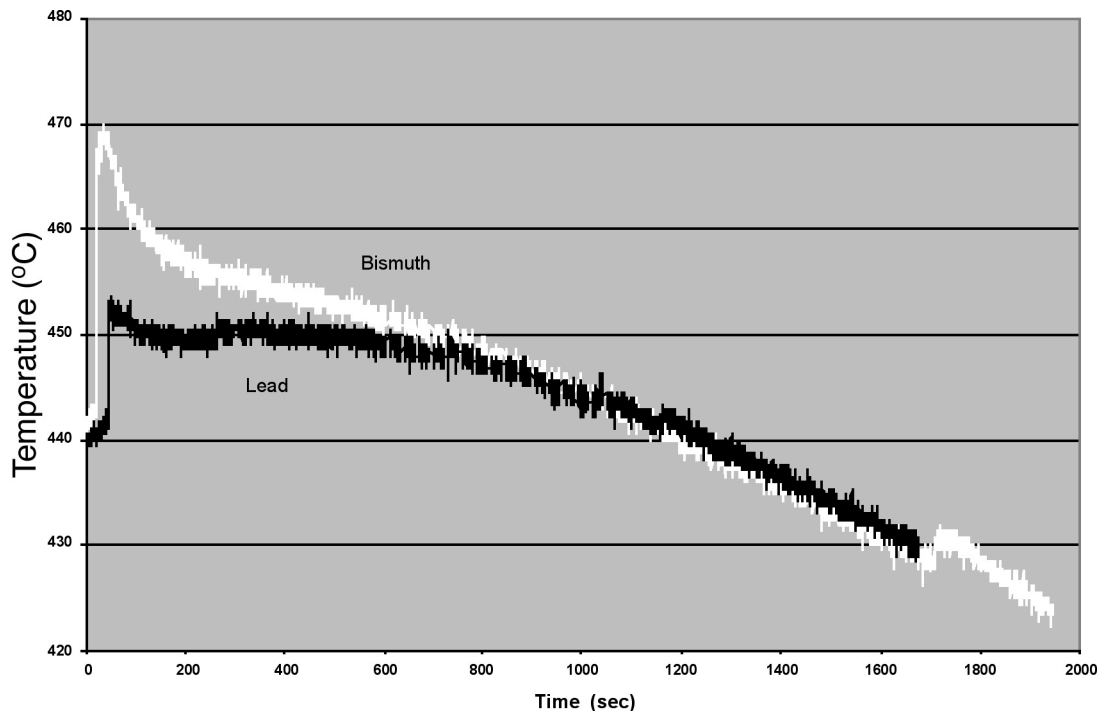


Figure 23. Temperature traces for the sodium-lead and sodium-bismuth mixing tests.

Several features of the plots are worth noting. The Na-Pb and Na-Bi reactions were obviously exothermic and led to nearly instantaneous temperature increases. The rapid temperature rise during the bismuth test was approximately double that measured when an equal volume of lead was mixed with sodium. Minor temperature increases are observable at approximately 250, 700, and 1150 seconds in the lead plot. A more noticeable increase can be seen in the bismuth plot near 1700 seconds. These slight jumps in temperature were no doubt caused when additional droplets of molten heavy metal fell into the pool and exothermically reacted with the sodium.

Additional tests with LBE, along with others to address test-temperature and injection-speed effects, are currently underway.

Irradiation Tests

The activities on four series of experiments in the Blue Room of the Weapons Neutron Research (WNR) facility at LANSCE began in this quarter and are discussed below.

Corrosion Experiments

A simple sample holder (furnace) was fabricated to expose pre-oxidized samples in contact with lead-bismuth eutectic to proton irradiation (Fig. 24). The purpose was to demonstrate that capacitance might be used as a real-time indicator of the corrosion properties of protective oxide layers on candidate target/blanket engineering alloys. Samples of SS-316L (austenite) and HT-9 (ferrite) steels, as well as the precipitation-hardened nickel-based alloy 718, were tested in a static liquid lead-bismuth eutectic bath. The samples were pre-oxidized in air and then exposed to LBE at 150°C before and during 800-MeV proton irradiation in the Blue Room facility. During exposure, the capacitance of the oxide was monitored as a function of time.

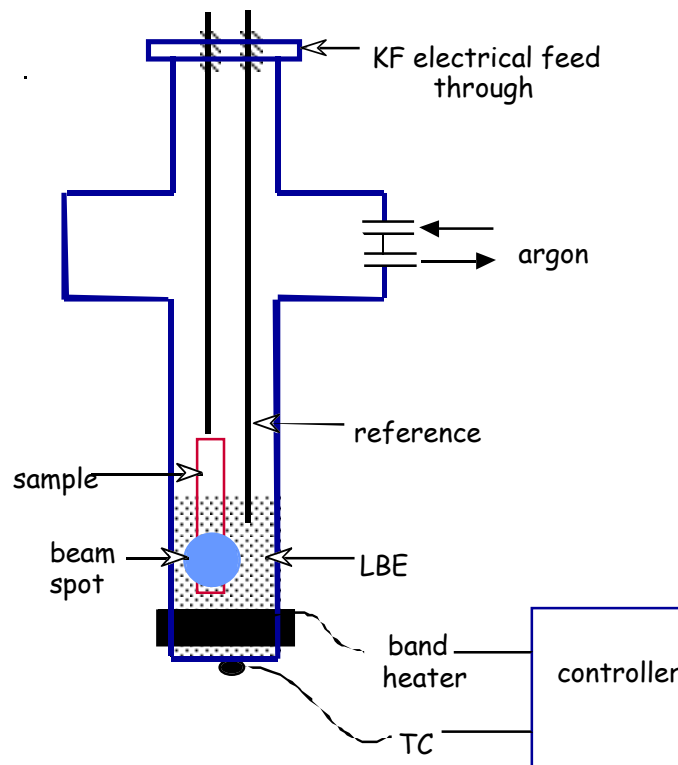


Figure 24. Schematic of the test section.

For alloy 718 and HT-9, the pre-oxidation layer was apparently nonprotecting in liquid LBE as indicated by a sharply increasing capacitance with exposure time independent of exposure to the proton beam. By comparison, in the absence of proton irradiation, the capacitance of the oxide on SS-316L decreased with exposure

time, indicating the layer formed by the pre-oxidation process was passivating and possibly self-healing. Irradiation of the SS-316L sample (after exposure to LBE for 2 hrs) at ~80 nA showed a small increasing trend in oxide capacitance, indicating a change in the transport properties during proton irradiation (and thus corrosion resistance). However, no catastrophic change in the oxide properties occurred, and hence, the ability of this oxide to protect the metal substrate from corrosion does not appear to fail catastrophically. Preliminary metallography of the samples revealed that the oxide on both SS-316L and HT-9 was a thick, dual-layer film enriched in chromium with respect to the alloy composition.

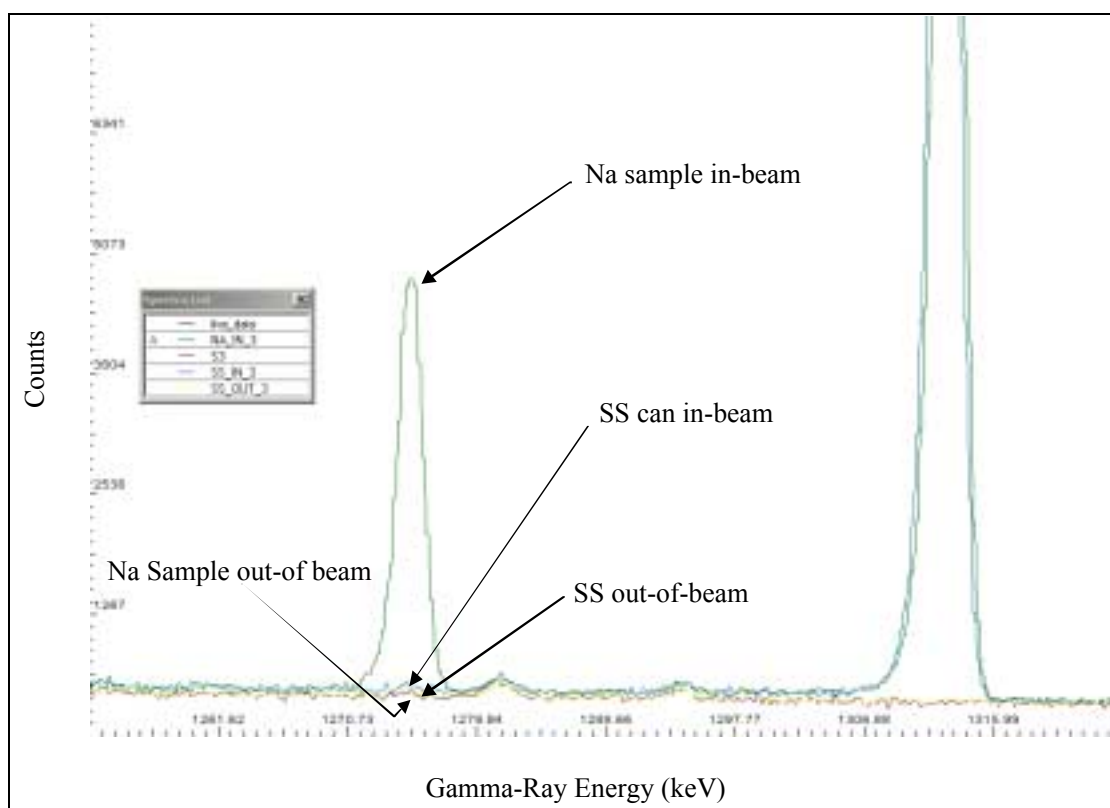
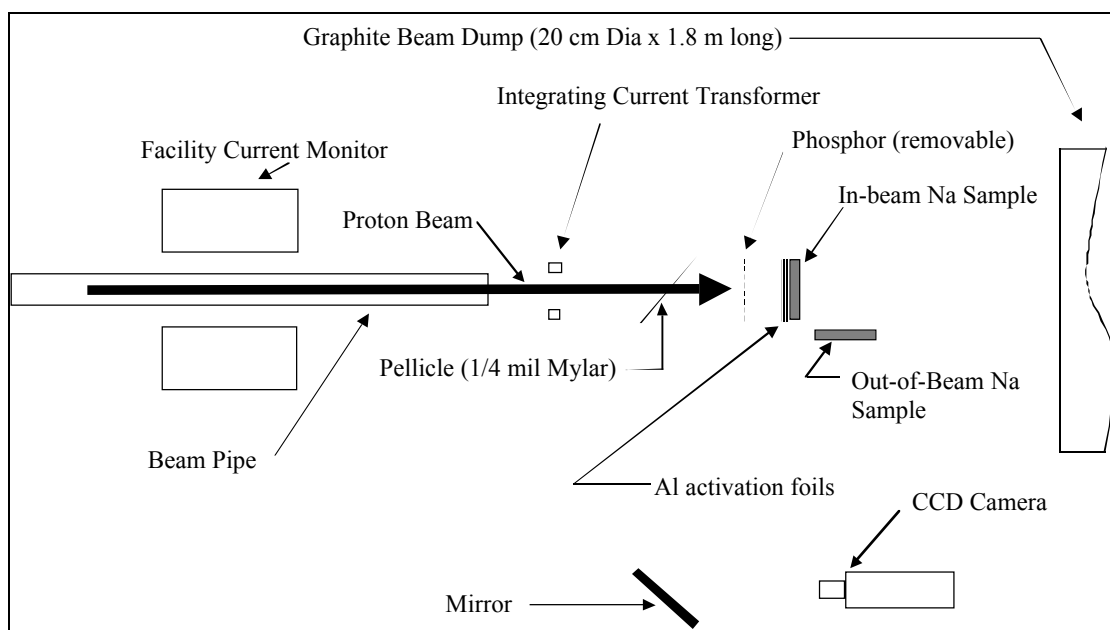
These tests were scoping experiments with little planning time prior to testing. The measurement techniques were checked, and an initial indication of the beam effects was investigated. In follow-on tests scheduled for FY02, some problems encountered during the scoping experiments will be corrected. A more prototypic pre-oxidation phase will be implemented. These oxides will be similar to oxides developed for LBE technology applications by the Russians as part of a preconditioning program. We anticipate more protective multi-layer oxide films will be generated. The test apparatus will be modified such that the thermodynamic conditions within the test chamber can be better controlled (including better assurance against air ingress during sample change-out). A detailed test plan and procedure are currently being written for the FY02 tests.

Sodium Activation Experiments

Two sodium cans (like the one shown in Fig. 25) were fabricated at ANL-West and shipped to Los Alamos for irradiation. One can was used in the beam for irradiation, and the other was outside the beam as a control sample. The test arrangement is illustrated in Fig. 26. The can was irradiated in the Blue Room at one beam energy (800 MeV). A number of pre-test calculations using MCNPX were performed. The ^7Be and ^{22}Na amounts are obtained by gamma-counting after irradiation. The gamma-ray spectra for ^{22}Na are shown in Fig. 27. The pre-test production predictions are shown in Fig. 28. The preliminary cross-section evaluation of the data is given in Table 6. A final test report is being prepared.



Figure 25. Sodium can used in Blue Room irradiation.



Yield in Sodium after 30 minutes

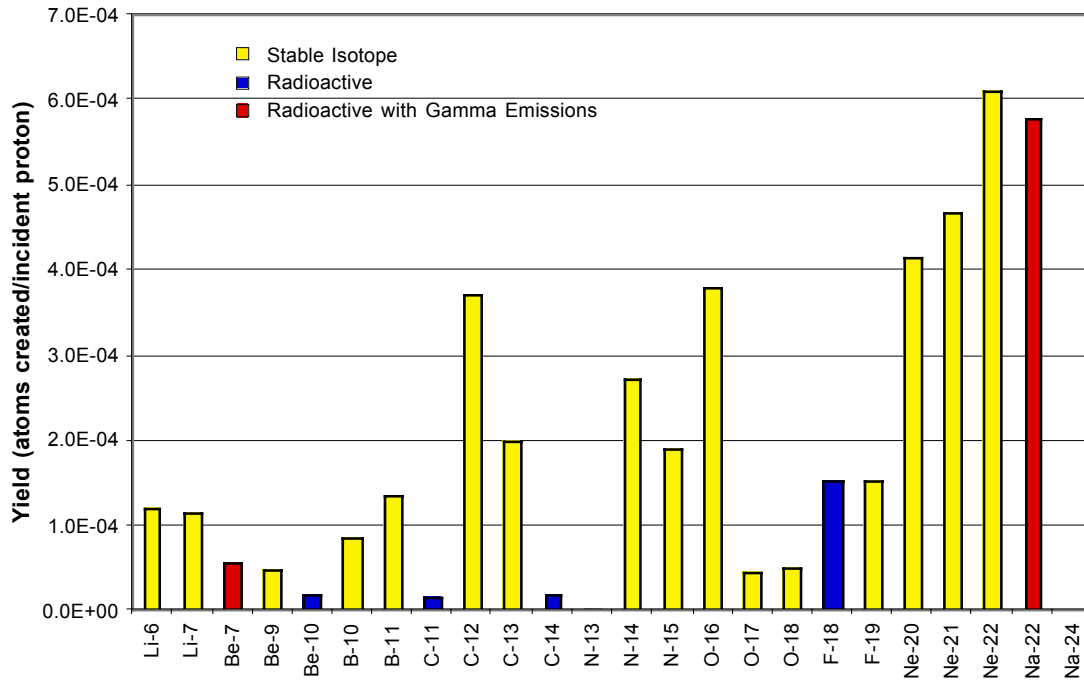


Figure 28. Test prediction.

Table 6. Preliminary Unreviewed Cross-Section Results

Isotope	Measured X-Section (mb)	Calculated X-Section (mb)
Na-22	29.6 ± 1	45.4
Be-7	6.5 ± 0.5	4.2

Hydrogen and Helium Production Experiments

The objective of these experiments is to measure hydrogen and helium production rates under a high-energy (up to 100 MeV) neutron irradiation. In the last quarter of FY01, the reaction chamber was assembled and detectors were positioned in the reaction chamber. Also, the cabling was completed for the data acquisition system. Images of the neutron beam were obtained in the reaction chamber to verify the positioning of the chamber. The collimation of the neutron beam to the chamber was improved. The commissioning tests were scheduled for September; however, we are still waiting for beam time for commissioning. We expect to perform commissioning tests in October. Figure 29 shows the reaction chamber and the test setup.

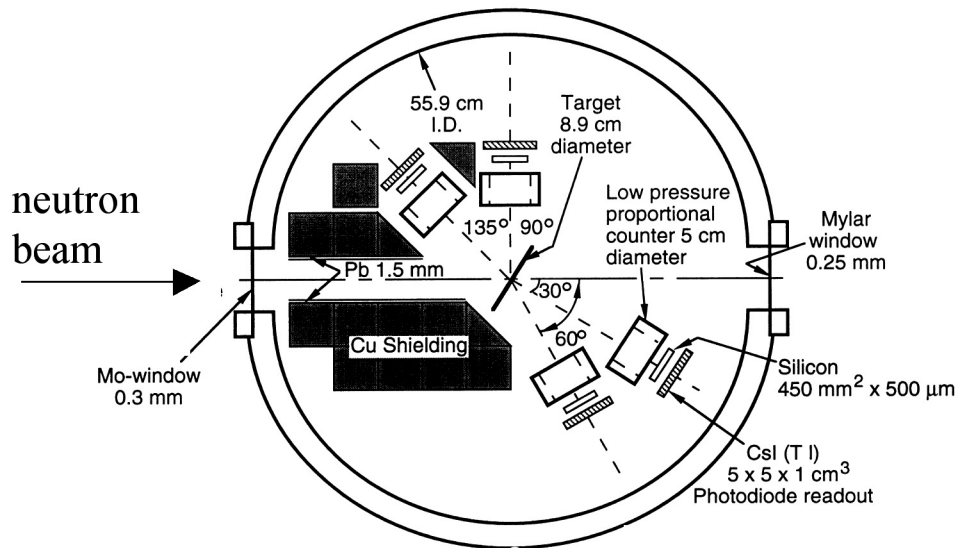


Figure 29. Reaction chamber for hydrogen and helium production tests.

Neutron Yield and Spectrum Tests for LBE Targets

Initial irradiations for activation foil measurements are planned for December. We will use a 10-cm radius target mounted on a support table with the ability to translate the target in the axial direction. The table, support structure, and target dimensions have been identified and designed. The LBE material and translation table were ordered, and delivery is scheduled for early November.

The four beam lines in the Blue Room required modifications to meet the current standards for personnel protection and safety. Work was performed on two flight paths that will be used in the initial measurements to bring them within current regulations. They are now ready for use. Detector and electronic systems for the four detector systems (one for each flight path) were also reactivated and tested.

Initial materials have been identified for the activation foil measurements. A combination of facilities at LANSCE and LANL TA-48 will be used for counting the activation foils. Facilities at LANSCE allow for easy transport of the foils after irradiation (facilitating shorter delay times), whereas the analytical capabilities and expertise at TA-48 allow for automated counting and a higher level of quality assurance during the process. The foils will be counted first at LANSCE for reactions with shorter half-lives, and then transported to TA-48 for additional counting of the longer reaction products.

Analysis Activities - Spallation neutron sources create high-energy neutrons whose energies extend up to the incident proton energy. In the design of accelerator-driven waste transmuters, the high-energy neutrons that leak from the spallation target require the following to be taken into consideration: (1) they dominate the shield design because they have long attenuation lengths (18 cm in steel); (2) they lead to the production of source neutrons in the fuel region, which generates a spatially dependent neutron source that influences the power density distribution in the blanket; and (3) they dominate the production of H and He atoms in the steel structural elements that reside in the multiplier region near the target. This gas production limits the lifetime of the structural materials near the target.

The experiment will rely on two different methods for determining the neutron leakage from the LBE target—activation foil data and time-of-flight measurements. These techniques are complementary and will each offer unique data for determining neutron flux levels. The time-of-flight measurements will offer very detailed neutron spectral data emitted from a region of the target at discrete angles. The activation foils will provide integral neutron spectral data at positions along the circumference of the target. These data are integral with respect to energy and angle, but they represent highly localized data due to the size of the activation foils. The neutron spectra at these specific points can then be determined by a process of spectral unfolding from the integral reaction-rate data. These unfolded spectra are based on an energy-group structure and, therefore, are not as detailed as spectra obtained from time-of-flight measurements. However, these group-wise data are still highly detailed and offer the advantage of being able to determine the total neutron flux as a function of position along the length of the target (compared to the differential data provided by time-of-flight measurements).

Initial calculations have been performed and are continuing to identify key experimental parameters and effects of slight modifications in the parameters, including the target radii, target length, proton beam profile, cross-section data, and calculational tools employed. The specific areas of concern are total neutron fluence leaking from the circumferential surface of the target, neutron spectra as a function of position along the circumference of the target, and angular distribution of the neutron flux along the target. These aspects are discussed in further detail in the experiment test plan. Several characteristic plots are shown in Figs. 30-32 for a few of the key issues. These figures include spatial distribution of the neutron flux from the target (Fig. 30), total neutron flux along the surface of the target for different target radii (Fig. 31), and spectral distribution of the neutron flux for different positions along the target (Fig. 32).

In addition to the initial parametric studies, reaction rate data are being reviewed for the spectral unfolding process from activation foil information. These data will continue to be reviewed and refined to meet the specific needs of this neutron leakage experiment.

University Collaboration

We expect that researchers from two universities will be involved in the LBE target experiments, including the University of Nevada-Las Vegas and the University of Michigan. Meetings were held with researchers from both universities to outline projects for student participation. A proposal was written and approved to fund activities at UNLV under the existing grant to UNLV through the Harry Reid Center. The University of Michigan also has an existing program through the AAA Office; tasks and effort under the existing contract may be redirected to support this experiment.

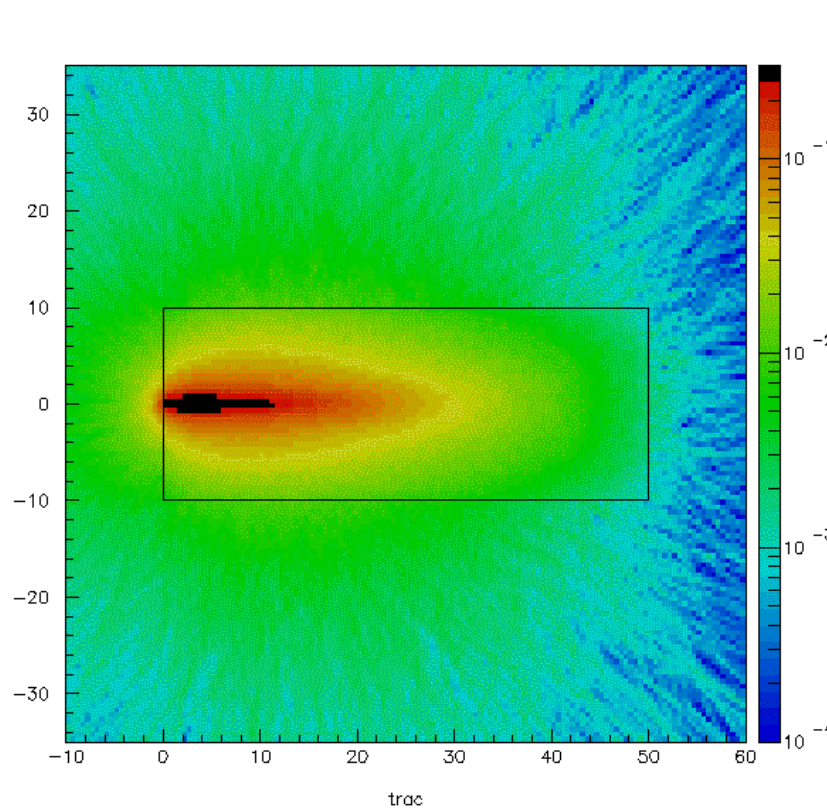


Figure 30. Spatial profile of the neutron flux. The proton beam enters the LBE target (outlined) from the left.

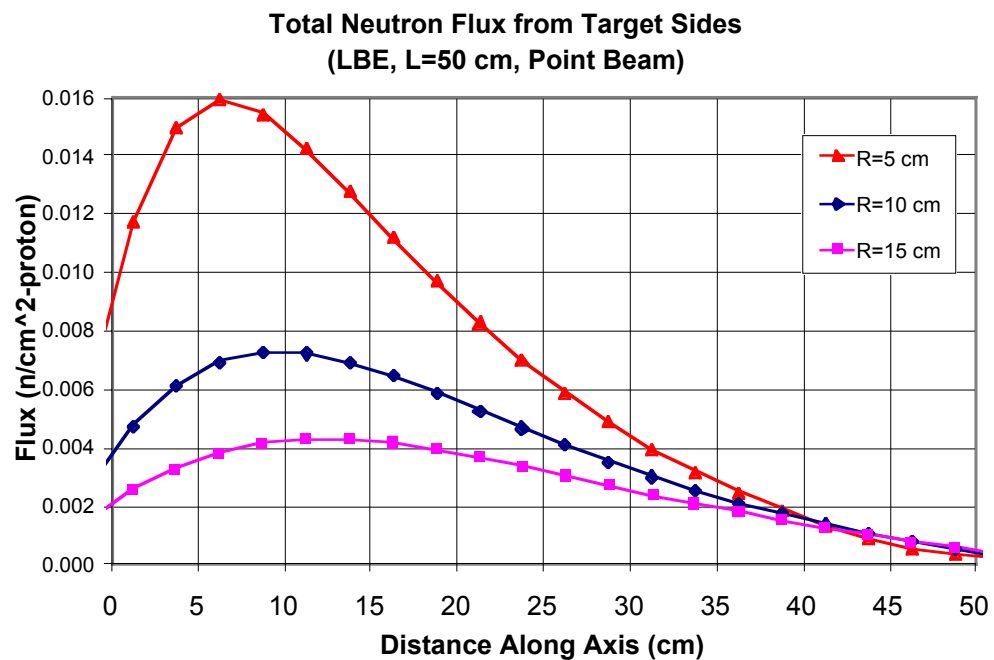


Figure 31. Total neutron flux along the surface of the target for different target radii.

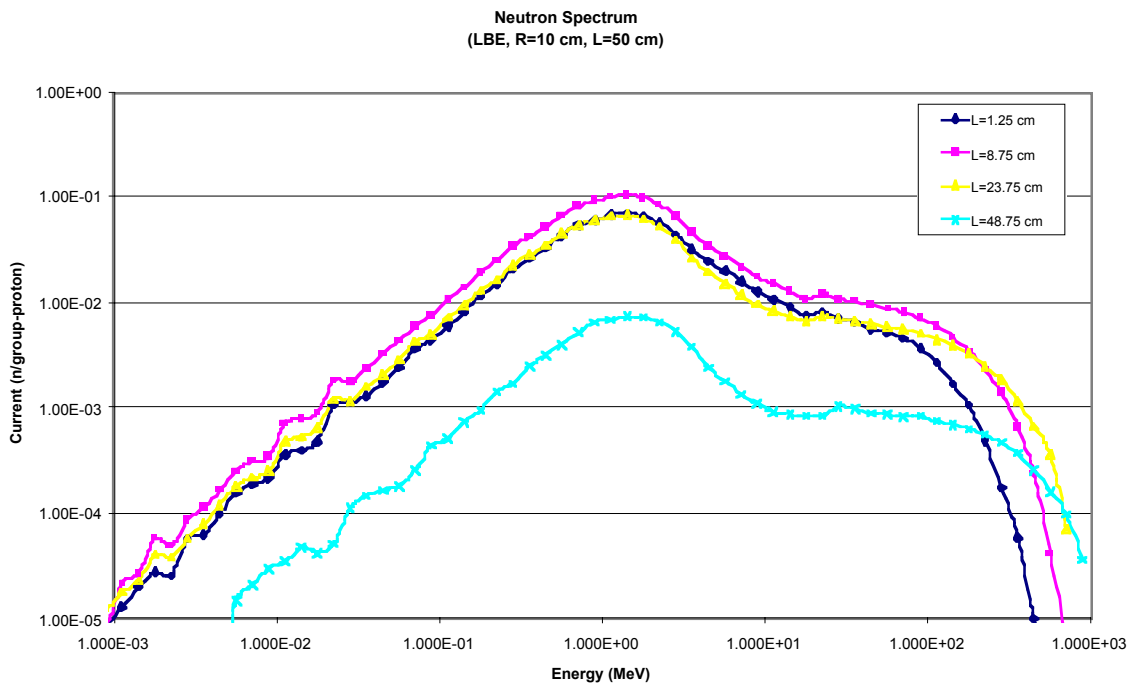


Figure 32. The spectral distribution of the neutron flux for several different positions along the surface of the target.

5. Spallation Target Development

Scope

For the spallation target development, the two main areas are the lead-bismuth eutectic technology and materials research.

- LBE Technology** – In FY01, the main activity in the LBE technology area was construction and operation of the Materials Test Loop (MTL). This is a large loop capable of delivering 15 m³/h flow rate of LBE using a mechanical sump pump. High velocities (up to 6 m/s) are achievable in the test section, whereas the nominal design velocity is 1 m/s. The vertical geometry allows for natural circulation with ~0.2 m/s velocity. The design specification for the power input to the loop is 50 kW (nominal) with 20% extra capacity. This loop is designed and being constructed to support the LBE technology development, in general, by providing a test bed for corrosion, heat transfer experiments, and instrument testing. Oxygen control strategy and probe testing is also a function for the MTL. At present, spallation target technology is the primary motivation for developing the LBE technology, but if needed, the loop can also be used to support the choice of LBE as a nuclear coolant.

- **Materials Research** – In the materials area, we are continuing to develop the *Materials Handbook*, along with supporting experiments.
 - High-Temperature Testing at PNNL and ORNL - The primary scope of the activities at PNNL and ORNL is to obtain high-temperature, structural test data for materials already irradiated at low temperatures under the APT Program, including high-temperature tensile testing and compact tension testing of 9Cr-1Mo and SS-316L specimens (irradiated and nonirradiated), microstructure investigations, reports on fatigue crack growth, fracture toughness, and tensile testing of weld materials. This includes transfer of small-scale testing capability from PNNL to LANL.
 - Materials Handbook and Related Activities - High-temperature structural testing of already-irradiated materials (at low temperatures) is being conducted. Additional testing of irradiated tungsten samples continued. The *Materials Handbook* will be maintained, and the scope will be expanded to include additional materials of interest to ATW applications.
 - Temporary Assignment at PSI (Materials Collaboration) - Robert Rutherford was invited to Paul Scherrer Institute in Switzerland to assist in tensile testing and TEM observations on irradiated SS-316L and F82H samples. This work also includes compression testing on various forms of nonirradiated tungsten.
 - LANL Hot-Cell Analyses – Post-irradiation tests such as bend, push-out, and hardness tests are being performed, and activated samples such as alloy-718 window, tungsten, and weld specimens are being analyzed. This work is a continuation of the APT Program.
 - Corrosion - Water corrosion tests to complete a Design Data Need (DDN) are being completed. Air corrosion tests were conducted to complete a DDN requesting air corrosion data to validate the design on components exposed to the APT cavity atmosphere, including the effects of exposure of construction materials for these components to expected APT mixed proton and neutron radiation and species produced from radiolytic reactions. This work is a continuation of the APT Program.

Highlights

- The readiness review for the Materials Test Loop was completed. Pre-start findings (mostly procedural shortcomings) are being addressed. The melt tank has been loaded with lead-bismuth eutectic.
- A final report was written that analyzed all the tensile data produced at PNNL from January 2000 through June 2001.
- The final reports on fatigue crack growth and weld tensile properties from ORNL were received.
- The closeout of DDN 031 (air corrosion) was completed and signed off (APT milestone).
- AAA employee Rutherford was invited to the Paul Scherer Institute in Switzerland to assist in the materials irradiation program.

LBE Technology – Materials Test Loop

During this quarter we started system testing, including several successful pressure tests, oxygen control system test, and data acquisition and control system (DACS) program module tests. We filled the melt tank with LBE. We also had a successful independent readiness review and addressed the majority of the pre-start findings. We updated the MTL Test Plan.

MTL Pressure Test - The LBE Material Test Loop has been successfully pressure-tested in the cold state (room temperature) using water with a helium cover gas. The previously specified flange bolt preload of 20 ft-lbs has been used. Water leaks in the LBE piping have been identified and corrected. In addition, gas leaks in the cover gas space of the various tanks have been reduced to an acceptable level of 6.5% per day at a pressure of 60 psig.

The retightening of the sump inlet flange to 30 ft-lbs during the initial (July 3) test increased the flange bolt preload above allowable levels. It was determined that the reason for the water leak at that time was a misalignment of the sump inlet flange. The piping was modified to correct the alignment by cutting and rewelding. Following this modification, a final pressure test was conducted to ensure the soundness of the system. The pressure-time history for this final test is shown in Fig. 33.

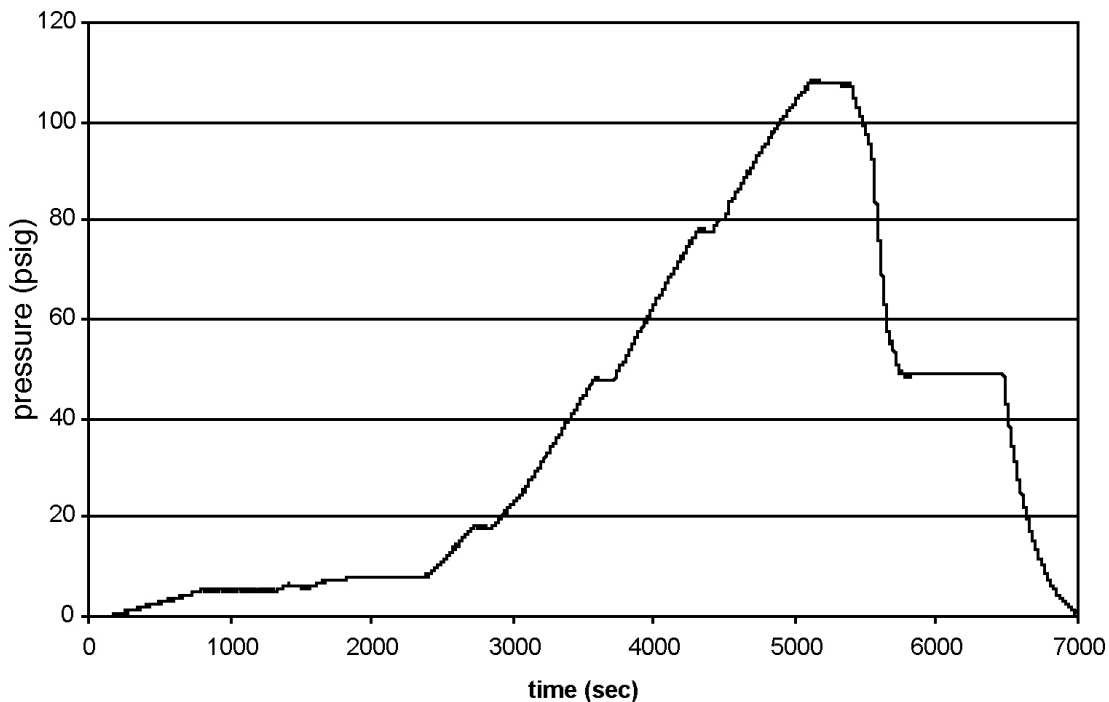


Figure 33. Pressure-time history for the pressure test.

Test of Oxygen Control System Mechanism - The oxygen control system mechanism was successfully tested using water and helium gas at room temperature. The mechanism for gas feeding, level and pressure control, and monitoring worked better than the design expectation.

Successful Fill of LBE into Melt Tank - The melt tank of the MTL apparatus was filled with approximately 4 tons of LBE. The LBE was in the form of 5-lb bricks. Many of the bricks were highly oxidized. Therefore, a process was developed to remove the oxidation prior to introducing the LBE into the melt tank. A small, heated fill tank was installed on top of the melt tank. The LBE bricks were melted in the fill tank where the oxidation could be skimmed from the top. The LBE was then drained into the melt tank through a valve between the fill and melt tanks in a continuous operation. The entire operation took about 2 1/2 days. The cooling curve of the melt indicated that the alloy is eutectic.

Test of DACS Modules - The DACS program is nearly complete and is under testing and tuning. Some of the modules were used successfully in the pressure test and LBE fill operation.

Independent Readiness Review - We provided the design, test/calibration, and safety documentation and presented pertinent materials to an independent readiness review panel. The review found some pre-start findings that were subsequently addressed. None of the findings was major, and many identified needed improvements in the formality of operations and document control. The responses to the pre-start findings will be issued shortly for final concurrence before the start of MTL test operations. A number of post-start findings will be addressed shortly during initial operations.

Professional Involvement - The MTL team submitted six papers to the American Nuclear Society (ANS) AccApp/ADTTA'01 conference to be held in Reno, Nevada, in November. "A Kinetic Model for Corrosion and Precipitation in Non-isothermal LBE Flow Loop" by X.Y. He was published in the *Journal of Nuclear Materials*.¹⁷ The paper "Active Control of Oxygen in Molten Lead-Bismuth Eutectic Systems to Prevent Steel Corrosion and Coolant Contamination" by N. Li was accepted for publication in the *Journal of Nuclear Materials*.

Materials Research

PNNL Activities

Technology Transfer to LANL - The new tensile test fixture that will be used in a tensile test frame in a LANL hot cell is currently being evaluated. The current design shows promise with some slight revisions.

Data Analysis at PNNL - A final report was written that analyzed all the tensile data produced at PNNL from January 2000 through June 2001. The results show that tensile properties obtained from SS-316L/304L irradiated in a mixed proton/neutron irradiation environment at low temperatures (50°C – 160°C) differ from tensile properties obtained from similar materials irradiated in a fission neutron irradiation environment at similar temperatures and doses. The most important difference is a reduced dose for the onset of loss of uniform elongation for the SS-316L/304L irradiated in the mixed proton/neutron environment. The results also show an increase in ductility in Mod9Cr-1Mo when tested at 400°C and 500°C after irradiation in a proton beam at 50°C – 70°C.

¹⁷ He, X.Y. *et al.*, "A Kinetic Model for Corrosion and Precipitation in Non-isothermal LBE Flow Loop," *Journal of Nuclear Materials*, **297** (2001) 214-219.

Shear-Punch Testing at PNNL - A new shear-punch test fixture is currently being evaluated that will be used to produce shear-punch mechanical properties data from APT TEM disks. The new fixture employs a displacement measurement device that more directly measures punch displacement. The result is a shear-punch load vs. displacement trace having greater similarity in appearance to a corresponding tensile load vs. displacement trace. The greatest benefit is that shear yield can now be measured at an offset shear strain in a manner analogous to the method used for measuring yield on a tensile test trace.

ORNL Activities

The final reports on fatigue-crack growth and weld tensile properties from ORNL were received and reviewed. We found that the fatigue-crack growth data determined from nonirradiated and irradiated subsize compact specimens are comparable with published data for the nonirradiated materials studied; in general, the present data indicate that high-energy, mixed proton/neutron irradiation may not have a significant effect on the fatigue-crack growth behavior of annealed SS-316L/304L out to 1 dpa, and out to 4 dpa for precipitation-hardened alloy-718, although it is recommended to investigate the rates after higher dose irradiations (Figs. 34 and 35).

ORNL also completed high-temperature fracture toughness tests on irradiated Mod9Cr-1Mo at 400°C and irradiated SS-316L at 300°C. Final analysis of the results is in progress.

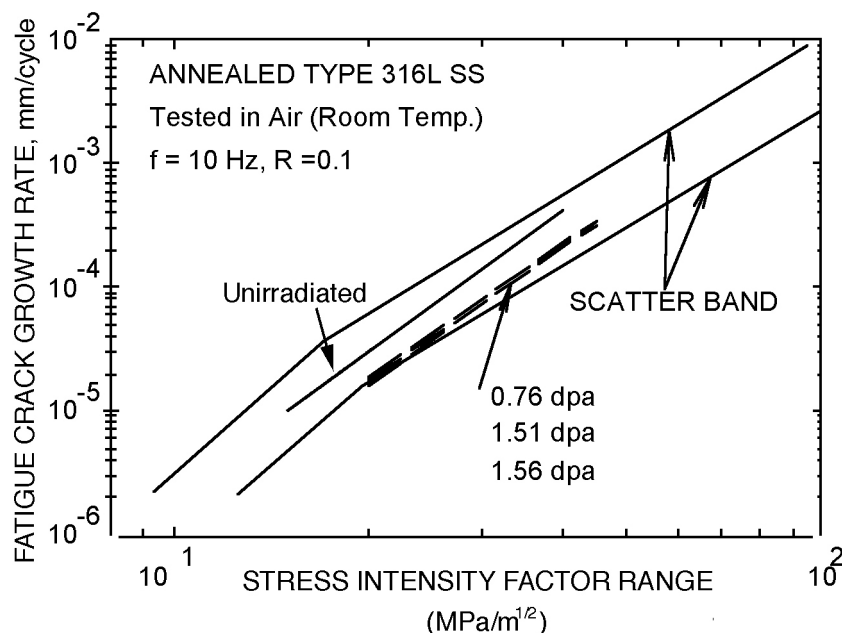


Figure 34. Fatigue crack growth data for annealed 316L stainless steel.

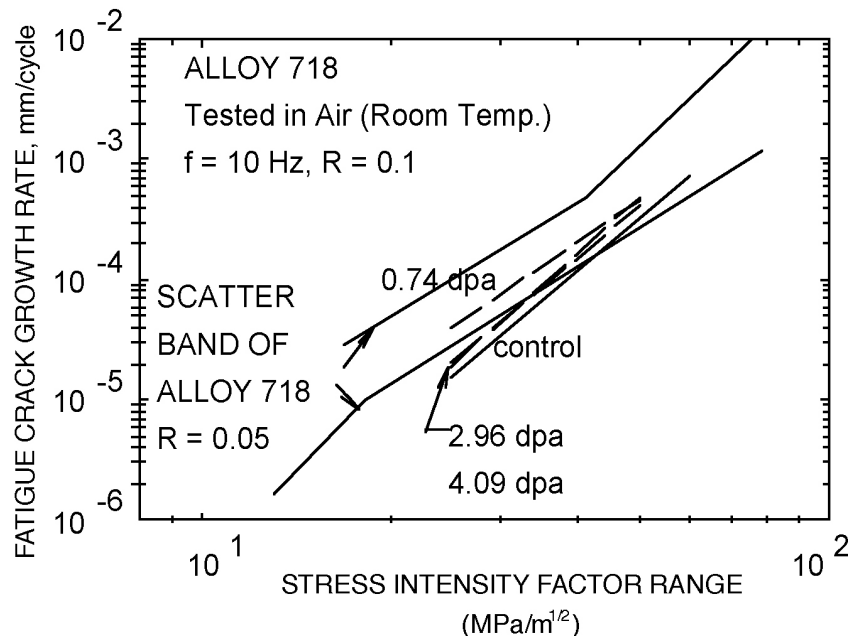


Figure 35. Fatigue crack growth data for precipitation-hardened alloy 718.

Materials Handbook Activities

Contacts were made with Cr-Mo steel experts at ORNL to obtain other information relative to the modified 9Cr material. They provided a list of more than 20 open literature references relative to the effects of irradiation on microstructure, swelling, tensile properties, fracture toughness, impact properties, and fatigue behavior. Copies of these documents have been obtained. Conditions represented in the references cover irradiation temperatures from 50°C to 600°C at doses up to 200 dpa. Drafting of a Handbook chapter [Chapter 19] on the Modified 9Cr ferritic steel is in progress.

We presented a paper on the *Materials Handbook* at the *Workshop on Materials Research for High-Power Accelerator Applications* at the *Fifth LANSCE User Group Meeting* in August. The paper was entitled "Materials Data for Particle Accelerator Applications: APT Materials Handbook."

The Handbook Coordinator visited the German Laboratory, Forschungszentrum Jülich (FZJ) in Jülich, Germany, at the Laboratory's invitation to discuss possible participation of the European Spallation Source (ESS) Project in the continued updating and expansion of the *Materials Handbook*. As a result, the ESS Project has offered to provide chapters on tantalum (a spallation target material and possible target containment materials) and mercury (the ESS spallation target material). FZJ personnel working to AAA specifications and requirements will author these chapters. Further, the chapters will be reviewed and approved by the AAA Program. Additionally, the ESS Project will provide new radiation effects data on alloy 718, SS-304L, SS-316L, and Modified 9Cr-1Mo-V ferritic/martensitic steel for incorporation into the Handbook.

During the same period, personnel from the Paul Scherrer Institute traveled to FZJ to discuss the possibility of providing a chapter on lead-bismuth eutectic (potential

spallation material in for AAA and several European spallation applications) for the Handbook. Whether we proceed with this collaboration will be confirmed in October.

Temporary Assignment at PSI

In the early part of summer, AAA employee Rob Rutherford passed his thesis exam and was subsequently awarded the Masters of Science Degree in Materials Science and Engineering from the University of Cincinnati. In June, he was invited to go to Paul Scherrer Institute (PSI) in Switzerland to participate in their materials irradiation program.

Tensile and TEM specimens were irradiated at PSI to a maximum dose of 12 dpa at temperatures from 300°C-400°C in the STIP I (Spallation Target Irradiation Program). These will be the first samples to be tested after irradiation in a proton beam at such temperatures, and the data are directly applicable to materials for the ATW program. The collaborative effort involves tensile testing and TEM observations on irradiated SS-316L and F82H samples. The work also includes compression testing of various forms of nonirradiated tungsten at room temperature to 300°C. The original three-month assignment was extended an additional month to November 2001. A detailed technical account of the work and its benefits to the AAA Program will be included in the next quarterly report.

LANL Hot-Cell Analyses

Hardness tests were performed and photos taken of the SS-304L and annealed alloy-718 cladding after irradiation to a maximum of 12 dpa. Hardness tests and photos were also taken on push-out specimens of SS-316L bonded to tungsten and annealed alloy 718 bonded to tungsten after irradiation to a maximum dose of 1.5 dpa at the high flux isotope reactor (HFIR) in ORNL.

Air Corrosion DDN

The production mechanism of nitric acid and its behavior is central to the disposition of the Air Corrosion Design Data Need. As a proton beam passes through air, nonradioactive O₃, NO, and NO₂ are produced by radiolysis of the air. The O₃ reacts with NO to produce more NO₂. In the presence of water vapor, NO₂ can then be converted by reactions with O₃ and radiation-produced free radicals such as HO and HO₂ to gaseous acid (HNO₃). In water, NO₂ (aqueous) can then be converted by reactions with O₃ (aqueous) and radiolysis products such as H₂O₂, to strong acid (H⁺ and NO₃⁻). These are all radiolytically enhanced chemical processes, not nuclear, and large quantities of materials are involved. (The general process is similar to *acid rain* production from NO and NO₂ produced during combustion, e.g., in gasoline-burning motor vehicle engines. In the acid rain case, the radicals are produced by ultraviolet light.)

In the APT cavity at 1 torr, conditions are expected to be predominantly dry; if HNO₃ is formed, continuous cavity pumping of the HNO₃ will reduce its concentration in the adsorbed water layer, thereby reducing corrosive effects. In the event that water is present, concentrated nitric acid can be present through the direct formation mechanism described above and because of the high solubility of the residual HNO₃. As the water is evaporated by pumping, the acid concentration goes up until its vapor pressure exceeds the partial pressure of the HNO₃ in the cavity, at which point it is volatilized. When the water is gone, so is the nitric acid, leaving HNO₃.

The HNO_3 production at low pressure should not scale with pressure since it is a multi-step set of reactions that depend on products of concentrations, which will all be much lower than those developed at LANSCE in the target area. As compared with the LANSCE target area, the HNO_3 concentration in the APT cavity is expected to be much less than the ratio of pressures (1 torr/590 torr). This reasoning supports the design assumption that the low pressure will be sufficient to decrease the air corrosion rates to acceptable levels.

The adverse corrosion effects of HNO_3 have been demonstrated at LANSCE, and many of the controlled observations were made in the course of the materials irradiation experiments conducted for the APT Project. The APT prototypic Al-6061-T6 to SS-304L blanket-tube transition joints irradiated at LANSCE were examined on the exterior surfaces exposed to the atmosphere in the target containment box. Observations using scanning electron microscopy (SEM) found that corrosion on the Al-6061-T6 alloy surfaces of the assemblies was clearly evident following irradiation and was attributed, primarily, to the presence of nitric acid. Energy-Dispersive X-ray Spectroscopy confirmed that the observed corrosion scale consisted of aluminum oxide.

The LANSCE target vacuum window (made from alloy 718) operated for nine months during APT irradiations. Corrosion was observed on the air side of the window, appearing as a dark area (presumably an oxide) that covered the area exposed to the proton beam. This type of corrosion appears to be uniform in the area exposed to the proton beam. The maximum calculated window temperature was 367°C in the center of the beam region.

The appearance of the external surfaces of the inserts in the 1998 irradiation was documented with photographs taken during packaging of the experimental assemblies for shipment to the hot cells and during examination in the hot cells. Al-6061-T6 surfaces were discolored while SS-304L stainless steel piping surfaces not in the direct beam were not discolored. Significantly, the type of corrosion on the Al-6061-T6 appeared to be uniform.

These observations can be considered a worst-case situation for APT, and even though conditions are not prototypic, they do represent air corrosion in the presence of air irradiated by an intense proton beam. These observations will be included in a DDN response. Further analysis of the surfaces of the APT inserts is recommended to determine oxide composition, the form of the scale, and the thickness.

Even though this work was performed in direct support of the APT DDN program, the results and the considerations are applicable to the AAA Program. Additional work is recommended. Low-pressure (1 torr of air) laboratory corrosion studies should be conducted on candidate materials under varying conditions of water vapor, HNO_3 concentration, and temperature. As further refinement, it appears feasible to undertake a calculation of the production rates of HNO_3 in the APT cavity vessel using radiolysis data, radiation field predictions from MCNPX, and the "acid rain" database. A measurement of total acid production at the LANSCE target has been accomplished and would provide a benchmark for such calculations.

This page left intentionally blank

IV. ENGINEERING DESIGN & DEVELOPMENT

6. APT Engineering Design

Scope

The focus of APT Engineering Design during this phase of the project is two-fold. First, we are completing the preliminary design phase to the extent described in the *APT Preliminary Design Plan*. This entails capturing the design in such documents as system design descriptions, general arrangement drawings, and piping and instrumentation diagrams (P&IDs), among others, and documenting the bases for the design in calculations and technical reports. Release of the *Preliminary Design Status Report* formalizes completion of the preliminary design phase. Second, we are archiving APT documentation to support an efficient Project restart, if required.

Highlights

- We released the *Preliminary Design Status Report*, meeting a Level 1 APT milestone on schedule.
- Fifteen Level 3 milestones were completed this quarter with the release of system design descriptions for APT systems and structures.
- Other Level 3 milestones completed this quarter include the release of the technical report, *Normal Conducting/Superconducting (NC/SC) Technology Study for the APT Linac*, and completion of the target/blanket preliminary design status review.

Preliminary Design Status

Preliminary Design Status Report - With DOE concurrence, we released the *Preliminary Design Status Report*, meeting a Level 1 APT milestone on schedule. The report summarizes the status of the APT design and technology as of September 2001 and provides a road map to the more detailed documentation making up the APT Preliminary Design Package.

APT Archiving - We completed archiving APT documentation and records. A total of 125 boxes of APT documentation was required to capture the Project. The archived material is stored at the Los Alamos National Laboratory Records Center. Access to APT document and records is unaffected by this archiving, and the APT Information Management System (IMS) continues to operate as usual. We also completed archiving the APT Design Basis Database, with its supporting files, and all APT computer-aided design (CAD) files.

Target/Blanket Status Review - The target/blanket preliminary design status reviews were completed. The reviews provided an update on progress in target/blanket design and analyses since the last review, held in July 1999. Among the topics addressed were target and blanket design, prototyping, physics, shielding, thermal-hydraulics, and seismic and structural analyses.

Top-Level Documents

APT Reference Design Cost Estimate - The APT cost estimate was updated and released, documenting revisions to the estimate made this year.

APT Environmental Requirements - We revised and released the *APT Environmental Design Requirements* document.

AAA Environmental Impact Statement - The *AAA Technology Report* was released. This report is a compilation of data required for the development of an Environmental Impact Statement (EIS) for the AAA Program. In July, the Operations Project Office (OPO) hosted a two-day meeting at the Savannah River Site (SRS) for the AAA EIS team to review support facilities for the project. Discussions covered material flows, schedules, and permitting.

System Design Descriptions

The release of updated and revised system design descriptions completed 15 Level 3 milestones. For most of systems, SDD work involved updating functions and requirements, and describing the designs that satisfy the requirements. SDDs released this quarter include the following:

- Radio-Frequency Power System
- High-Energy Linac System
- Cavity Vessel System
- External Shielding System
- Target/Blanket Building Remote-Handling System
- Integrated Control System
- Isotope Recovery System
- Main AC Power System
- Radiation Exposure Protection System
- Health Protection Monitoring System
- Balance-of-Plant (BOP) Heat-Removal System
- Target/Blanket Hot-Cells System
- Production Building HVAC System
- Liquid Radioactive Waste System
- Cryogenics Building

Technical Reports, Calculations, and Models

Accelerator Reports - We completed the technical report, *Normal Conducting/Superconducting (NC/SC) Technology Study for the APT Linac*, completing a Level 3 milestone. Other reports released include the *APT Coupled-Cavity Drift Tube Linac (CCDTL)*, *Coupled-Cavity Linac (CCL) Thermal/Mechanical Analysis*, and *High-Energy Linac Cryomodule Structural Analysis*, as well as technical reports on the waveguide coupling to coupled-cavity linac cavities and on the design of the higher-order-mode coupler for superconducting cavities in the high-energy linac.

CCT Code - We completed the document, *CCT: Coupled-Cavity Tuning Code - Specifications and Design Description*, which presents the specifications for the computer code CCT and describes the design of this code.

Cryomodule Model - We completed a model of the cryomodule assembly for the $\beta=0.175$ spoke cavity section of the all-superconducting low-energy linac as part of the technology study for the low-energy linac. We developed initial layouts of the cryomodules in the tunnel integrated with the RF power system and cryogenics system.

Target/Blanket Reports - We released *APT Blanket Assembly Fabrication Development*, satisfying a Level 3 milestone. We also released the *APT Clad Tungsten Target Prototype Development Report* and the calculation report, *Stress Analysis of Large-Diameter Target/Blanket Jumpers*.

Electrical Calculations - We released the *Power Distribution System Equipment Sizing and System Analysis Calculation*. The analysis calculates short circuit duties at various distribution bus locations. Results confirmed that the selected distribution equipment ratings envelop the calculated device duties. The short circuit and circuit analysis calculation was also completed and released. This calculational result confirmed that the designed distribution equipment ratings envelop the calculated device duties.

Master Equipment List - We completed a final check of the consolidated *APT Master Equipment List*. This list includes all tagged electrical distribution equipment pertaining to the Main Power Supply, NonSafety Class DC/Uninterruptible Power Supply (UPS), Safety Class DC/UPS, and Construction Power Supply Systems.

Seismic Analysis - We completed and released the accelerator tunnel 3-D seismic analysis report.

Transient and Availability Analyses - We released the *APT Transient Analysis Report*. This document describes the transients specified in the plant design duty cycle. The *Methods and Data for APT Availability and Reliability Analysis* report was also released. This document provides details and data sources used for APT availability analyses and probabilistic risk assessments.

Safety Calculations - Calculation reports documenting accident analyses prepared for the draft *Preliminary Safety Analyses Report* were released, completing the APT safety milestones for FY01. We also began the ADTF hazard analysis effort. A two-day meeting was held with the target materials test facility and subcritical multiplier design teams. The initial draft of the hazard analysis tables were prepared and circulated for comment.

Design Changes

Accelerator Design Change - The design change request to reconfigure the low-energy linac into smaller modules, was approved.

Drawings and Specifications

Intertank - The last two intertank documents, *Fabrication & Assembly Specification for the High-Energy Linac Medium Beta Intertank* and *Design Specification for the High-Energy Linac Power Supply*, were released.

Heat Removal and RadWaste P&IDs and PFDs - The piping and instrumentation diagrams for the BOF Heat-Removal System and for accelerator heat removal were released. We completed the process flow diagrams (PFDs) for the Window Heat-Removal System and the Gaseous Radioactive Waste System.

Site, Building, and Electrical Drawings - A number of site, building, and electrical drawings were released, including the following:

- Architectural and structural drawings for the accelerator tunnel, klystron gallery, and injector building;
- Target/blanket building structural drawings;
- Tritium Separation Facility (TSF) architectural plan drawings;
- Klystron gallery, mezzanine, and mechanical service building general arrangement drawings;
- Large-bore underground piping arrangement drawings that show piping among the mechanical service buildings, accelerator tunnel, and cooling towers;
- Approximately 60 civil engineering drawings;
- Site grading and road drawings;
- NonSafety Class DC and UPS System SS Group-A and Group-B single-line diagrams;
- Electrical grounding details sheets 1 & 2; and
- Primary Substation #1 grounding plan.

Archived Work in Progress - The Radiation Exposure Protection block diagrams, the Window Heat-Removal System P&ID, and plan architectural drawings for the general warehouse, simulator and training, administration, construction management, and security portal buildings were designated works in progress and were entered into the APT IMS for archiving.

7. Accelerator-Driven Test Facility

Scope

The scope of work covering the preconceptual and conceptual design activities for the Accelerator-Driven Test Facility is as follows:

- **Design** – The design covers both the preconceptual and conceptual phases of the ADTF project and includes the Target and Material Test Station, the Subcritical Multiplier, the accelerator, and the balance of facility segments. The preconceptual design will support a Critical Decision 0 (CD-0) for the

Project, *Approval of Mission Need*, originally scheduled at the end of the second quarter FY01. The conceptual design will commence thereafter and continue throughout the remainder of FY01, ultimately leading to CD-1 (*Approval of Preliminary Baseline Range*) at the end of FY02.

- **Systems Integration** – Integration activities include:
 - Development of the functional and performance requirements for the ADTF project;
 - Definition and control of the design interfaces between major facility segments;
 - Coordination of internal and external design reviews;
 - Technical risk assessment; and
 - Cost estimating.
- **Project Management** – Project Management activities include:
 - Definition and control of work scope;
 - Budget allocation and management;
 - Preparation and maintenance of integrated project schedules; and
 - Issuance of periodic technical and management progress reports.

Highlights

Systems Integration

- The *ADTF Missions, Functions, and Performance Requirements* document was approved and issued. This document establishes the initial requirements baseline for the facility.
- A revised ADTF preconceptual cost estimate was prepared to define the direct construction cost of the Target and Material Test and Subcritical Multiplier stations. These costs will be used to evaluate alternate project strategies to meet the AAA Program goals.

Target Multiplier Test Station

- Calculations have been performed, indicating that for a given beam power, an annular target geometry (where the test section is inside an annular target region with inward leakage of spallation neutrons) can provide twice the fast flux achieved as the configuration with the test section on the side (analyzed previously).

Subcritical Multiplier

- The assessment of the four options being considered for the SCM design (vertical and inclined beam entry; inner vessel, and redan) has been completed, and the vertical entry option with an inner vessel was formally selected as the reference design.
- A conceptual design for the structure supporting a high-energy beam transport (HEBT) above the SCM has been completed. The structure includes systems for refueling operations and for replacement of the in-pile beam tube (IPBT).

- A reference design for the lead-bismuth target has been completed for the SCM vertical entry configuration. Neutron characteristics for the reference design have been estimated. Thermal-hydraulics and structural analyses have been conducted to support the reference design.
- The effects of minor actinides and plutonium in the multiplier core physics are being studied as part of the DOE/CEA collaboration. Preliminary results for several loadings with a metal-fueled driver multiplier have been obtained.
- The comparison of oxide and metal-fueled driver-multiplier assemblies is also being studied as part of the DOE/CEA collaboration. Preliminary comparisons of multiplier physics parameters have been obtained.

Balance of Facility

- The TMT hot cell has been sized to provide post-irradiation examination capability for the SCM experimental fuel. Functional flow block diagrams were prepared to show movement of materials between the SCM and the hot cell.
- A trade study was completed, evaluating alternate shielding designs for the SCM building.

7.1 Systems Integration

Overall Facility Design and Arrangement

The ADTF is configured as a multiple-station facility. The baseline project scope will include construction of two target stations:

- **Target and Material Test Station** – This station will provide a test environment for materials and fuel experiments and the evaluation of alternate coolant and target technologies. The design basis will also include the potential to demonstrate tritium production, as well as the potential for isotope production.
- **Subcritical Multiplier 100 MW** – This will provide a test environment for the demonstration of coupled operation of the accelerator, target, and multiplier. Its design basis will include the capability to irradiate significant quantities of fuel, with the eventual transition to an actinide core.

A third target station, an international user facility, would be constructed at a later date. A schematic arrangement of the ADTF is shown in Fig. 36 below.

ADTF Major Elements

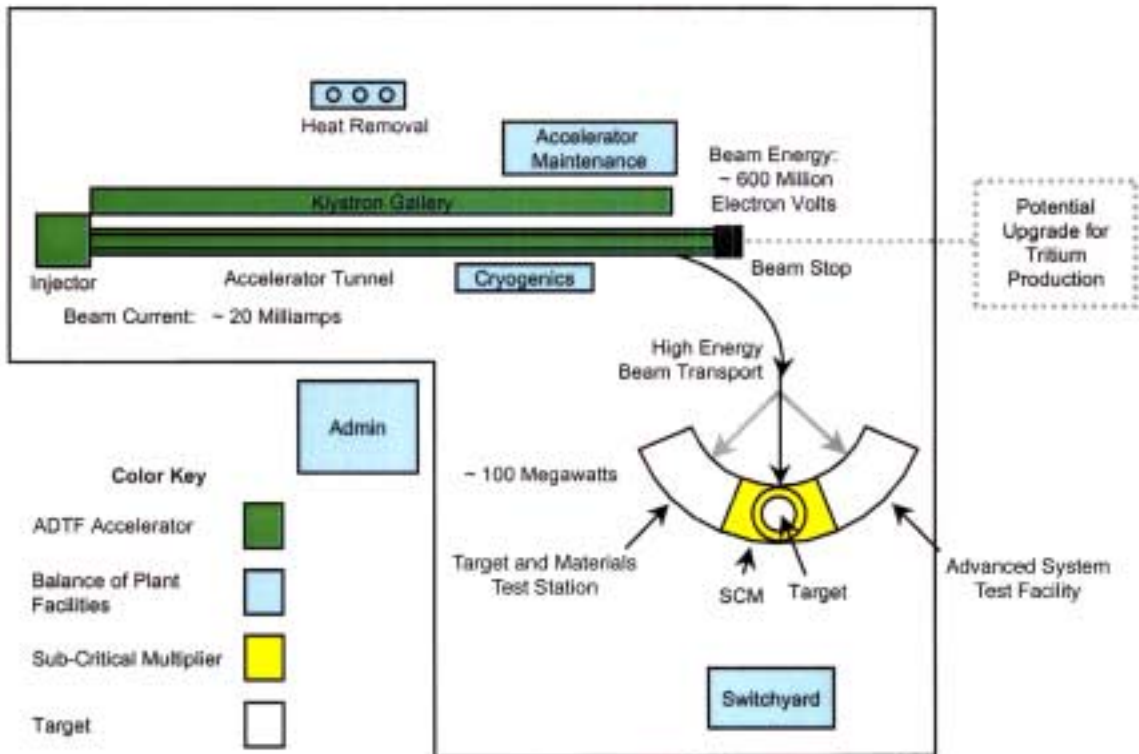


Figure 36. Schematic of the Accelerator-Driven Test Facility.

ADTF Missions, Functions, and Requirements

After completing several reviews, both internal and external, the Missions, Functions, and Requirements document for the ADTF was approved and issued. This document reflects the initial requirements baseline for the facility at the completion of preconceptual design.

Cost Estimate

Using the best available design information, a revised preconceptual cost estimate was prepared for the direct construction cost of the TMT and SCM stations. Vendor quotes were solicited for the major process mechanical equipment. Some difficulty was encountered in finding interested or qualified vendors for the major nuclear components (e.g., vessel) of the SCM. Where vendor quotes were not available, scaling factors were applied based on historical data either from the Spallation Neutron Source Project (for the TMT) or the Experimental Breeder Reactor (EBR-II) facility (for the SCM). The civil-structure estimate was developed by quantity takeoffs from design sketches of the major buildings. Other elements of costs (such as electrical, instrumentation, and cooling water) were derived parametrically by scaling from the APT estimate.

The cost estimates will be used to evaluate alternate project strategies for the ADTF. The following options can now be costed:

- A multi-station ADTF, as envisioned in the CD-0 package submittal, that will have both TMT and SCM stations coupled to a 600-MeV, 13-mA accelerator.
- A single-station ADTF with only the TMT station initially constructed, but with the capability to append a SCM sometime in the future.
- A TMT station constructed at LANL and coupled to an upgraded LEDA facility.

7.2 ADTF Target and Material Test Station

TMT Design

The TMT station is comprised of a spallation neutron source driven by a continuous proton beam operating at 600 MeV and 13-20 mA of current. The configuration is designed to provide optimum flexibility in the testing of materials, coolants, targets, and fuels that are envisioned for use in accelerator transmutation of waste systems. In addition, this station provides a versatile irradiation environment that allows for testing of advanced nuclear systems such as Generation-IV fuels, and production of isotopes for commercial and medical use. The concept consists of a centrally located irradiation chamber that contains the spallation neutron source (target) and surrounding reflectors, moderators, and closed coolant loops. The entire chamber is shielded with 5 meters of steel and concrete to protect workers. The proton beam, target, and materials tests are all brought into the cell horizontally or vertically (Figs. 37 and 38). This provides for a simple, straightforward beam transport system

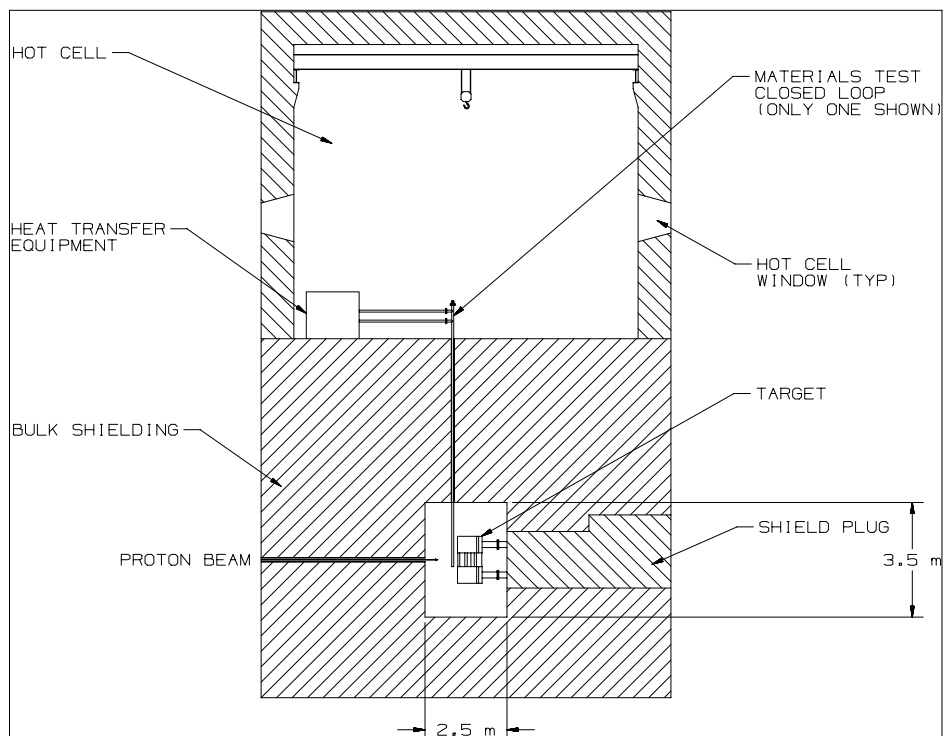


Figure 37. TMT elevation view.

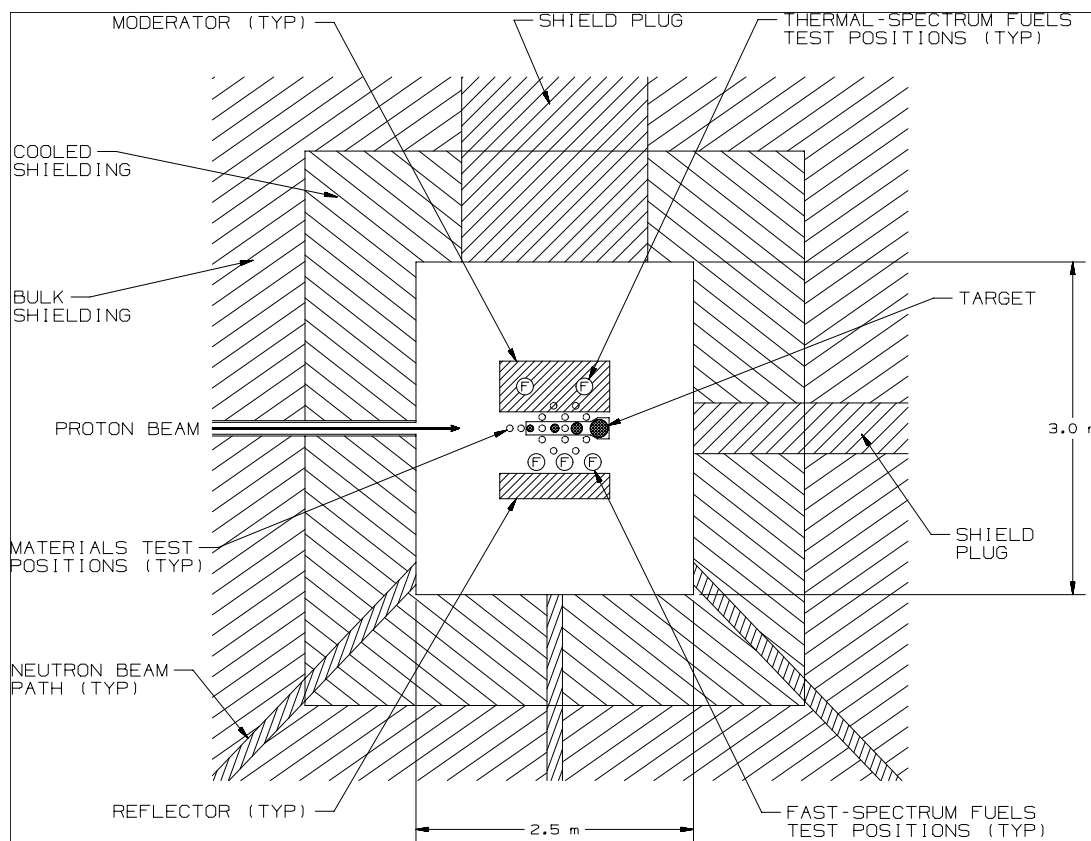


Figure 38. TMT plan view.

from the accelerator to the irradiation chamber. In addition, the mechanisms for implementing a horizontal target and multiplier insertion configuration are a demonstrated technology based on existing and planned facilities. At the completion of an irradiation cycle, target and test components are moved into and out of the irradiation chamber from adjoining hot cells. All primary heat-removal equipment resides in the hot cells, providing for safe operation and maintenance similar to operations at the Spallation Neutron Source.

Target Design Options

To provide optimum flexibility for both fast-spectrum and thermal-spectrum irradiations, two major target/reflector/moderator configurations are being investigated: wing geometry and annular geometry (Fig. 39). The base-case system employs a reflector adjoining the neutron source in *wing* geometry where the neutron source is centrally located, and the test region sets off to the side (Fig. 40). Neutrons produced in the target by spallation leak radially outward into the adjoining reflector. Using this geometry, and with the accelerator providing a continuous flow of protons at 600 MeV (13 mA), a fast-spectrum neutron flux of 1×10^{15} n/cm²/s is generated in the reflector. Within this region, closed loops are used to irradiate fuels and materials in either a sodium, lead-bismuth, or helium coolant. In addition to the fast spectrum, a thermal spectrum is possible by replacing the reflector with a moderator. In this region, thermal fluxes of up to 4×10^{14} n/cm²/s are possible, providing an excellent environment for the irradiation of advanced fuels and materials for next-generation

reactors. For example, advanced fuel for a graphite-moderated, helium-cooled system can be tested using this configuration.

The design studies for the spallation target technologies of interest—lead-bismuth eutectic, sodium-cooled tungsten, and helium-cooled tungsten—were reported in the previous quarterly report (April–June 2001). The emphasis in this quarterly report is the design studies for the annular target option.

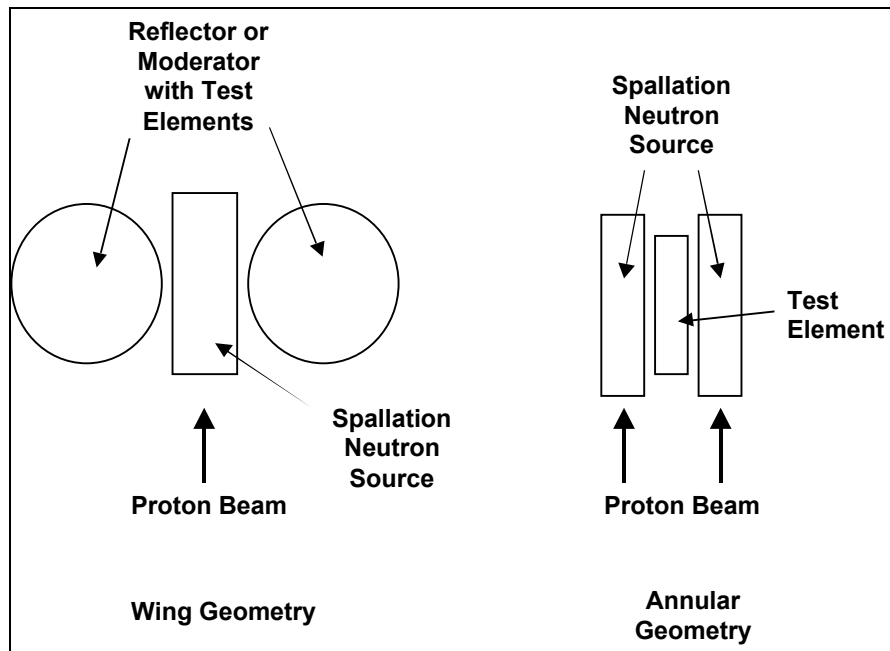


Figure 39. Target design geometry options.

Annular Target Geometry Option

Because of the need for a more intense neutron flux for irradiating fast-spectrum fuels and materials above what is achievable with the wing geometry, the annular geometry was investigated. The conceptual layout of this target geometry is shown in Fig. 40. For this option, the beam is rastered into an annulus (inner and outer radii of beam spot are approximately 5 cm and 15 cm, respectively). This spot matches the location of the spallation target with adequate margin for beam position. Neutrons produced in the target leak inward towards the test section, as well as radially outward towards the reflector. Analyses show that at 600 MeV and 13 mA, a fast-spectrum neutron flux of 2×10^{15} n/cm²/s is achievable in the test section. Therefore, for a given beam power, this target option doubles the neutron intensity over that of wing geometry.

Although the flux can be doubled using this innovative geometry, it is still below the 3×10^{15} n/cm²/s value desired by the fuel and materials researchers. Therefore, scoping physics calculations were performed to determine the beam current and energy required to reach a fast neutron flux of 3×10^{15} n/cm²/s. As shown in Fig. 41, with the annular target geometry, a 600-MeV, 20-mA beam can achieve this flux level. Since higher beam energies are more efficient at producing neutrons, the beam

power requirement decreases with energy. A beam energy of 600 MeV offers the benefit of the power density in the target reaching a balance between the Bragg peak and the spallation peak. Thus, from a power density and target size standpoint, this energy offers an optimum. From a cost standpoint, the lower beam energies are preferred because the accelerator is shorter. The 600-MeV proton energy offers a reasonable compromise between target engineering, efficiency, and cost.

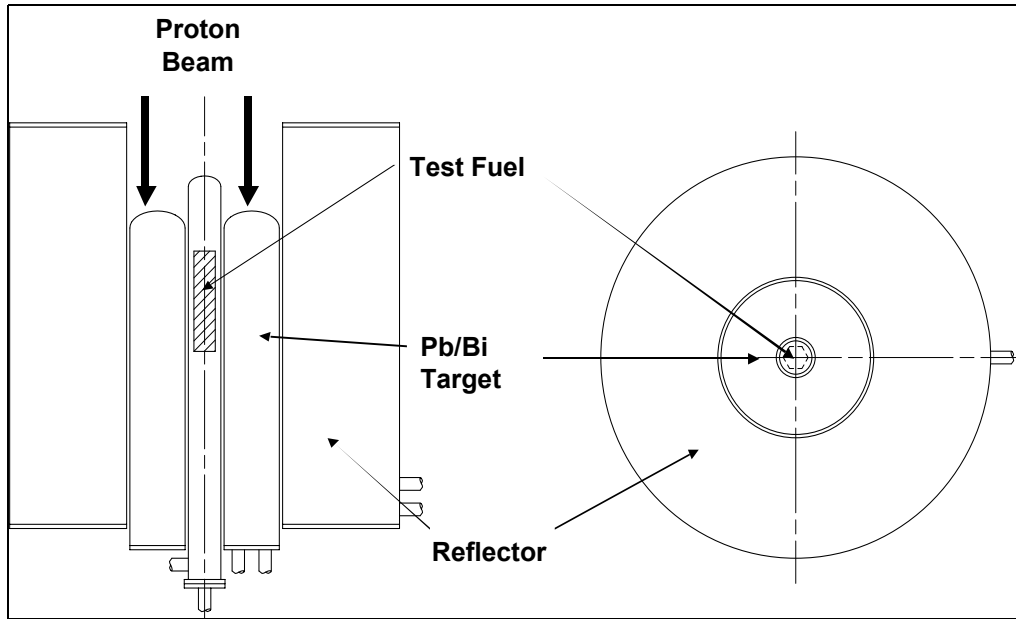


Figure 40. Annular target geometry.

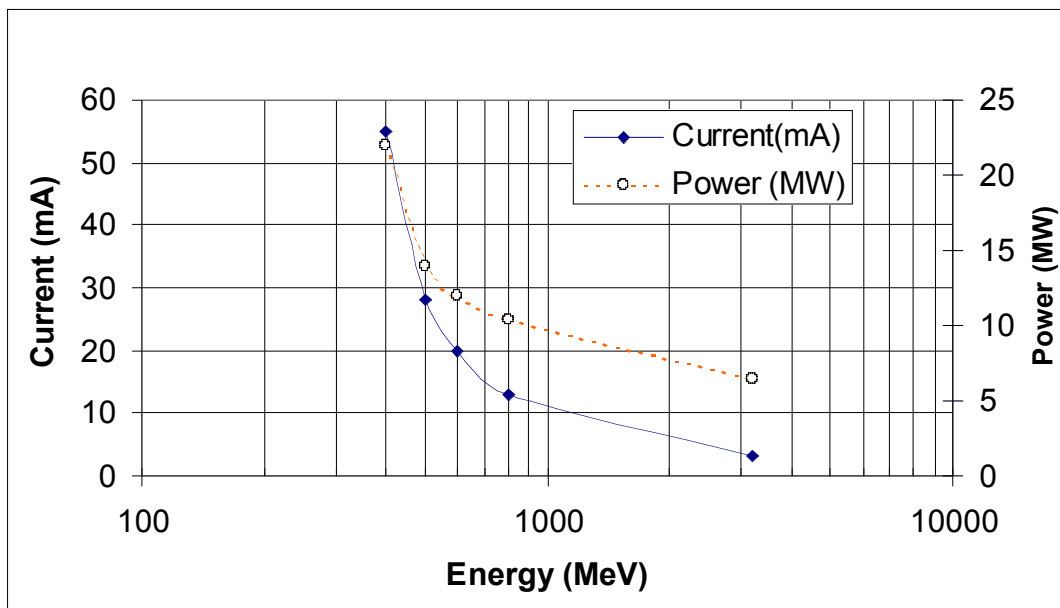


Figure 41. Beam current vs. energy to achieve 3×10^{15} n/cm²/s.

Table 7 summarizes the flux, radiation damage and burnup of fuel for this system. Very high flux intensities and fuel burnups are achievable. Assuming a fuel region in the test section that is representative of a 19-rod bundle, a very uniform flux distribution is calculated both axially and radially. Spectra are similar to that of fast reactors with the addition of a high-energy tail caused by the spallation neutrons.

Table 7. Neutronic Performance of the Annular Target Option

Parameter	Value
Total neutron flux in the test section	3.3×10^{15} n/cm ² /s
Fast neutron flux (<0.1 MeV) in the test section	3.1×10^{15} n/cm ² /s
High-energy neutron flux (<20 MeV) in the test section	1.3×10^{15} n/cm ² /s
Fuel Burn-up in 300 full-power days	
Minor Actinide Fuel	10.0 atom % / year
Plutonium-239 based fuel	15.5 atom % / year
Uranium-235 based fuel	11.9 atom % / year
Radiation damage in steel in 300 full-power days	75 dpa/y
Helium production in steel in 300 full-power days	500 appm/y

Calculations of the radiation damage are also shown in Table 7. Here, we observe that for a 300-day year of operation, 75 displacements per atom (dpa) of damage are realized in the test section. This is very similar to what is expected in a fast reactor with similar flux intensity. However, in addition to this damage, 500 atomic parts per million (appm) of helium are generated in the structural materials. Thus, although the very high fluxes and burnups are achievable, the helium production is high for cladding materials and needs to be reduced in order for the pins to achieve higher burnups before the cladding reaches its end-of-life. Based on studies of accelerator-driven systems, our goal is to achieve no more than 75 appm helium per year of irradiation. To achieve this reduced helium production, we are investigating the use of buffers between the spallation target and the test section.

Sample results are shown in Figs. 42 and 43 for the neutron flux and helium production in and around the target. In this example, a 14-MW beam is used with an energy of 500 MeV and a beam current of 28 mA, irradiating a lead-bismuth eutectic target. The beam is rastered over an annular surface of 400 cm² (target inner and outer radii are 9 cm and 17.8 cm, respectively). Inside the target, a depleted uranium buffer is used with a radii thickness of 6 cm. The buffer is used primarily to filter the high-energy neutrons responsible for high helium production rates, with minimal loss to fast neutrons. In this specific example a burnup rate of 6.2% is achieved for minor actinide fuels.

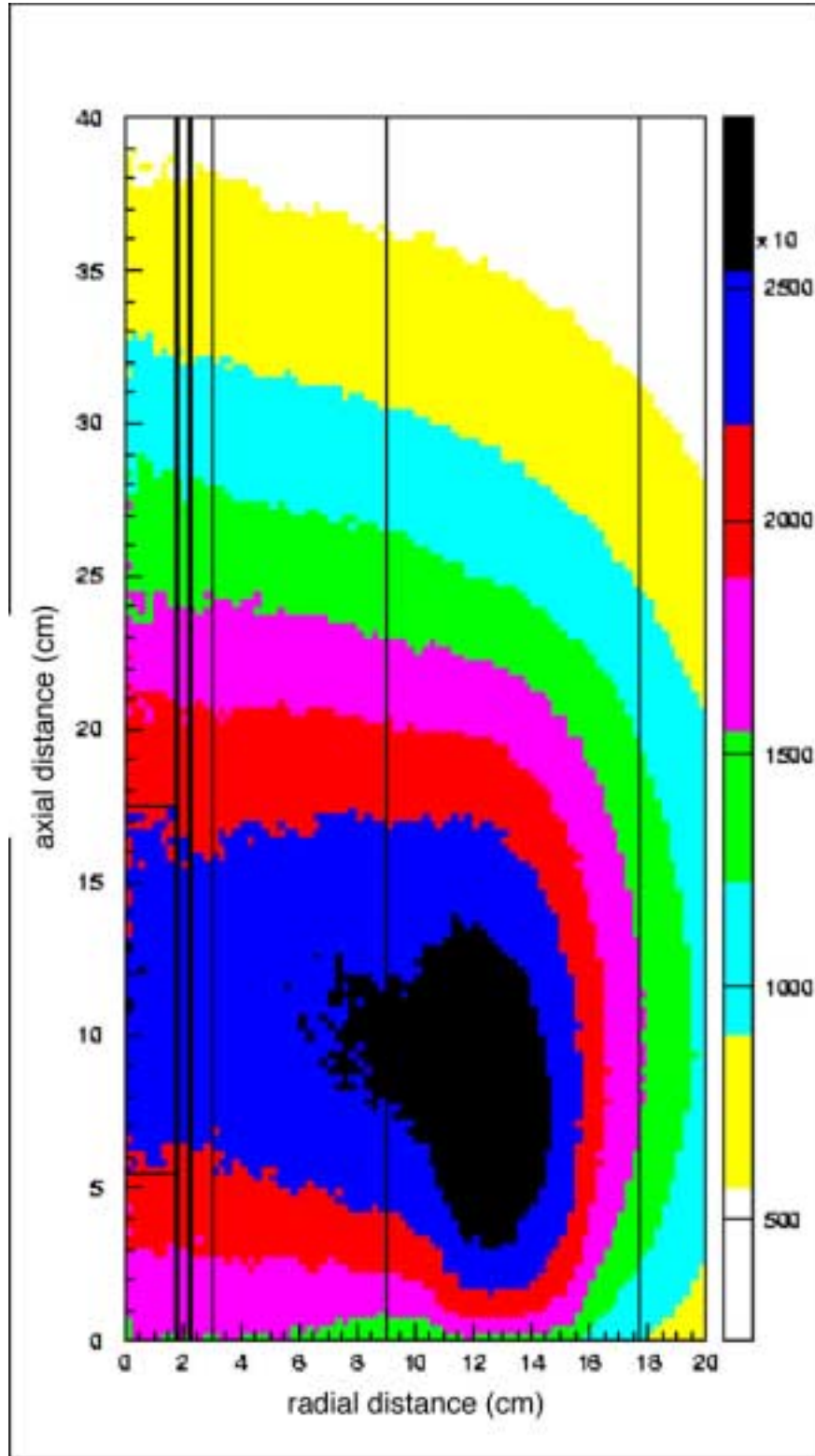


Figure 42. Neutron flux distribution around the target (fast-flux; unit: $\text{n}/\text{cm}^2/\text{s}$)

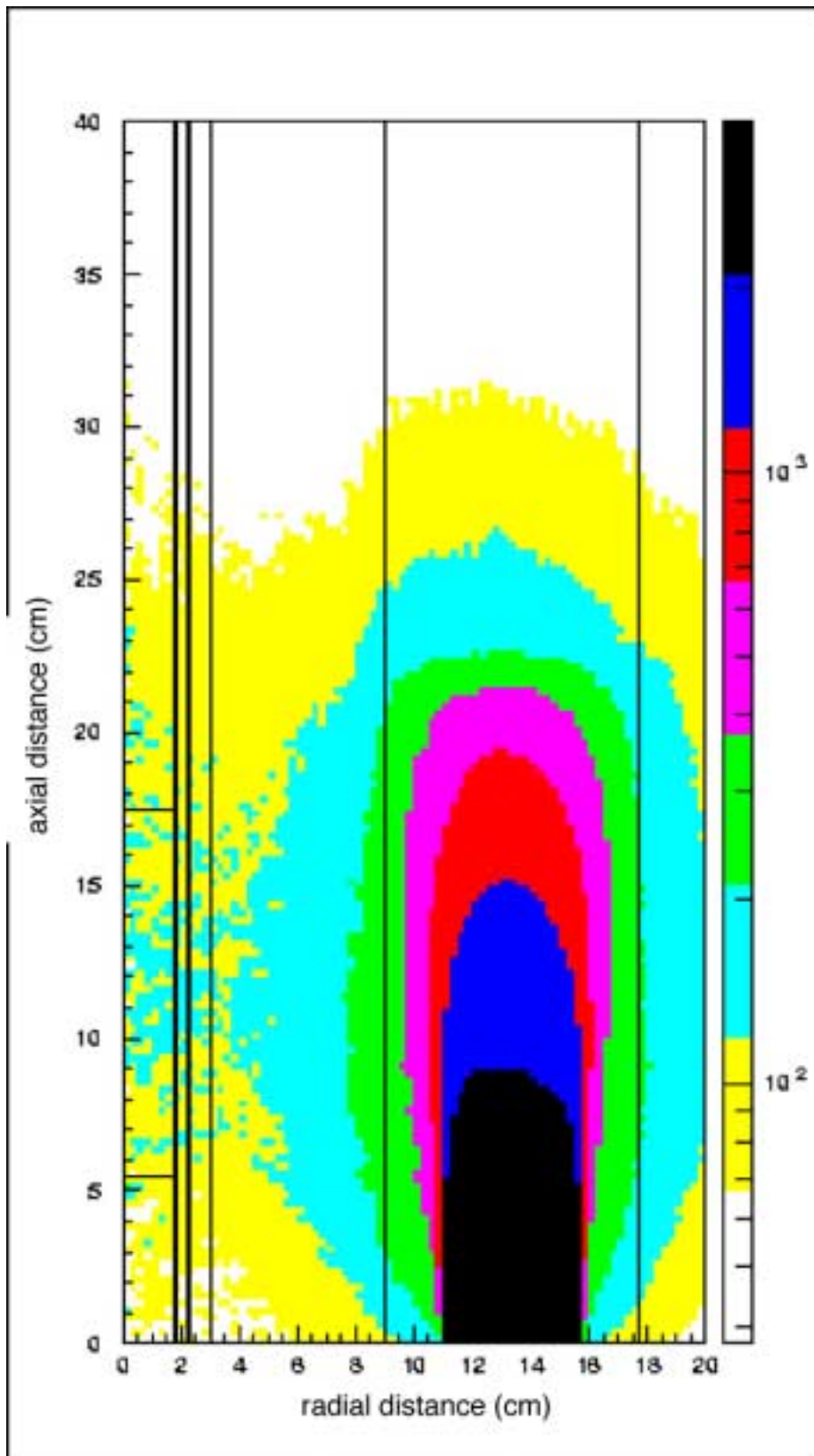


Figure 43. Helium production rate around the target (unit: appm/y).

Conclusion

The ADTF TMT preconceptual design studies have been performed to determine the optimum target geometry and materials for irradiations. Both wing geometry and annular geometry have been considered for the spallation neutron source, as well as LBE and tungsten targets. Calculations show that the wing geometry offers excellent flexibility for the irradiation of materials, especially in a moderated spectrum. However, to achieve fast-flux levels of interest to fuel and material designers, the annular geometry performs significantly better, with a doubling of the flux intensity. The results show that for a 600-MeV, 20-mA proton beam, a fast neutron flux level of 3×10^{15} n/cm²/s is achievable. Future studies will be performed to reduce the helium production in the test section to more representative levels expected in ADS systems. For the target material, an LBE target is preferred over that of sodium-cooled tungsten and helium-cooled tungsten. This target provides a very high power density capability and high neutron leakage. In addition, the waste stream is reduced over the solid target options because the target structure only needs to be replaced. Nevertheless, the facility will provide the capability to test the various target options in order to support the transmutation research program.

ADTF Subcritical Multiplier - 100 MW (SCM-100) Design

The design activities for the sodium-cooled, pool-type subcritical multiplier continued during the quarter in several major areas. The overall facility design progressed in preparation for the conceptual design phase that will start after the approval of CD-0. Four major configuration options have been assessed (different geometries for the beam insertion, consideration of an inner reactor vessel in the sodium pool or use of a redan design). The vertical entry with an inner vessel has been formally selected as the reference design after carefully verifying that all equipment could be placed above the SCM primary vessel cover and rotating plugs. The feasibility of performing the refueling operations and replacement of the in-pile beam tube has also been verified.

After the formal selection of the reference design, further work on the design of vessel cover penetrations for the major pieces of equipment was done. The decay-heat removal systems have also been added to the design.

A reference liquid lead-bismuth target design has also been selected based on the thermal-hydraulics and structural analyses. Neutron characteristics of the spallation source have also been estimated.

A draft report on the selection of a pool-type design for the SCM, as opposed to a loop configuration, has been prepared. The draft report has been submitted for review.

Several coordinated activities were also continued during the quarter. Meetings have been held with the other ADTF design teams to coordinate the design of the different pieces of the ADTF (SCM, TMT, common facilities, balance of facility, and beam transport). A meeting to initiate the ADTF hazards assessment was also conducted. The SCM team also participated in meetings to provide information for the ADTF cost estimate, to be completed at the end of the fiscal year.

The DOE/CEA collaboration in the area of the SCM has been progressing, with core physics studies addressing the loading of minor actinides and plutonium in different proportions to the multiplier. Comparison studies of the neutron physics performance of metal and oxide driver fuel in the multiplier has also been initiated.

Support for development of the Environmental Impact Statement and the experimental plan continued during the quarter. Process flow diagrams for the ADTF were developed as a function of the various research and operational phases of the project, identifying the various support facilities and mass flows. A report on the mass flows for the SCM and TMT is in the final stages of preparation.

Sodium-Cooled Fast-Spectrum SCM Design

During this quarter, the vertical-entry internal-vessel design was formally chosen as the preferred approach for the SCM-100, and documentation of the selection process was initiated. Before this selection was finalized, it was necessary to verify that all equipment, including the high-energy beam transport tube, could be placed in the reduced space above the primary vessel cover, in the small rotating plug, and that the design was indeed feasible.

Space for the control-rod drives, the fuel-handling gripper, the internal-vessel cover-lifting mechanisms was laid out on the small rotating plug, along with a more realistic interface with the in-pile beam tube (IPBT). Mutual sealing and support of the rotating plug and the permanent cover were also included with realistic dimensions, along with pathways for movement of equipment, including the IPBT and its handling cask, the fuel-unloading machine, and the large sodium pumps and heat exchangers mounted on the cover, should they ever need to be removed. The control-rod drives are assumed to be minimal units (e.g., servo or stepper motors) capable only of accurate placement of the rods within the multiplier region, with no provision for rapid shutdown or scram. The possibility of a removable fuel-handling gripper was evaluated as a means of reducing the congestion on the small rotating plug, and it is felt to be a viable option, if necessary.

Layouts of vertical and plan views of the SCM-100 were further refined to include the high-energy beam transport support structure, which allowed us to verify that the dimensions of a structure capable of supporting the ~50 metric tons of magnets, vacuum pumps, beam monitoring instrumentation, etc., were consistent with the placement of the other multiplier-related equipment as reported previously. The current SCM reference design, including the HEBT support structure, is shown in Fig. 44.

After verifying the feasibility of the vertical entry, efforts began to include other, less space-critical systems and components such as the shutdown heat-removal (SHR) NaK loops, their piping runs, and the piping runs for the secondary Na system. Routing of this piping may pose some challenges because it must penetrate the buried SCM containment shell and extend to the Na-to-air heat exchangers located at grade; the SHR piping may be especially difficult because it will probably penetrate the earthen berm around the containment, which is envisioned as providing the necessary shielding for the HEBT.

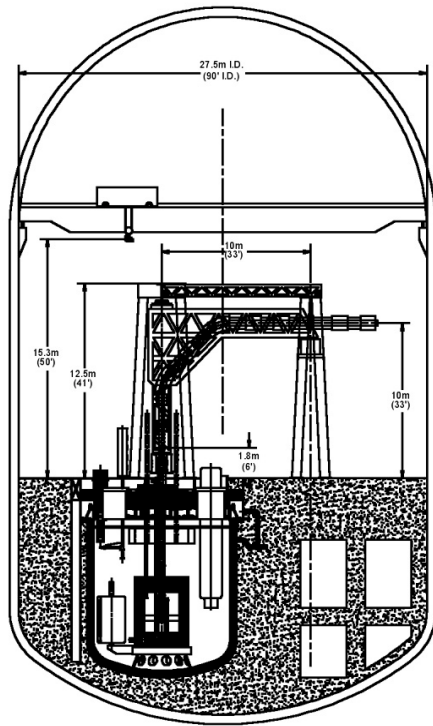


Figure 44. SCM-100 reference design.

Routing of the SHR NaK piping up the inside of the containment wall and penetration near the crane elevation for placement of the NaK-to-air heat exchangers (HXs) outside containment on or within the earthen shielding berm led the team to select two SHR loops. An alternative would have been the use of three loops the same size as those used in EBR-II.

Further consideration of the operating floor, with allowance for work areas among the various piping runs, has led to considerable rethinking of how to arrange equipment. With addition of the accelerator HEBT support structure and the LBE target with its support loop, handling, and movement of large equipment such as the IPBT shielding cask, rearrangement of some major pieces of equipment on the primary vessel cover has been necessary.

A concept has been developed for the LBE target IPBT, including the interface with the SCM core, the backshine shield, and connections to the external support loop and to the accelerator HEBT. The connections to the external support loop are shaped roughly like a fire hydrant, with LBE inlet and outlet piping connecting to flanges at the sides and the HEBT connecting to a flange at the top. Routing of the LBE target loop piping, along with that of the secondary Na system and SHR NaK piping, should be in troughs under removable panels in the operating floor to keep them out of the way. They must skirt the areas where the HEBT support structure is mounted to the floor, and they should not be in areas allocated for set-down of heavy equipment such as shielding casks. This makes optimization of the equipment layout difficult, and the location of the SCM tank within the containment building is being reevaluated.

The backshine shield of the LBE target IPBT is a multi-piece structure that fits inside the central vacuum pipe and in the annuli between the various tubes comprising the LBE flow path and the outermost guard tube. Each piece has several spiral slots along the outside; those in the inner piece allow higher vacuum pumping effectiveness in the downstream target tube, and those in the flow annuli allow for flow of the LBE in both directions. The thicknesses of the annuli are increased in the backshine shield area to permit roughly the same flow area through the slots as in the downstream annuli. The spiral prevents radiation streaming. The interface with the core is a separate structure that uses a *scalloped* shape on the outside to match the surrounding hexagonal fuel assemblies and a circular inner surface to match the IPBT. It is removable through the hole in the core barrel cover and the small rotating plug for occasional replacement. This piece is part of the buffer region surrounding the target and may be made of solid steel or may be just a hollow sheet-metal structure.

SCM Neutron Physics Design

As part of the support for the trade study between vertical and inclined proton beam tube entry into the multiplier vessel, scoping physics calculations were performed to confirm the feasibility of an inclined-entry configuration with a lead-bismuth target. The calculations showed that a multiplier assembly with 98 fuel elements would produce approximately 100 MW of power. The subassemblies, of the EBR-II Mark III type, would produce about 1 MW each. However, the power-peaking factors are of the order of 2.15, compared to 1.46 for EBR-II. Consequently, cores of this type cannot be driven to 100 MWt without substantially increasing the number of fuel elements and changing other design parameters. Doing so would reduce the achievable peak neutron flux proportionately, and this key design objective would not be achieved. This adds a disadvantage to the inclined-entry concept, which was taken into consideration in the final selection of the preferred beam entry option.

Nuclear responses in the SCM fuel assemblies next to the target were analyzed as a function of the target buffer thickness. The main parameters estimated are the helium-to-atomic displacement (He/dpa) ratio in the cladding material and the fuel bin power density. The ratios of He/dpa in HT-9 as a function of buffer thickness are shown in Fig. 45 for both the liquid lead-bismuth and the solid tungsten target.

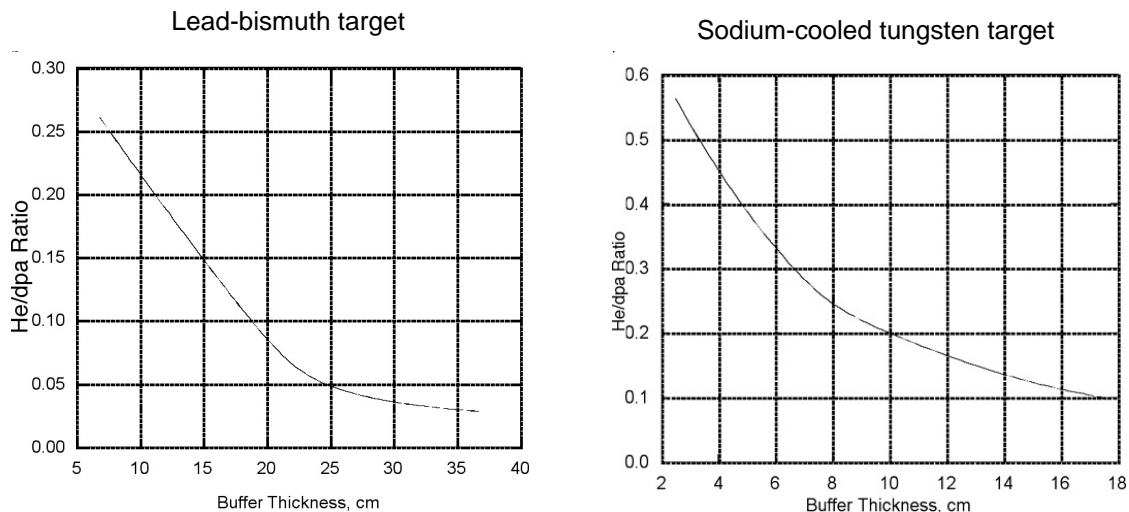


Figure 45. Ratio of helium formation to atomic displacement as a function of the buffer thickness, estimated for cladding material at the inner row of multiplier assemblies.

The neutron flux spectrum for the SCM with a LBE target has been calculated using an MCNPX model for the selected vertical-entry configuration. The multiplier contains 126 fuel assemblies of the EBR-II Mark-III design, with reduced enrichment. The enrichment was adjusted to achieve a total power of 100 MW with 5 MW of beam power using 600-MeV protons. In this SCM-100 configuration, the required enrichment is 62%. The neutron flux was calculated at locations off the core center but at the axial mid-plane of the core. The neutron flux (Fig. 46) is obtained at the outside surface of the assembly (on one flat) of rings 7, 8, and 9. Ring 7 is the inner fuel ring, 8 is the middle fuel ring, and 9 is the outer fuel ring.

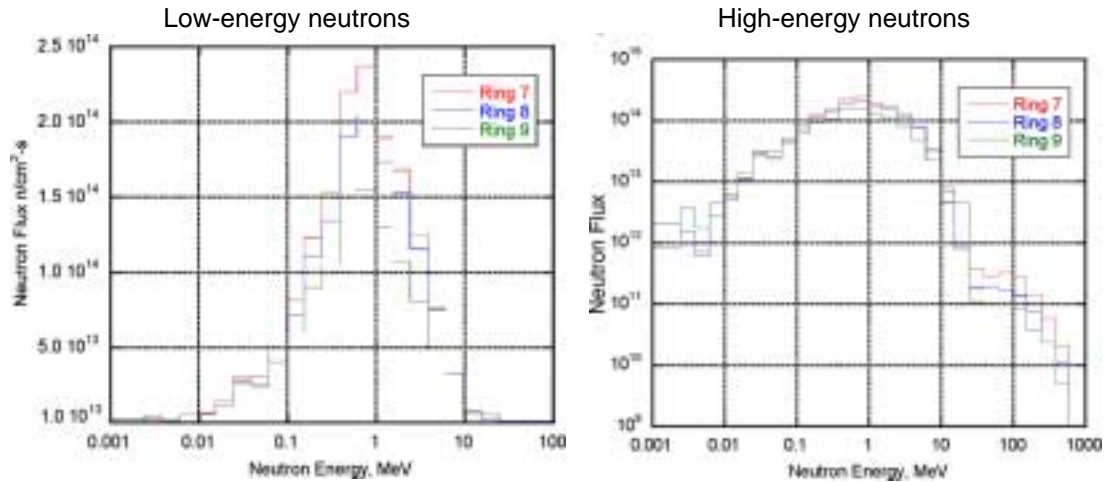


Figure 46. SCM neutron flux at different locations.

SCM Target Designs

LBE Target Design

Neutron Spectrum and Spatial Distribution for the LBE Reference Target -

Previous analysis had shown that a 7-cm-thick buffer would satisfy the physics and engineering design requirements. An MCNPX analysis was performed using this buffer size to estimate the spectrum and spatial distribution of the spallation neutrons. The neutron energy spectrum was calculated over the radial boundary of the buffer because these neutrons drive the subcritical multiplier. The neutron spectrum peaks in the energy range of 0.6–0.7 MeV as shown in Fig. 47. The high-energy tail extends to about 600 MeV. The spatial distribution of the spallation neutrons in the axial direction has a direct effect on the power distribution in the subcritical multiplier. Fig. 48 shows the axial distribution at the radial boundary of the buffer. The total distribution peaks at ~12 cm measured from the upper surface of the lead-bismuth material, while the high-energy (above 20 MeV) neutrons peak at ~14.5 cm. The peak-to-average is 1.33 and the peak-to-minimum is about 4.11.

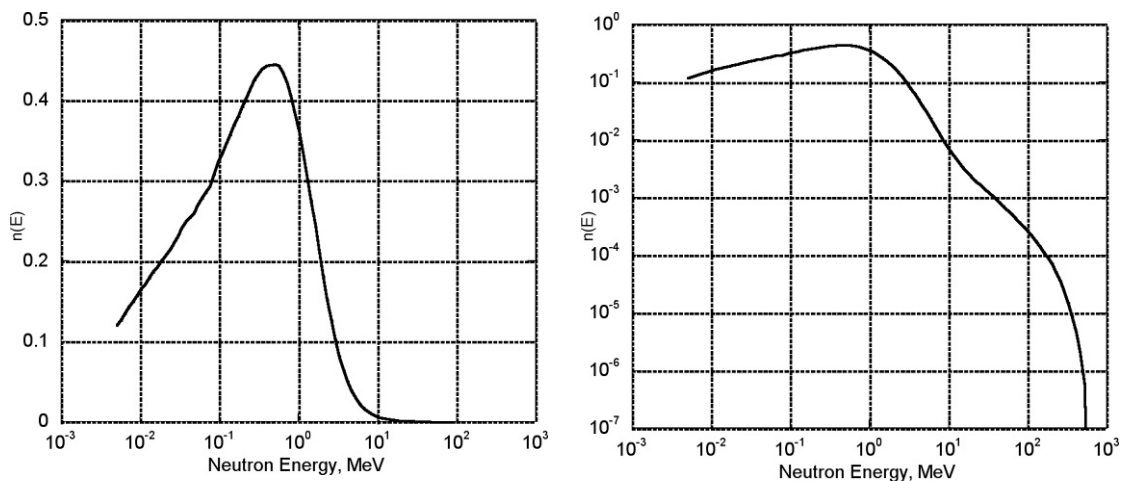


Figure 47. Spallation neutron source spectrum, with details of the high-energy neutrons.

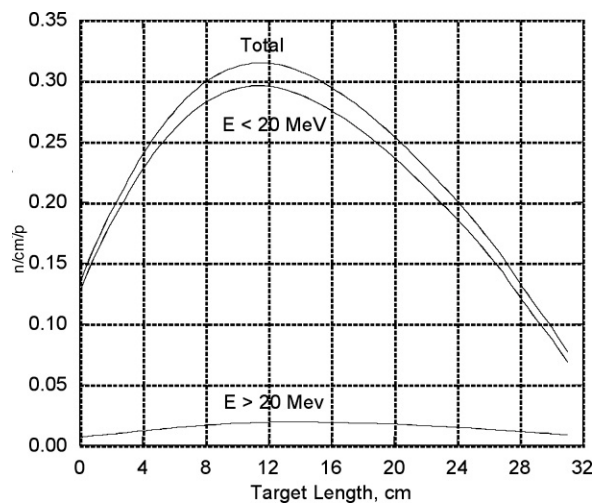


Figure 48. Spallation neutron distribution along the beam axis.

Thermal-Hydraulics and Structural Performance of LBE Reference Target Design -

The thermal-hydraulics characteristics of the LBE target have been simulated using the commercially available computational fluid dynamics (CFD) code Star-CD, and transferred to the ANSYS structural analyses. The emphasis of the thermal-hydraulics analysis has been on the design of the beam window. Analyses were conducted for a conical and a hemispherical window to investigate the effect on the window maximum temperature. The window thickness was 5 mm. The radial temperature distributions along the adiabatic and wetted surface of the beam window are shown for both the conical and hemispherical cases in Fig. 49. The maximum temperature with a 5-mm-thick window exceeds the desirable limit, so further analysis was conducted for

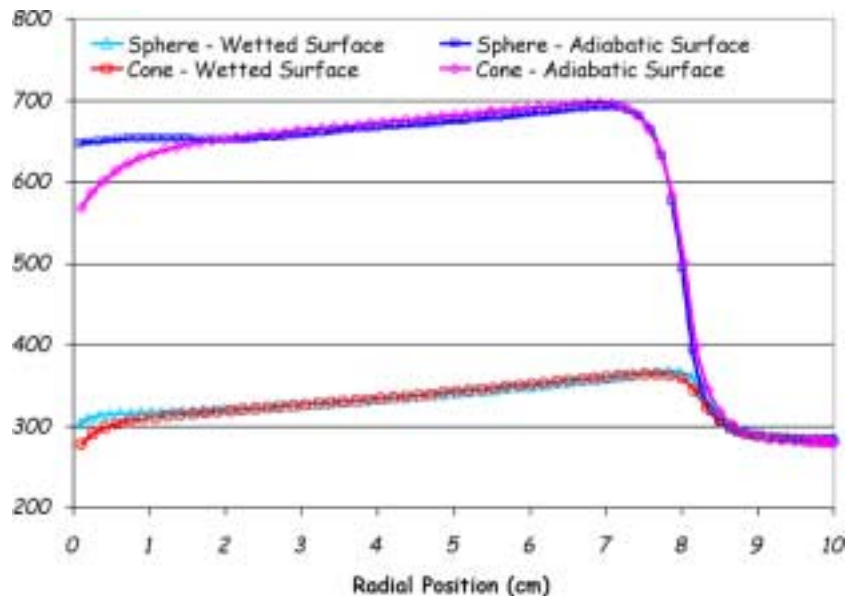


Figure 49. Comparison of temperature distributions along the adiabatic and wetted surfaces of an LBE target window for the SCM-100 with conical and hemispherical geometries.

window thicknesses of 4 mm and 3.5 mm. CFD simulation results of the target concept indicate that the thermal-hydraulic constraints are satisfied. The axisymmetric model of the target with 3.5- and 4-mm-thick windows has been analyzed with modifications for the flow geometry. The end-cap geometry is optimized, and a turning fairing is included at the leading edge of the middle wall (soft turning edge in the inner tube carrying the upflowing liquid Pb). For the 3.5-mm case, the maximum temperature in the beam window structure is 517°C. Figure 50 shows a sample of the results for the 3.5-mm-thick window.

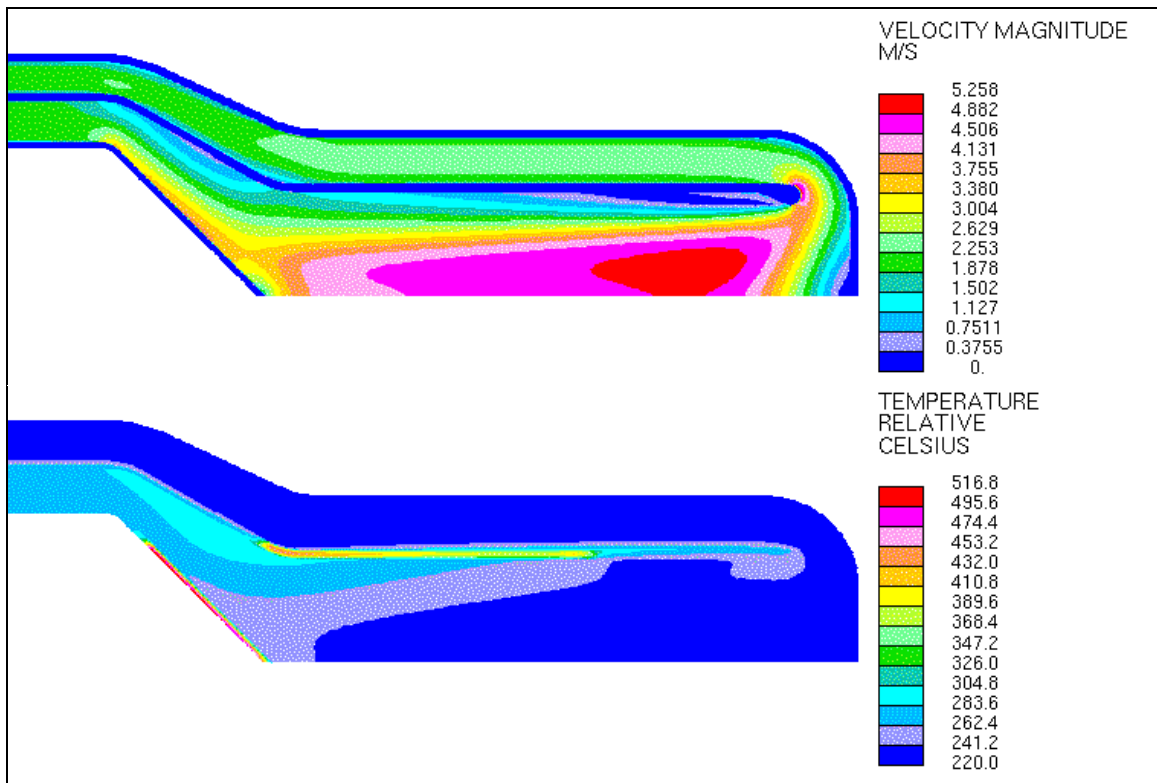


Figure 50. Axisymmetric velocity and temperature profiles for the current target concept with a 3.5-mm beam window.

As a result of these thermal-hydraulic studies, the reference lead-bismuth target design has been established with a 3.5-mm-thick hemispherical window and a 5-mm-thick beam tube. The LBE target has a uniform inlet velocity of 2 m/s and an inlet temperature of 200°C. The design satisfies the temperature limits specified for both the peak and surface temperatures. The hemispherical configuration is preferable to the conical configuration because of the higher margin for buckling, shown from stress analysis results. Additionally, the thickness of the cylindrical beam tube is 5 mm to ensure adequate margin for buckling.

The structural and thermal-hydraulic analyses with geometrical configurations were performed iteratively to define the reference design. General Atomics performed the structural analyses using ANSYS models to satisfy the structural design criteria developed for APT target blanket components and the ITER fusion reactor. HT-9 steel is the structural material used in the analysis. The results show that the reference design satisfies all structural requirements.

LBE Removal for Target Module Replacement - The ADTF target module will require periodic replacement due to radiation damage in the target structural material. The LBE will need to be drained before the target module is removed. Due to the high density of the LBE, a sufficient suction cannot be generated using standard pumping tools and methods. The module can be partially drained by pressurizing the inner annulus with a cover gas and driving the LBE out through the outer annulus. The target cannot be completely drained in this manner because a stable interface cannot be maintained when the liquid LBE is completely above the cover gas in the outer annulus. The interface will collapse and the cover gas will bubble through the LBE. The instability of this interface is described as Rayleigh-Taylor instability.

The maximum gap width or tube diameter in which a stable interface can be maintained is determined from the Rayleigh-Taylor critical wavelength, which is a function of the surface tension, the acceleration rate, and the density difference of the two fluids. After draining the majority of the liquid LBE from the target through the outer annulus, the remainder could be removed by inserting a small diameter tube through the outer annulus of the target module to serve as an outlet as the target module is pressurized. To guarantee stability of the interface until the tube is completely drained, the tube diameter must be less than 3 mm. If the presence of a small residual LBE volume does not significantly impact the removal procedure, absolute interface stability may not be required and larger tubes may be used to reduce the time required to drain the target. Additional studies will be required to define the tube diameter and the number of tubes for the target drainage procedure.

Alternate LBE Target Concept Development - An advanced LBE target design (Fig. 51) has also been studied as an alternative to the reference design. The concept uses fully asymmetric streamlines and large pressure losses to ensure flow stability. Reductions in local flow velocities and turbulence intensity resulting from the complete stabilization of the flow field will likely reduce heat transfer in the heated region. The alternative concept also includes a separate cooling channel to reduce the temperature of the beam window region. Initial simplified 2-D simulations indicated that the peak temperature in the beam window could be up to 50°C lower than the reference concept with similar window thickness. To provide a reasonable bound for the temperatures of the internal structure and the target fluid, a simplified 3 D model was developed. The cylindrical target is represented by a Cartesian geometry that maintains cross-sectional flow areas and reasonably approximates the heated surface areas. The 3-D flow field is currently being analyzed.

Solid Tungsten-Target Design

Further design work has been performed this quarter for a solid tungsten design. Two alternate configurations are being studied. Unlike the reference tungsten target design, these configurations do not use parallel sodium flow to cool the target and window, but an upward flow that sequentially cools the target plates first and the window second. In the first design, the tungsten plates are placed horizontally in the spallation zone, whereas in the second design the tungsten plates are arranged vertically. Preliminary modeling indicates that both configurations allow the tungsten plates to be sufficiently cooled down. Modeling of the window cooling has begun.

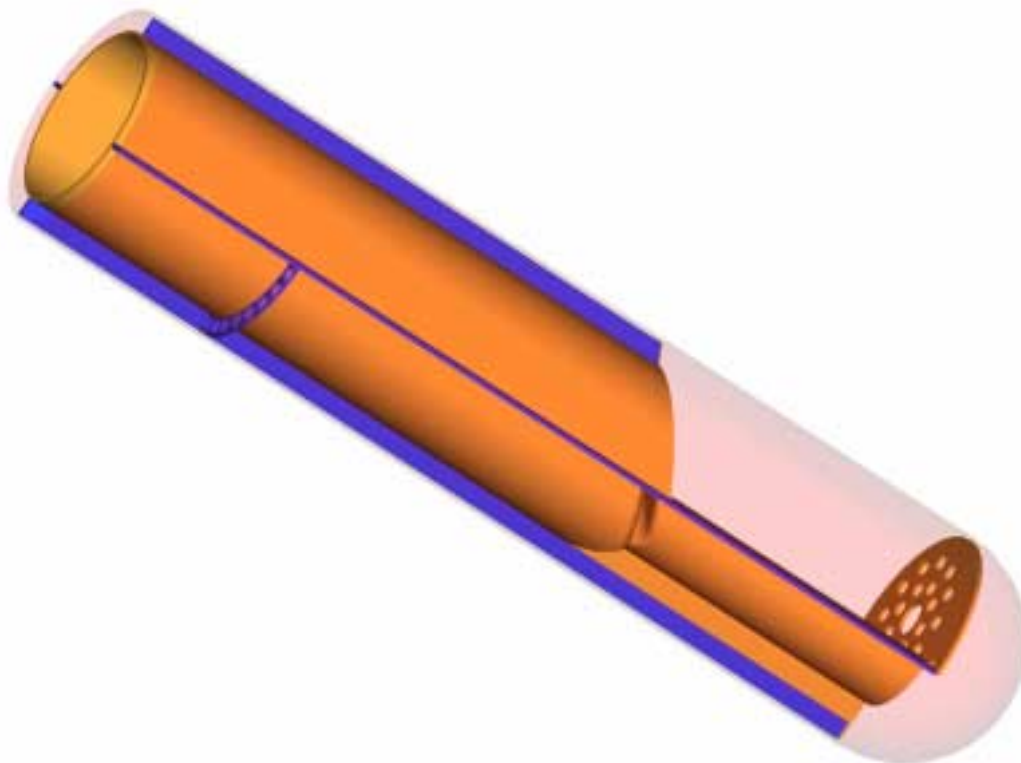


Figure 51. Advanced lead-bismuth eutectic target design concept

Shielding Design

The 3-D MCNPX shielding model for the SCM facility has been used to obtain preliminary dose results during operation inside the building. The calculations show that the neutron dose above the backshine shield during operation is $\sim 2 \times 10^6$ rem/hr. Above the SCM working floor, this dose drops fast in the range of 1 to 10 rem/hr. The model requires further enhancement to provide detailed dose maps. The model was provided to Los Alamos for calculating the biological dose after shutdown during the target replacement process.

Other SCM Design Team Activities

Coordination With Other ADTF Activities

The SCM design team participated in the ADTF preliminary hazards assessment (PHA) activities. Characteristics of the systems, existing hazards in the SCM buildings, and expected transient responses were provided to the PHA team. SCM information has been provided to the ADTF cost estimators. The draft cost estimate for the TMT and SCM were reviewed, and feedback was provided to the cost estimating team.

The SCM design team also collaborated closely with the Balance of Facility designers and the TMT designers to support designs of the structures, material handling, and

common facilities (hot cells). Close collaboration has existed with the HEBT design team to support the design of the multiplier primary vessel cover and the support structure for the HEBT.

ADTF EIS Support Activities

The Project is working toward reaching agreement on all ADTF support facilities, both direct and indirect, that need to be included in the EIS. Direct support facilities are those that produce physical products for use in the ADTF.

Process flow diagrams for the ADTF have been developed as a function of various research and operational phases of the project, identifying various support facilities and mass flows. The mass flow diagrams for each facility have been modified to show time-phasing of functions. The proposed phases are shown in Table 8.

The report on the mass flows for the SCM and the TMT for use in development of the EIS is in the final stages of preparation. The goal is to envelop anticipated or reasonably anticipated actions of the ADTF. The report covers the direct support facilities, i.e., facilities that provide or receive a product from the SCM or TMT. The purpose of the report is to define the following:

- 1). The potential fuels that can be used as driver and research fuel in the TMT and the SCM, their burnup levels, and the shipments between facilities;
- 2). The hot cells and the experimental facilities anticipated for both the fuels development and the separations programs;
- 3). The potential functions of the various facilities;
- 4). The various irradiation facilities; and
- 5). The mass flows as a function of time for the various facilities.

Table 8. ADTF EIS Schedule - Project Phases

Phase	TMT	SCM	Pilot Scale Front-End Separations Facility	Pilot Scale Back-End Separations Facility
1	Design; Construction	Delayed start of design & const.	R&D	R&D
2	Operational	Construction	R&D	R&D
3	Operational	Operational	Design / Construction	R&D
4	Operational	Operational	Operational	Design / Construction
5	Operational	Operational	Operational	Operational

A draft review of this document will take place in early October. After completion of the draft review, the report will be submitted for further review and approval.

International Collaboration - DOE/CEA Work Package on ADTF Design

Work has been performed on development of an SCM-100 neutronic model. A complementary study is being performed by CEA (Cadarche), using an R-Z model previously prepared at ANL. The main goal of the current study is to investigate certain safety aspects of different SCM-100 configurations loaded with metal or oxide fuel and to study the impact on safety performance of fractional loading of special assemblies containing minor actinides. For this purpose, a model (126 assemblies of the EBR-II Mark III type with metal fuel enriched to 67%) was created using the ERANOS code system.

Preliminary β_{eff} calculations were performed. Results from these calculations are summarized in Table 9, which also contains the contributions from ^{235}U and ^{238}U to the overall β_{eff} value. The results show that ^{235}U contributes about 93% of the total value of 0.00724. We also see a 2% difference in the values obtained using the transport R-Z and diffusion hexagonal-Z models. R-Z geometry was used in the transport calculation because ERANOS does not have a transport perturbation module for 3-D geometries.

Table 9. Preliminary β_{eff} Results

Model	Components		
	U-235	U-238	TOTAL
Transport (R-Z)	0.00656	0.00548	0.00711
Diffusion (Hexagonal-Z)	0.00671	0.00527	0.00724

Analysis continued on the investigation of the safety parameters for different configurations loaded with metallic fuel and transuranic-containing assemblies. Using a base core design with metallic fuel enriched to 57.5%, the impact of fractionally loading the TRU assemblies on the core safety parameters has been studied.

Three isotopic vectors were considered for the TRU-containing assemblies. These vectors were derived from the high-burnup pressurized water reactor (PWR) spent-fuel inventory after 10-year cooling. For the three cases, it was assumed that the Pu and MA contents of the spent fuel could be separated and recombined into ratios of interest. The MA/Pu fractions considered for the three cases are 0.5/0.5, 0.1/0.9, and 0.9/0.1. The fuel form employing these three vectors is TRU-40Zr. Preliminary core physics and safety performance parameters for the base core have been estimated. Table 10 contains a summary of the core parameters for the three cores employing six TRU assemblies.

These preliminary results are indicative of the issues to be considered in designing TRU-containing assemblies. First, it is apparent that as the Pu content of the TRU assemblies is increased, the initial k_{eff} increases, suggesting a limit to the number of assemblies that can be accommodated (to ensure subcriticality level) or a need for assembly redesign (lower fuel volume fraction). Additionally, the β_{eff} is observed to decrease with the Pu content in the fuel, as expected, indicating the need to manage the number of such assemblies in the core.

A representative layout of these cores is shown in Fig. 52 (the reflector and sodium pool zones are not represented in the figure). The performance of this design has been compared with an alternative design using oxide fuel and Fast Flux Test Facility (FFTF) assemblies (Fig. 53).

The oxide fuel configuration consists of nine hexagonal rings with 48 drivers containing mixed-oxide fuel (U-PuO₂) with a plutonium-in-heavy-metal content of about 24% wt.%. Target and buffer regions cover the first two rings; the core region is surrounded by a reflector making up rows 6-9. Table 11 contains a summary of results for the SCM base core fueled with FFTF driver assemblies compared with a core fueled with EBR-II driver assemblies.

Table 10. Results for Na-Cooled SCM-100 Cores Loaded with 6 TRU Fuel Assemblies

MA/Pu (%)	Keff	Power Peaking Factor	Ave Pwr Density (W/cc)	Flux (Max./Ave) (10^{15} n/cm ²)	β_{eff}	$\Delta\rho_{\text{void}}$ (pcm)
10 / 90	0.98798 (BOC)	1.24	737	3.34 / 2.57	690	-1649
50 / 50	0.97336 (BOC)	1.24	748	3.37 / 2.61	692	-1756
90 / 10	0.95718 (BOC)	1.25	760	3.42 / 2.65	695	-1673

Comparing assembly dimensions, the FFTF assembly has a height ~2.5 times that of the EBR-II assembly and about twice the EBR-II assembly pitch. Comparing the results obtained when utilizing EBR-II and FFTF driver assemblies, we find that the FFTF case gives a lower β_{eff} because of its plutonium content; the EBR-II driver assembly does not initially contain plutonium. The sodium void coefficient of the SCM-100 loaded with FFTF assemblies is more positive than that loaded with EBR-II assemblies because the latter's active core is much smaller (approximate factor of 4), resulting in a leakier core. It was also observed that the SCM-100 core with FFTF assemblies has a larger (more negative) Doppler coefficient. This is attributed to the higher ²³⁸U content in this fuel, relative to the EBR-II driver fuel. Because of the larger core size, the SCM-100 with FFTF driver assemblies has a lower power density and higher power-peaking factor than the EBR-II case. The flux level achieved in the FFTF core is not significantly different despite the much lower power density because of the lower fissile fraction in its fuel assembly.

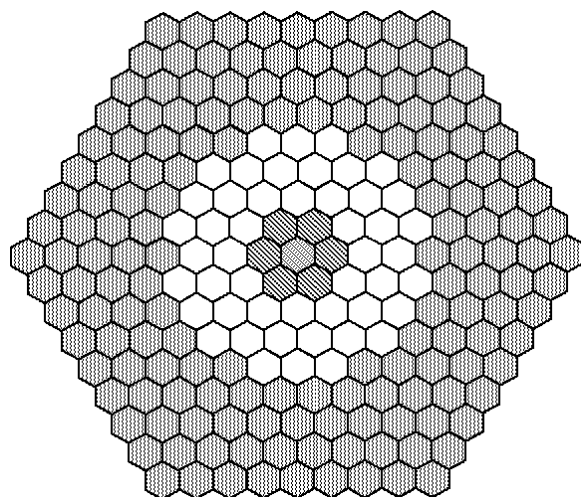
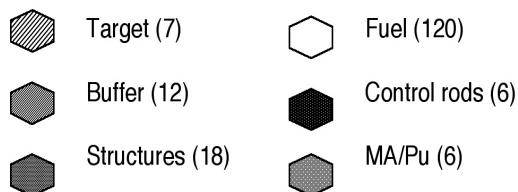
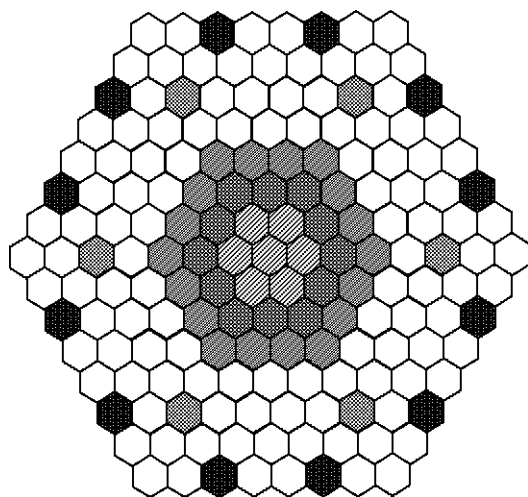


Figure 52. Layout of the SCM-100 loaded with U-10Zr and TRU fuel assemblies.

Figure 53. SCM-100 loaded with FFTF driver assemblies.

**Table 11. Performance Parameters for SCM-100 Base Cores with
EBR-II and FFTF Driver Assembly Types**

Case	State	EBR-II	FFTF
Power-Peaking Factor	BOC	1.24	1.44
	EOC	1.23	1.43
Average Power Density [W/cc]	BOC	744	176
	EOC	744	175
Neutron Flux (Max./Avg.) [10 ¹⁵ n/cm ² /s]	BOC	3.33 / 2.61	2.49 / 1.63
	EOC	3.41 / 2.68	2.55 / 1.67
k _{eff}	BOC	0.97114	0.97056
	EOC	0.95512	0.95402
β_{eff} [pcm]	BOC	730	332
	EOC	754	340
$\Delta\rho_{\text{void}}$ [pcm]		-1813	-824
Doppler, K _d [pcm]		-70	-676

7.3 Balance of Facility Design

A point design has been established for the Balance of Facility design of the ADTF multiple-station concept. The current plant arrangement has the following features:

- The general site arrangement will be largely based on the APT site plan. The target stations will be offset so as not to interfere with an upgrade path to extend the accelerator tunnel and construct a target station for tritium production.
- The SCM and TMT stations will be arranged such that the beam will enter at the same elevation. This will require a deep subsurface excavation for the SCM containment structure.
- The SCM and TMT stations will be arranged to allow a single hot-cell facility to support the operational needs of both stations.

The preconceptual design has evaluated and refined the equipment and building layouts for both the TMT and SCM stations. Progress in these areas is discussed below.

TMT and Hot Cell Building

To define the necessary functions within the TMT hot cell, the design team performed a step-by-step evaluation of the movement of material from the SCM to the hot cell and ultimately to an offsite location for further examinations, processing, or disposal. Functional flow block diagrams were prepared that defined the sequence of functions that would be performed within the hot cell. If possible, the associated performance requirement was also defined. This process was then used to define the required areas and equipment stations within the hot cell. It was determined from this analysis that both an air and argon hot cells would be required to support SCM operations. To supplement this evaluation, the design team also visited other hot-cell facilities at ANL-West and SRS to better evaluate the potential scope of the ADTF hot cells. The general arrangement of the proposed hot cell for ADTF is shown in Fig. 54.

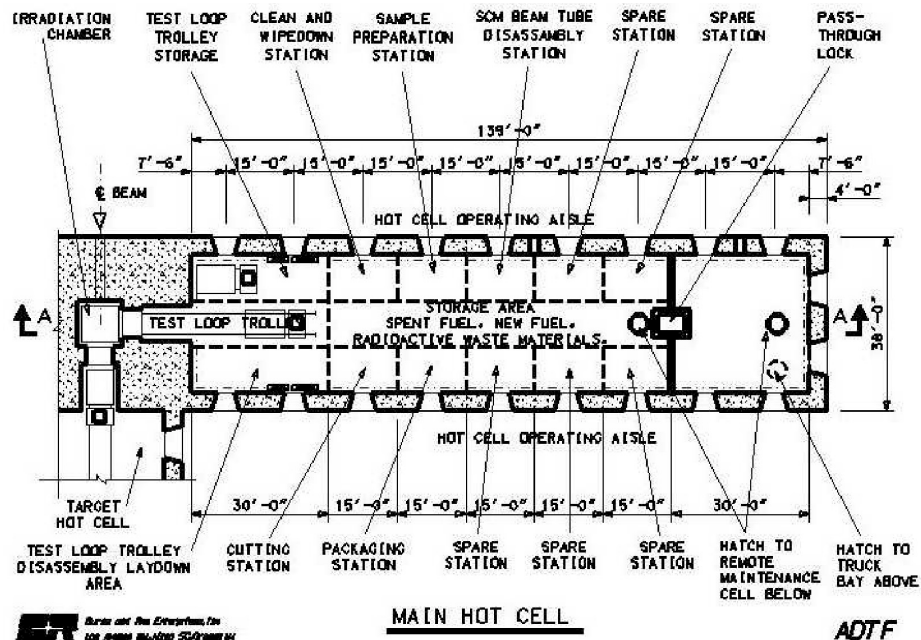


Figure 54. TMT main hot cell.

SCM Building

Since the SCM nuclear design requires a vertical beam entry, the beam tube will require significant shielding, either internally or externally to the SCM containment. The point design selected for the preconceptual cost estimate assumed that the building would be located below grade, with the necessary shielding provided by an earthen berm as seen in Fig. 55. Although providing the necessary shielding, this arrangement does present some construction and operational challenges.

Specifically, access would be restricted and the movement of large components into and out of the building is more difficult than for a facility at grade. To evaluate alternate arrangements, a simplified trade study was performed. Several at-grade arrangements were

considered. Shielding would be provided by either an earthen berm over the structure or by shielding internal to the building (either steel or high-density concrete). The conclusion of the study was that an at-grade facility would be feasible without a significant cost increase and would provide significant improvements with respect to access for maintenance and operation activities.

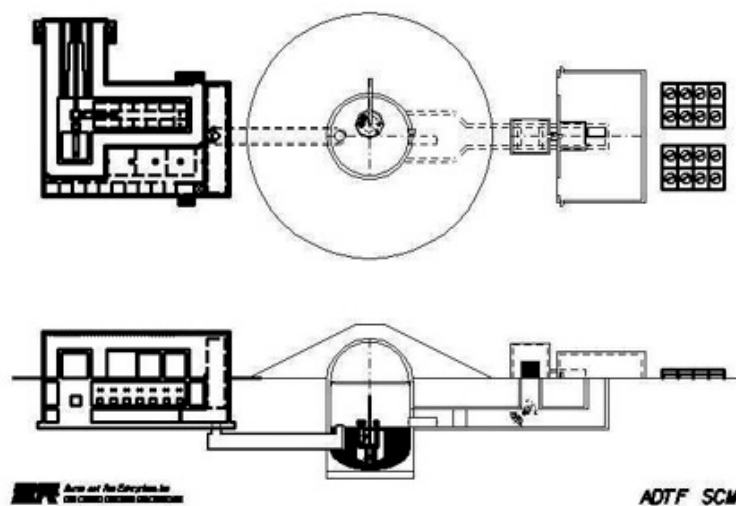


Figure 55. Below-grade SCM building.

V. PROJECT INTEGRATION

8. Systems and Technology Integration

Scope

System and Technology Integration coordinates all technical elements in defining requirements, performing system-level evaluations, developing preconceptual designs, and establishing technology development activities into a comprehensive research and development/proof of performance (POP) effort. Overall system objectives, system performance requirements, and POP requirements are used to correlate R&D needs, data quality objectives, experimental facilities, resources, and materials. System-level modeling evaluates the performance of multi-strata options in establishing a technically feasible spent nuclear fuel (SNF) management program, especially with regard to proliferation, economics, environment, safety, and institutional issues. Likewise, preconceptual designs serve as fundamental bases in defining critical R&D and focusing POP testing. Woven together, the system and technology integration activities can provide a solid foundation for focused and coordinated AAA research and development.

Highlights

- The Systems and Technology Integration Team completed the extensive multi-tier evaluations and produced the technical report entitled *Candidate Approaches for an Integrated Nuclear Waste Management Strategy—Scoping Evaluations* (AAA-PDO-GEN-01-0051, September 2001).

Multi-Strata Evaluations

This quarter, System Integration activities focused on completing the multi-tier evaluations and producing the technical report *Candidate Approaches for an Integrated Nuclear Waste Management Strategy—Scoping Evaluations*. As reported last quarter (April–June 2001), the evaluations employed an isotopic feed stream of 10-year, cooled, SNF irradiated in advanced light-water reactors (ALWR) in the commercial *Nuclear Future* infrastructure. In Case 1, plutonium is separated from the SNF and irradiated in a thermal-spectrum reactor (first tier); minor actinides and thermal spectrum residuals are sent to the second tier, accelerator-driven system for further transmutation. In Case 2, all transuranics are irradiated in the first-tier thermal-spectrum reactor; residuals are sent to the second-tier ADS. In Case 3, transuranics and long-lived fission products are sent directly to fast-spectrum systems with either a conversion ratio of 0.0, such as an ADS in the original Roadmap, or with a conversion ratio of 0.5, as with the Integral Fast Reactor.

The performance of each of the fundamental approaches (and appropriate variations) was compared to an established set of high-level programmatic goals supporting the nuclear waste transmutation mission.

The goals and supporting criteria are expressed as follows:

Improve long-term public safety

- Radiotoxicity Criterion - Reduce radiotoxicity of spent nuclear fuel below that of source uranium within 1,000 years.
- Dose Criterion - Reduce maximum predicted peak dose to future inhabitants of a region containing a repository by at least 99% as compared to current predictions.

Provide benefits to the repository program

- Heat-Load Criterion - Reduce long-term heat load of spent nuclear fuel by at least 90% after 500 years as compared to unprocessed spent fuel.
- Criticality Criterion - Preclude possibility of future criticalities by reducing and degrading the transuranic content.
- Mass Criterion - Reduce mass of commercial spent fuel by separating the uranium and either recycling the uranium or diverting it to alternate disposal.

Reduce proliferation risk from plutonium in commercial spent fuel

- Plutonium Inventory Criterion - Reduce or potentially reverse the build-up of the inventory of plutonium in the nuclear fuel cycle, reversing the long-term trend of plutonium build-up from the once-through fuel cycle.
- Plutonium Disposal Criterion - Reduce the inventory of plutonium passing to the nuclear waste repository by 99% and decrease the fissile fraction within that plutonium.
- Plutonium Accessibility Criterion - Minimize the risk of plutonium diversion throughout the alternate fuel-cycle and materials-handling processes.

Improve prospects for nuclear power

- Viability Criterion - Provide a viable and economically feasible waste management option for commercial spent nuclear fuel.
- Technical Risk Criterion - Minimize technical risk to achieve solutions to the nuclear waste challenge.
- ES&H Criterion - Improve upon ES&H characteristics of the once-through fuel cycle.

To ensure that the performance of each approach would be assessed in an unbiased manner, expert judgment was solicited in the technical areas of fuels and materials, separations chemistry, and reactor physics to determine not only the range of technical options and important variables, but also to determine key elements of various processes. Using the expert input with reference to previous evaluations, an integrated system process was established to serve as a flow-sheet structure for defining each of the approaches and variations. Burn-up and separations calculations were performed, which allowed the system process structure to integrate mass flows and process variables throughout the system. A base data set was then constructed for each approach, using system mass concentrations, thermal loading, and

radioactivity for all nuclides at relevant points in the system process. Using the base data sets, and derived factors when appropriate, each approach was assessed to determine its performance against the established criteria. To ensure material balances in the system, separations chemistry and irradiation calculations were correlated at all steps in the process. Likewise, the outputs of those calculation sets were incorporated into approach-specific spreadsheets for integration, which were then used to derive data for the criteria assessment.

A common set of assumptions were used as boundary conditions in the overall assessment, and to ensure that the evaluation results could be compared to the criteria in an unbiased fashion. All evaluations were performed using *established* models for advanced light-water reactors, gas-cooled reactors, accelerator-driven systems, and advanced liquid-metal reactors. No system optimization was performed prior to criterion assessment, but it is recommended in subsequent evaluations. An abbreviated set of major assumptions includes the following:

- Transmutation system performance is normalized to projected spent nuclear fuel input from commercial sector, *not* to commercial energy production.
- The commercial spent nuclear fuel feed vector is based on the isotopic charge and discharge of a pressurized water reactor with 50,000 MWd per metric ton burnup.
- U, Pu, and MA are separated at 99.9% efficiency.
- Tier-1 LWR burnup/irradiation calculations are performed with the same ORIGEN decks to ensure consistency.
- An equilibrium cycle is assumed in Tier 2 such that the feed from commercial ALWR or Tier 1 is introduced at the same rate (makeup) that the TRU is destroyed in Tier 2.

Comprehensive assessments were performed to evaluate the approaches, and the reader is directed to the technical report for appropriate detail. However, at this point in the evaluation process, the following principal conclusions can be drawn:

- *All* of the assessed approaches can fundamentally meet the transmutation criteria as stated, within the fidelity of the available data, assumptions, and analytical methods. It appears technically feasible to move toward an integrated waste management strategy using future reactors.
- Virtually every criterion, and the transmutation performance of each approach, is most significantly influenced by the ability to achieve 99.9% separation of TRU materials from spent nuclear fuel.
- The current state of knowledge about separations and fuel fabrication losses is quite limited. While industrial-scale plutonium uranium extraction (PUREX) plants have systematically achieved separation losses equal to or lower than 0.1% for uranium-oxide fuel, and to a very limited extent for mixed-oxide fuels, other processes, particularly those designed for as-yet-undeveloped fuel types, cannot yet be assessed with precision. Thus, detailed sensitivity studies must accompany the development of flow sheets, and a major R&D effort is required to develop and demonstrate the separations and fabrication technologies.

- Another important factor is the achievable burnup rates, which also strongly affect the overall transmutation losses (by changing the number of separations passes) and require an extensive fuel development and demonstration program.
- For two-tier systems, there is a clear advantage to trying to maximize the overall burnup rate in the first tier. As mentioned, theoretical studies indicate high potential burnup rates, but practical considerations usually limit the achievable rate. The issue needs to be studied carefully, taking into account all practical considerations in the fuel cycle.

Regarding the performance of candidate approaches vs. the goals, criteria, and metrics, we can conclude the following:

- Each assessed approach *can* reduce the radiotoxicity of spent nuclear fuel to below the radiotoxicity of natural uranium ore within 1,000 years, assuming 0.1% separation losses.
- From a qualitative approach, it appears that each assessed approach *can* reduce maximum predicted peak dose to future inhabitants by at least 99% in comparison to current predictions.
- Each assessed approach can reduce the inventory of materials that contribute to long-term heat loads in the repository by 90% or more.
- Each assessed approach reduces the transuranic mass by greater than 99%, under the given assumptions, but each case exhibits a percentage increase in fission product mass. Likewise, there is a sharp percentage increase in TRU and fission product waste volume, but this condition can be alleviated by reassessing the assumption for two-year cooling rather than a longer period. It should be noted that appropriate disposition paths for graphite fuel element material must be explored.
- Each assessed approach reduces plutonium inventory by greater than 99%, which certainly exceeds the 90% nominal basis.
- The support ratio assessments clearly demonstrate that the scope of the transmutation enterprise necessary to support a nuclear future assumption is very large. Likewise the support ratios are very dependent on assumptions regarding electricity production at each tier.

This evaluation has provided a set of preliminary conclusions that are strictly limited by the overriding assumptions and their variability. However, the robustness of system performance and comprehensive, systematic analytical approaches must be verified in future analyses such as:

- Assess economic performance of approaches with attention to support ratios.
- Assess the sensitivity of transmutation performance to variations in assumptions, especially the 99.9% separation efficiency assumption.
- Perform R&D on process factors that most significantly impact separation efficiency, and seek process approaches that ensure efficient separations.

- Perform R&D on process factors that most significantly impact the efficiency of fuel processing, and seek process approaches that ensure efficient fuel fabrication.
- Determine the maximum achievable Tier 1 burnup in balance with radiotoxicity and dose of materials sent to the repository, as well as increases in fission product inventories and waste volumes.
- Assess uncertainty incurred by lack of data, assumptions, and analytical methods.
- Assess alternate approaches and variations on current approaches.

9. University Programs

Scope

The AAA University Programs consists of four major aspects:

- **University Fellowships Program (UFP)** – The Amarillo National Research Center (ANRC) is acting as the executive agency for the AAA Program to select, award, and administer fellowships for 10 graduate students beginning in FY01.
- **UNLV University Participation Program (UNLV UPP)** – The University of Nevada at Las Vegas (UNLV) is supporting the AAA Project through “research and development of technologies for economic and environmentally sound refinement of spent nuclear fuel...”¹⁸ The Program has three components: student-based research, infrastructure, and support.
- **AAA Directed University Research** – Three universities currently support R&D and technology development: University of Michigan, University of California-Berkeley, and University of Texas-Austin.
- **University Research Program (URP)** – A future program to create a NERI-like competition for faculty and student research proposals (not funded in FY01).

The AAA University Program also involves coordination between other AAA projects and academia.

Highlights

AAA University Fellowship Program

- The Amarillo National Research Center submitted to DOE/NE a report of student feedback from the June visit of the AAA Fellows to Washington, D.C.

¹⁸ ref. H.R. 5483, P.L. 106-377

- The AAA University Participation Program PI and the Intercollegiate Programs Coordinator attended a meeting at the ANRC to discuss a variety of potential intercollegiate collaborations.
- Three students completed summer internships, two at LANL and one at ANL-W. In addition, one AAA Fellow was supported during the summer with AAA funding at UT-Austin.
- All 10 Fellows began their academic programs with the start of the fall semester at their respective universities. Several have begun their research projects, and others are formulating their topics and programs.

AAA University Participation Program

- A second call for student-based research proposals was issued, and 10 proposals were received and reviewed by a Blue Ribbon Review Panel (DOE/NE, LANL, and ANL). The UNLV AAA Finance Committee selected, and DOE/NE approved, eight student-based research projects. The UNLV PI submitted a Statement of Work for this research to DOE-AL for student research to begin in September. The titles of the funded proposals are:
 - Modeling Corrosion in Oxygen Controlled LBE Systems with Coupling of Chemical Kinetics and Hydrodynamics;
 - Neutron Multiplicity Measurements for AAA Target/Blanket Materials;
 - Development of Dose Conversion Coefficients for Radionuclides Produced in Spallation Neutron Sources;
 - Development of a Systems Engineering Model of the Chemical Separations Process;
 - Design and Evaluation of Processes for Fuel Fabrication;
 - Development of a Mechanistic Understanding of High-Temperature Deformation of alloy EP-823 for Transmutation Applications;
 - Nuclear Criticality Analyses of Separations Processes for the Transmutation Fuel Cycle; and
 - Radiation Transport Modeling of Beam-Target Experiments for the AAA Project
- The AAA UPP Director traveled to Obninsk, Russia, to visit the Institute of Physics and Power Engineering (IPPE) and other nuclear science institutes, to attend a conference, to discuss potential research collaborations, and to recruit scientists and students for AAA research at UNLV.

AAA Directed University Research

- Contracts were awarded to the University of Michigan and to the University of California at Berkeley for work in support of reactor design and analysis, systems studies, planning for experiments, and repository performance studies.
- The University of Michigan PI submitted an annual report for the period April 1, 2000, to July 31, 2001 (ATW research with FY00 funds). The report included three technical papers that have been submitted for presentation at international meetings.

- The AAA University Programs Coordinator visited the University of California at Berkeley to review progress on their research, to give a graduate colloquium on the AAA Project, to meet with faculty, and to give a speech for the student section of the American Nuclear Society.

Other

- DOE/NE sponsored five students (two fully and three partially) to attend the Glenn T. Seaborg Institute for Transactinium Science (GTS-ITS) Summer School at Lawrence Livermore National Laboratory.
- A summary report on total student support from the FY01 AAA budget was transmitted to DOE/NE for communications purposes. Approximately 80 students, from high school through the doctorate level, have been, are, or will be supported by the program this year. This information was also disseminated at the meeting of the Nuclear Engineering Department Heads Organization during the summer conference of the American Nuclear Society.

Technical Progress

Technical progress of ongoing investigations by directly supported university research projects is reported under the appropriate sections in this report.

10. Collaborations

Scope

There is great potential for beneficial international collaborations, with over a dozen nations currently evaluating nuclear waste partitioning and transmutation. The AAA Program, primarily through the technical community, has informal contacts with many of these programs; however, formal international collaborations, which are in the best interests of the Program, must be carefully developed so as to avoid over-commitments or other programmatic challenges. Through the fourth quarter of 2001, the following collaborative activities were *formalized* and will be pursued:

- Participation in technical collaborations with the French CEA in developing technologies related to materials, fuels, physics, safety, and a proposed accelerator-driven test facility. Also under discussion are separations, accelerator technology, and systems.
- Participation in a Working Party on Partitioning and Transmutation (WPPT) under the auspices of the OECD/NEA (Organization for Economic Cooperation and Development / Nuclear Energy Agency).

Other collaborative efforts under consideration include the European Union, JAERI (Japan), and work under the auspices of the IAEA (Austria). Several other national programs are also of interest, but discussions on collaborations have not progressed as far with these parties.

Highlights

- The report, *Internal Plan for International Technical Cooperation*, summarizing opportunities for international collaborations, was finalized and published with a limited distribution.